OCTOBER 2, 1967

COORDINATED SCIENCE LABORATORY

PROGRESS REPORT FOR MARCH - AUGUST, 1967

UNIVERSITY OF ILLINOIS - URBANA, ILLINOIS

The research reported in this document was made possible through support extended the Coordinated Science Laboratory, University of Illinois, by the Joint Services Electronics Program (U. S. Army Electronics Laboratories and U. S. Army Research Office, Office of Naval Research and the Air Force Office of Scientific Research) under Contract Number DAAB07-67-C-0199.

Portions of this work were also supported by:

National Aeronautics and Space Administration

Grant NsG-443, Grant NsG-376, Grant NsG 228-62

National Science Foundation

Grant NSF GK-36, Grant NSF GK-690, Grant NSF GK-1663

Advanced Research Projects Agency

Through U. S. Army
Contract DAAK-02-67-C-0546

Air Force Office of Scientific Research

Grant AFOSR 931-66, Grant AFOSR 931-67

Office of Naval Research

Contracts
N00014-66-C0010-A01, N00014-67-A-0305-0001

U. S. Office of Education

Contract
OE C-1-7-071213-4557

Syracuse University Research Corporation

Contract SURC 66124

Owens-Illinois, Incorporated

Bi-University Institutional Liaison for Development

University of Illinois

as acknowledged in footnotes in the text

(OVERLEAF BLANK)

SUMMARY OF

PROGRESS REPORT FOR MARCH THROUGH AUGUST 1967

1. Surface Physics.

Measurements of the adsorption and desorption of N_2, CO, and H_2 on polycrystalline, 110, and 111 tungsten have been made utilizing the Auger electron-emission technique. These measurements indicate various types of adsorption states having, in general, complex desorption characteristics. The electron spectrometry technique developed in this laboratory has been applied to the study of the adsorption of gasses on polycrystalline tungsten and platinum. The instrument is being modified to allow temperature control of the sample over a wide temperature range starting at about $100^{\circ}K$. The heating technique has also been modified. Work on the experiment for the study of the angular distribution of secondary electron has proceeded. Preliminary measurements with the analyzer system have been made showing some design changes to be necessary. Initial measurements with the improved system are being started. An experiment to study the emission of ions from solid surfaces due to electron impact has been started. Progress in the design and construction of this instrument is discussed. Some measurements of the yield of photons emitted from surfaces by impinging ion have been made indicating values in reasonable agreement with theoretical predictions.

2. Applied Physics.

Difficulties experienced in using an omegatron as a relative standard for comparing ionization-gauge sensitivities to ionization cross sections are reported. Size effects in thin, epitaxial gold films are

discussed, as are the techniques used for the data analysis. The preparation of thin, unbacked, aluminum films for use as optical filters, and of replicas for electron microscopy of film surfaces is also considered.

3. Plasma Physics.

The high-frequency instability resulting from the interaction of a cold electron beam with a cold plasma is investigated in the collisionless as well as the collision-dominated regime. Measurements of the beam distribution function show that the instability is heavily damped at high plasma densities and exhibits a maximum at intermediate densities. The results are in good agreement with theoretical calculations invoking Coulomb collision as the main damping mechanism.

4. Rarefied Gas Dynamics.

Solutions of the nonlinear Boltzmann equation have been obtained for two problems: a strong shock wave (Mach number 4.0); and heat transfer in a rarefied gas for several values of the Knudsen number and of the ratio of the plate temperatures. These solutions can be compared in detail with results of Navier-Stokes and Krook theory by using a new program that calculates mean values and probable errors for each of some 80 functions of interest at each station in the gas.

5. High-Voltage Breakdown.

An improvement by a factor of three in the voltage-holding capabilities of copper electrodes at ultrahigh vacuum may be realized by gas conditioning of the electrodes. Under certain conditions, whiskers are found to grow or appear on tungsten tips in the field-

emission microscope. No whisker growth has been observed on clean tungsten tips.

6. Space Sciences.

The accuracy requirement of the general-relativity-effect measurement has been reappraised. Realistic data were used to estimate the center of noisy photographic images by computer simulation. From these data the overall readout accuracy was estimated. Possible flash-angle distributions for the satellite for various orbital inclinations are presented. A computer program for calculating the solar-radiation-pressure-induced precession has been extended to include the effects of orbital regression and advance of perigee for orbital inclination values. An experiment for estimating the sensitivity to NO of a proposed balloon-borne system has been conducted and evaluated. A prototype sunseeker is described and evaluated. A theoretical and experimental investigation to determine the optimum tubing diameter and matching termination for good response of fluidic transmission lines as a function of line length is being carried out.

7. Semiconductor Physics.

Defects are introduced into semiconductors by high-energy radiation. These defects influence the electrical, optical, and thermal properties of these materials. The luminescence that results from recombination of free holes with electrons trapped at these defects is a particularly sensitive means of determining the location of the energy levels arising from these defects and the nature of the interaction of

the trapped charge with the lattice. The impurity band in highly-doped semiconductors has been investigated by studying the tunneling current between a superconductor, In, and the semiconductor, p-type Si. The results of these studies give information about the density of states of the impurity band and about the coupling of electrons to the K=0 optical phonon.

8. Computer.

Computer statistics are reported. The properties of the CRT display are presented together with photographs of display output. Programming systems are described, and a new research program applying computer graphics to structural analysis is discussed.

9. Plasma Display.

Further observations of gas-composition effects are summarized; results of a study of the use of phosphors to provide displays with several colors are described; preliminary work on the use of plasma cells in logical structure is presented; and the problems of providing starting particles for the initial discharge in a sequence are discussed.

10. Infrared Converter.

Work on the infrared-converter, thin-film display, has continued. The properties of light-emitting, tunnel-injection, CdS devices are given. Techniques for preparing films of semiconducting CdS, InSb, and insulating films are under development.

11. Information Sciences.

In the area of information retrieval, effort is continuing in establishing the data base, and theoretical investigations have been undertaken in clustering theory and file-organization techniques. The main effort, however, has concentrated on developing an interactive display system on the CDC 1604. New results have been obtained in coding theory, specifically as regards geometrical considerations on cyclic codes, decoding of BCH codes, and the general properties of linear residue codes. A study has been completed in row-column minimization of sequential machines and related problems, such as covering problems and identification of combinable classes. Several results have been obtained in the area of nonlinear filtering.

12. Networks.

Pseudocuts of a graph are being studied in the belief that they will lead to necessary and suffieicnt conditions such that a linear graph can be mapped onto a doughnut. In addition, new topological formulas have been derived for the analysis of electrical networks containing ideal transformers. In the area of nonlinear circuits it has been found that a linear, time-invariant, passive RC network, in which is embedded a nonlinear time-varying capacitor with finite, positive, incremental capacitance, is always bounded-input, bounded-output, stable. Also, the behavior of a system of coupled oscillators is being studied. Some results have been obtained in the case of weakly-coupled oscillators, and the case where the coupling is very strong is under investigation. Some

new frequency-domain criteria have been obtained for the stability of uniformly distributed networks.

13. Control Systems.

Investigation of parameter-variation effects (sensitivity) on control-system performance in continuing. Emphasis has been placed on the design of minimum-sensitivity systems, using several techniques including comparison sensitivity, sensitivity functions, and the theory of differential games. Several computer simulations have been made, and some numerical techniques for parameter optimization have been studied. An investigation of the connections between optimality and sensitivity is continuing.

14. Switching Systems.

Further progress is reported in methods for the selection and generation of diagnostic tests, and the modular decomposition of combinatorial logic. The relationship between flow graphs and the traveling-salesman problem has been further investigated, and the results of the study of applicability of An+B codes to an error-checking arithmetic unit have been extended. Work on the Computer Compiler has been intensified.

COORDINATED SCIENCE LABORATORY PERSONNEL

Faculty, Research Associates, and Research Engineers

Compton, W. D.
Director
Alpert, D.
Anderson, R. W.
Anner, G.
Ash, R. B.
Bitzer, D. L.
Bohmer, H.
Bouknight, W. J.
Brown, R. M.
Carroll, D. E.
Chien, R. T.
Cooper, D. H.
Cruz, J. B., Jr.
Culton, J. W.
Ettinger, S. Y.
Fenves, S. J.
Gooch, J.
Haddad, A. H.
Hicks, B. L.
Hohn, F.
Huggins, R. W.
Jackson, E. A.
Kirkwood, B. D.
Knoebel, H. W.
Kokotovic, P.
Krone, H. V.
Lee, D. A.
Lyman, E. M.
Lyman, E. R.
Mayeda, W.
Medanic, J.
Metze, G.
Peacock, R. N.
Perkins, W. R.
Preparata, F.
Propst, F. M.
Prothe, W. C.
Assistant to Director
Raether, M.
Ray, S.
Skaperdas, D.
Slottow, H. G.
Smith, S. T.
Steinrisser, F.
Stifle, J.
Trick, T. N.
Trogdon, R.
Tulumello, A.
Voth, B.
Wax, N.
Wolf, E. L.
Wu, Y.
Yen, S. M.

Research Assistants

Agashe, S.
Arndt, G.
Arora, B.
Bahl, L.
Biss, K.
Bleha, W. P., Jr.
Bollinger, L. D.
Bourquin, J.
Brachhausen, E.
Carr, W.
Chang, J.
Chen, C.
Chow, D.
Cooper, T.
Cummings, J.
Davidson, E.
Depp, S.
Edwards, D.
Eisenman, D.
Goede, W.
Hartmann, C.
Heller, J.
Herner, J.
Hong, S.
Hosken, R.
Hsu, J.
Isenhart, R.
Jacobs, J. T.
Johnson, E.
Johnson, H. R.
Johnson, R.
Jones, C.
Karr, G.
Kraybill, D.
Lie, T.
Mehta, N.
Metze, V.
Moore, J.
Myers, J. L., Jr.
Nishijima, M.
Ong, A.
Pinsky, H.
Reilly, B.
Reilly, O.
Robinson, J.
Salmon, D.
Sannuti, P.
Schmeichel, H.
Schmidt, H.
Schneider, R.
Seth, C.
Spry, R.
Stahl, F.
Stefanek, R.
Tibbetts, G.
Toida, S.
Tzeng, K.
Wolterbeek, H.

Fellows

Butler, D.
Gaddess, T.
Lipovski, G.
Powell, T.

Administrative Secretary

Schmidt, R.

Secretary

Rudicil, J.

Typists and Stenographers

Bensyl, C.
Curtis, J.
Dabelko, E.
Day, L.
Franek, J.
Haley, J.
Hanoka, N.
Lane, R.
Shaw, C.
Siler, J.
Smith, J.
Williams, D.

Chief Clerk

Drews, C.

Duplicating Machine Operator

Potter, R.

Chief Engineering Draftsman

MacFarlane, W.

Draftsmen

Conway, E.
Harmon, D.

Res. Lab. Shop Supervisor

Bandy, L.

Res. Engineering Asst.

Burr, J. G.

Laboratory Mechanics

Bales, K.
Beaulin, W.
Bouck, G.
Fults, R.
Merritt, K.
Zackery, R.

Stores Supervisor

Lofton, C.

Storekeepers

Jordan, F.
McElwain, W.

Glassblower

Lawrence, W.

Photographer

Gladin, R.

Electronics Engr. Assts.

Carter, E.
Gardner, O. E.
Hedges, L.
Neff, E.
Vassos, N.

Physical Sci. Staff Asst.

Thrasher, W.

Electronics Technicians

Casale, T.
Coad, D.
Crawford, G.
Deschene, D.
Holy, F.
Johnson, M.
Knoke, J.
Merrifield, F.
Moule, G.
Roberts, G.
Schmidt, W.
Streff, L.
Susedik, A.
Turpin, F.

Student Assistants

Arnold, C.
Baran, J.
Barkley, N.
Birtcher, R.
Bonanno, J.
Chew, R.
Corcoran, J.
Duchamp, T.
Everhart, G.
Hansen, J.
Hasz, K.
Hickok, L.
Hoffman, R.
Kelley, K.
Lamos, J.
Mindock, R.
Nanninga, J.
Nelson, H.
Nichols, W.
Reynolds, P.
Roberts, D.
Rudolphi, T.
Rundgren, W.
Shapiro, M.
Soto, R.
Tao, B.
Trombi, P.
Tucker, P.
Tummelson, J.
Veach, R.
Ward, W.
Woodall, J.

1. Journal Articles Published or Accepted

S. Barnett, C. Storey, J. B. Cruz, Jr., and W. R. Perkins, "Comment on 'On Invariance and Sensitivity,'" IEEE Trans. on Automatic Control, AC-12, 210-211 (April, 1967).

G. G. Dodd, "On Unistor Graphs," IEEE Trans. on Circuit Theory, CT-14, 154-159 (June, 1967).

A. H. Haddad, K. Yao, and J. B. Thomas, "General Methods for the Derivation of Sampling Theorems," IEEE Trans. on Information Theory, IT-13, 227-230 (April, 1967).

T. Kamae, "Notes on a Minimum Feedback Arc Set," IEEE Trans. on Circuit Theory, CT-14, 78-79 (March, 1967).

T. Kamae, "A Systematic Method of Finding All Directed Circuits and Enumerating All Directed Paths," IEEE Trans. on Circuit Theory, CT-14, 166-172 (June, 1967).

P. Kokotovic' and J. Heller, "Direct and Adjoint Equations for Parameter Optimization," to be published in IEEE Trans. on Automatic Control, AC-12, October, 1967.

S. C. Lee, "Non-Senes--Parallel Realization of Symmetrical and Bisymmetrical Two-Element-Kind Two Ports to Minimize Multiparameter Sensitivity," IEEE Trans. on Circuit Theory, CT-14, 159-166 (June, 1967).

W. Mayeda, "Graph-Theoretical Network Analysis Using New Equivalent Transformations," Journal of Electronic Communication (Japan), 50, 115-121 (July, 1967).

J. Medanic', "Bounds on the Performance Index and the Riccati Equation in Differential Games," to be published in IEEE Trans. on Automatic Control, AC-12, December, 1967.

F. P. Preparata, G. Metze, and R. T. Chien, "On the Connection Assignment Problem of Diagnosable Systems," to appear in the IEEE Trans. on Electronic Computers.

T. N. Trick and J. A. Resh, "Transducer Power Gains in Optimally Matched Networks," IEEE Trans. on Circuit Theory, CT-14, 105-107 (March, 1967).

N. Wax, "On Some Periodic Solutions of the Liénard Equation," IEEE Trans. on Circuit Theory, CT-13, 419-423 (December, 1966).

2. Meeting Papers

B. M. Arora, D. L. Bitzer, H. G. Slottow, and R. H. Willson, "The Plasma Display Panel--a New Device for Information Display and Storage," Proc. of the 8th Annual Conf. of the Soc. for Information Display, San Francisco, Calif., May, 1967.

H. Böhmer and M. Raether, "Observations of Enhanced Diffusion During a Beam-Plasma Instability," International Symposium on Fluctuations and Diffusion in Plasmas, Princeton University Plasma Physics Laboratory, June 26-30, 1967.

J. J. Bourquin and T. N. Trick, "Stability of Distributed R-C Networks," Tenth Midwest Symposium on Circuit Theory, pp. XII-2-1 to XII-2-11, May 18-19, 1967.

R. T. Chien, "Computer-based Information Retrieval Systems: A Status Report," Proc. of the 1st Princeton Conf. on Information Sciences and Systems, March, 1967, pp. 48-52.

R. T. Chien and F. P. Preparata, "Search Strategy and File Organization in Computerized in Information Retrieval Systems with Mass Memory," FID/IFIP 1967 Conf., Rome, Italy, June, 1967.

D. H. Cooper, "Distortion Mechanisms in Disc-Recording Playback," Midwest Acoustics Conf., Chicago, Ill., April, 1967.

A. H. Haddad, J. B. Thomas, and D. S. Kuykendall, "Series Approximations for Optimum ZNL Filters," IEEE International Conf. on Communication, p. 216, Minneapolis, Minn., June, 1967.

A. H. Haddad, "On a Nonlinear Feedback Filtering System," International Symposium on Information Theory, San Remo, Italy, September, 1967.

A. H. Haddad, "Optimum Filtering with a Class of Nonlinear Systems," The Fifth Annual Allerton Conference on Circuit and System Theory, October, 1967.

J. T. Jacobs, R. N. Peacock, and E. L. Wolf, "Size Effects in the Temperature Variation of Electrical Conductivity of Epitaxial Gold Films," the Gordon Conference on "Thin Films--Structure-Sensitive Properties," Tilton, New Hampshire, August, 1967.

W. R. Perkins, J. B. Cruz, Jr., and P. Kokotovic', "Parameter Sensitivity in Circuits and Systems," Conf. Record, Tenth Midwest Symposium on Circuit Theory, pp. VIII-4-1 to VIII-4-2, May 18-19, 1967.

F. P. Preparata and R. T. Chien, "On Clustering Techniques of Citation Graphs," Proc. of the First Annual Princeton Conf. on Information Sciences and Systems, March, 1967, pp. 53-56.

F. P. Preparata, "Binary Sequence Convolutional Mapping: The Channel Capacity of a Non-Feedback Decoding Scheme," International Symposium on Information Theory, San Remo, Italy, September, 1967.

3. Technical Reports

R-312 Control System Synthesis to Minimize Multiparameter Sensitivity, Richard L. Gonzales (August, 1966) UNCLASSIFIED.

R-317 Weight Distribution of Bose-Chaudhuri-Hocquenghem Codes, Tadao Kasami (August, 1966) UNCLASSIFIED. Thesis

R-343 Kinetic Theory of Radiometric Photophoresis in a Knudsen Gas, Yau Wu (March, 1967) UNCLASSIFIED.

R-344 A Superconducting Parametric Amplifier for the Measurement of Small d-c Voltages, Roger Reis (March, 1967) UNCLASSIFIED.

R-345 Binary Sequence Convolutional Mapping: The Channel Capacity of a Non-Feedback Decoding Scheme, Franco P. Preparata (March, 1967) UNCLASSIFIED.

R-346 The Plasma Display Panel--A New Device for Information Display and Storage, B. M. Arora, D. L. Bitzer, H. G. Slottow, and R. H. Willson (April, 1967) UNCLASSIFIED.

R-347 Numerical Studies of Strong Shock Waves Part VIII: Properties of a Shock Wave for a Mach Number of 2.5, B. L. Hicks and M. A. Smith (April, 1967) UNCLASSIFIED.

R-348 Numerical Studies of Strong Shock Waves Part IX: Error Analysis for a Mach Number of 2.5, B. L. Hicks and M. A. Smith (April, 1967) UNCLASSIFIED.

R-349 On Clustering Techniques of Citation Graphs, F. P. Preparata and R. T. Chien (May, 1967) UNCLASSIFIED.

R-350 Initial Behavior of the Pseudo Shock, S. M. Yen and B. L. Hicks (May, 1967) UNCLASSIFIED.

R-351 Necessary Conditions for Transformerless Realization of One-Terminal Pair RLC with One Resistor, Abelardo Cases Sabino (May, 1967) UNCLASSIFIED.

R-352 Incoherent Scattering of Microwaves from Enhanced Density Fluctuations in a DC-Discharge, Wayne E. Carr (May, 1967) UNCLASSIFIED.

R-353 Sensitivity Reduction Using Optimally Derived Controllers, James P. Herner (May, 1967) UNCLASSIFIED.

R-354 A Procedure for Ranking Diagnostic Test Inputs, Theo J. Powell (May, 1967) UNCLASSIFIED.

R-355 Compatibility and Row-Column Minimization of Sequential Machines, Gerald J. Lipovski (May, 1967) UNCLASSIFIED.

R-356 Some Generalizations in System Theory and Their Applications to Control Systems, Sadanamd D. Agashe (May, 1967) UNCLASSIFIED.

R-357 A Cathode Ray Tube Display, Jack Stifle (June, 1967) UNCLASSIFIED.

R-358 Minimax Controller Design, David Salmon (July, 1967) UNCLASSIFIED.

R-359 Communication Networks with Specified Survivability, David E. Butler (July, 1967) UNCLASSIFIED.

R-361 Teaching the use of the Library to Undergraduates: An Experimental Comparison of Computer-Based Instruction and the Conventional Lecture Method, Marina E. Axeen (August, 1967) UNCLASSIFIED.

R-362 An Improved Method of Finding all Largest Combinable Classes, Gerald J. Lipovski (August, 1967) UNCLASSIFIED.

R-363 Application of the Auger Process to the Study of Gaseous Adsorption on Tungsten, Gary Tibbetts (August, 1967) UNCLASSIFIED.

R-364 Size Effects in the Temperature Variation of Electrical Conductivity of Epitaxial Gold Films, J. T. Jacobs (August, 1967) UNCLASSIFIED.

R-365 Simplified Switching Functions for Time-Optimal Control Systems, Harry Schmeichel (August, 1967) UNCLASSIFIED.

R-367 An Improved Polarity Coincidence Detector, W. E. Carr, M. Raether and R. Trogdon (September, 1967) UNCLASSIFIED.

Page

(OVERLEAF BLANK)

F. M. Propst
F. Steinrisser
T. L. Cooper
D. Edwards
N. Nishijima
G. G. Tibbetts

1.1. Electron Spectrometry on Solid Surfaces.

In a recent publication,[1] we reported measurements of the vibration frequencies of H_2, N_2, CO, and H_2O on 100 tungsten. These measurements were interpreted to indicate that at low coverage H_2, N_2, and CO are dissociatively adsorbed and multiply bonded and that H_2O dissociates to produce the adsorption of atomic oxygen which is also multiply bonded. Since this publication, we have calculated the vibration frequencies and the desorption energies of H, N, O, and C for the model shown in Fig. 1.1. The detailed results of these calculations will be reported later. The qualitative results are that

1. The model gives the vibration frequencies and binding energies measured for these atoms.
2. The values of the parameters required to give the experimental quantities are quite physically reasonable.
3. There is internal consistency in the values of the parameters for the four atomic species.

We feel that, although the model is very simple and certainly not an absolute description of the physical system, it does give substantiation to our interpretations. Further, it gives promise that quantitative information can be obtained concerning the atomic structure of adsorption systems through the analysis of the experimental results of electron spectrometry.

---

[1] F. M. Propst and T. C. Piper, J. Vac. Sci. and Tech. 4, 53-56 (1967).

(OVERLEAF BLANK)

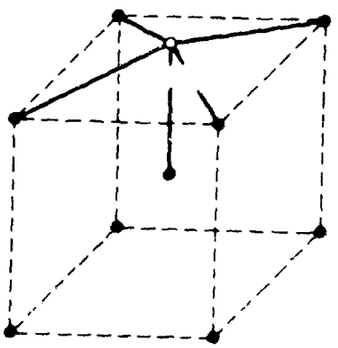

● W Atom o Absorbed Atom

$$V = V_0 \sum_{i=1}^{5} (1 - e^{-\beta(R_i - R_0)})^2$$

Fig. 1.1. Model used for the calculation of the vibration frequencies and binding energies of H, N, C, and O on 100 tungsten.

(OVERLEAF BLANK)

Preliminary measurements on polycrystalline tungsten and platinum indicate that atomic adsorption does not produce well-defined vibrations like those observed in the case of the single crystal. This is very likely associated with the intrinsic heterogeneity of the polycrystalline surfaces. Molecular adsorption on the polycrystalline surfaces gives rise to vibrational structure very similar to that observed in the case of the single-crystal surface. This is a reasonable result since molecular adsorption implies a relatively weak perturbation of the molecule.

One deficiency in the measurements made to date is that the target temperature is not controlled. Due to the heat of the cathode, the target temperature has been about 80°C. We have begun making modifications to allow temperature control over a wide temperature range starting at about 100°K. This will be accomplished by circulating liquid nitrogen through thin-walled tubes in intimate contact with the target holder. In addition to the lack of temperature control, we have found difficulties due to contamination. We have also seen indications that the high-energy-electron bombardment of the surface of the sample (to raise the temperature for cleaning) gives rise to a stabilization of the surface contaminants. To correct these difficulties, the target in the revised configuration will be heated by electron bombardment from the side opposite that which is under measurement. In addition, a sputter-ion pump is being substituted for the oil-diffusion pump.

1.2. Adsorption of Gases on Metal Surfaces†.

Measurements of the adsorption and desorption of N_2, CO, and H_2 on polycrystalline, 110, 111 tungsten have been made utilizing the Auger electron-emission technique described in previous Progress Reports. These measurements indicate various types of adsorption states having, in general, complex desorption characteristics. Detailed description and discussion of these results are given in the CSL Technical Report, R-363.

1.3. Study of the Energy-Angular Distributions of Secondary Electrons.

1.3.1. Target Clamp.

The electron-bombardment-heater modifications outlined in the previous Progress Report[2] have been completed. With the modifications, temperatures up to 2600°K were obtained with no difficulty. This is well above the temperature required for cleaning the targets to be used in the angular-distribution measurement. The power required to heat the target was within a few percent of power requirements calculated on the basis of the tables in Langmuir.[3]

A second target assembly using bombardment heating was constructed for another experiment. The target in this system was circular and in intimate contact with the end of a thin-walled tungsten cylinder. The filament was mounted inside the cylinder as close to the target as

---

†Supported in part by the National Aeronautics and Space Administration under Grant NsG-376.

[2]Progress Report for Sept. 1966-Feb. 1967, Coordinated Science Laboratory, University of Illinois.

[3]The Collected Works of Irving Langmuir, Vol. 2, pp. 282-283.

possible. By putting a plate with a negative voltage with respect to the filament across the open end of the cylinder, the bombardment electrons can be contained within the cylinder, thus allowing scattering measurements to be made on the target surface while it is heated by bombardment from the opposite surface. The target and cylinder assembly were heated to well above 2600°K with a power requirement very near that calculated. No noticeable temperature gradient existed across the target.

1.3.2. Electron Gun and Collector.

In the previous Progress Report,[2] some preliminary results from the electron gun and collector test system were reported. All the results are essentially correct but one. The rise in the collector current before cutoff[4] has not been eliminated or reduced sufficiently.

The spatial spot size[5] was measured, and is about 0.040 in. for beam energies from 100eV to about 20eV. Below 20eV the spot begins to broaden and increases to about 0.150 in. at 10eV. For energies less than 10eV the beam current is estimated to be too low for angular distribution measurements. The spot size and beam current (5×10^{-6} amperes at 100eV to about 10^{-7} amperes at 10eV) are both good enough for the anticipated measurements, but both could probably be improved by the elimination of stray 60-Hz magnetic fields that are now present in the system. Circuit modifications have already been made to reduce the capacitive 60-Hz noise to an acceptable level.

---

[4] Progress Report for March-August 1966, Coordinated Science Laboratory, University of Illinois, pp. 27-37.

[5] Full width at half maximum.

A typical energy distribution measured for a 100eV beam is shown in Fig. 1.2. The energy distribution for such a system should be a single, narrow (less than about a volt), spike at 100 volts. There are, then, three immediately apparent problems:

1. The structure of the peak;
2. The broadness of the peak;
3. The strong negative derivative effect.[6]

Further measurements were made with this system to attempt to understand these problems. Although many measurements were made and many parameters varied, only three definite results were obtained:

1. The structure is not associated with the electron gun;
2. The structure is not associated with the detection electronics;
3. The negative derivative effect is caused by the grid deflection mechanism described previously.[4]

Measurements were made on a second similar system which was constructed for testing an electron gun for another experiment. This system is illustrated in Fig. 1.3, and differs from the first in the following ways:

1. The collector is a conducting phosphor, which allows a visual observation of the beam;
2. A square mesh is used for the grid;
3. The geometrical transparency of the grid is less than 80%;

---

[6]"The Negative-Derivative Effect," refers to the effect described in Ref. 4, pp. 27-37, by the phrase "The rise in collector current immediately preceding cutoff."

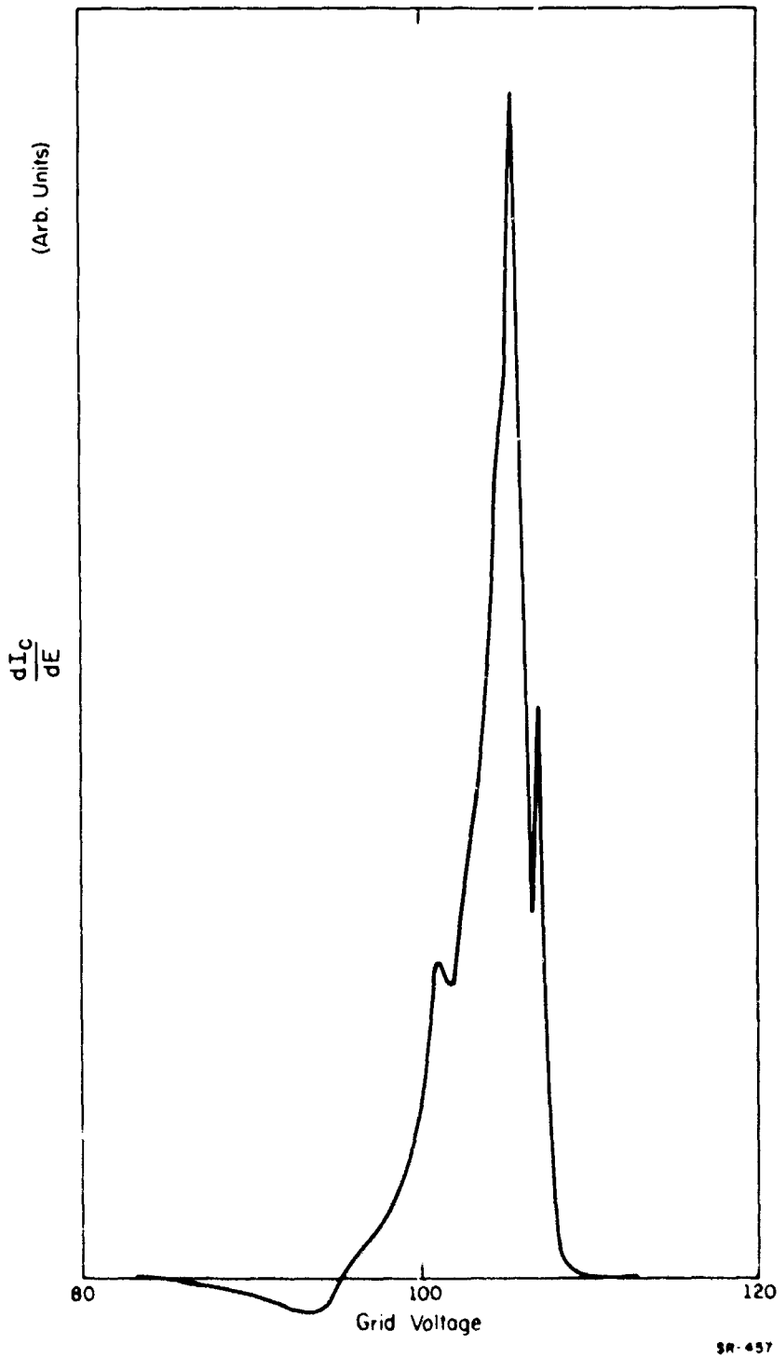

Fig. 1.2. Typical energy distribution for 100eV electron beam.

(OVERLEAF BLANK)

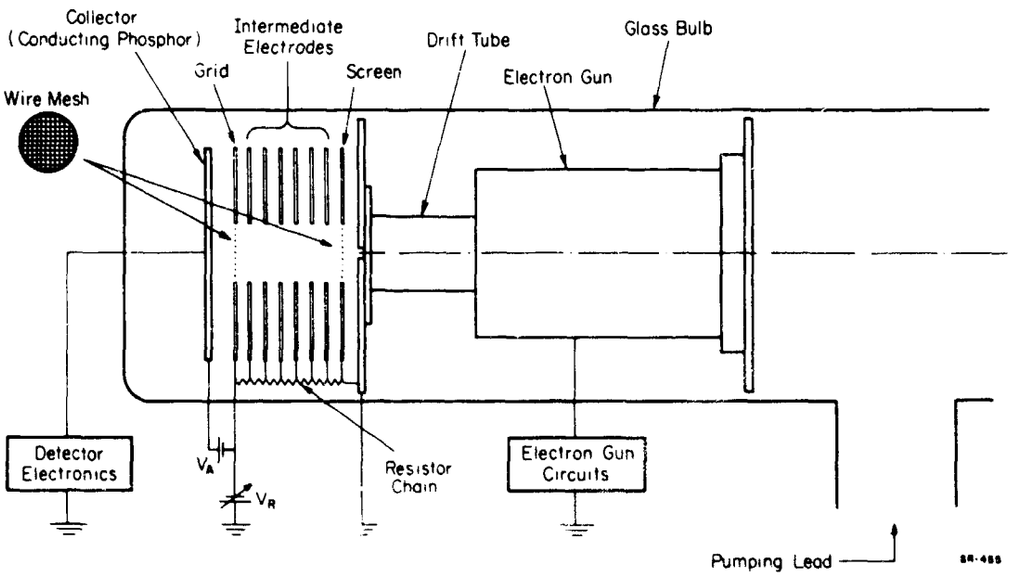

Fig. 1.3. Electron gun--analyzer system.

(OVERLEAF BLANK)

4. The ratios of grid wire spacing to retarding electrode spacing (i.e., screen to grid and grid to collector spacing) are much smaller than those of the first system. By decreasing these ratios it was felt that better resolution could be obtained. Because of the square mesh, however, a quantitative comparison of these ratios is not possible.

The use of the intermediate electrodes connected by resistors allows the grid-wire spacing to retarding-electrode spacing ratio to be made small without making the total size of the grid large compared to the retarding-electrode spacing. Experiments are now underway on this system with the intermediate electrodes replaced by a glass tube coated with tin oxide. This technique should allow the construction of an analyzer with small ratios of grid-wire spacing to retarding-electrode spacing without making the analyzer so large that it is of limited practical use.

The energy distribution of a 100eV beam in this system is a narrow (less than about 1 volt), spike with a tolerable negative-derivative effect. By applying either 60-Hz capacitive noise to the electrodes, or 60-Hz magnetic fields sufficiently strong to deflect the beam, a small amount of structure (one or two extra peaks) and broadening could be induced.

As was previously reported,[2] the resolution of the analyzer in the first system is about 10%. The ratios of grid-wire spacing to retarding-electrode spacing are about 1/4. On the basis of the measurements described above, it was decided to attempt to increase these ratios to about 1/40 in order to obtain a resolution of about 1%.

The screen-to-grid and grid-to-collector spacings are both equal to 0.125 in. Thus the grid wire spacing would have to be about 0.003 in. In order to retain a high transparency (more than about 90%), the wire diameter chosen was 0.0003 in. The technique used to make the grids will be described in the following section. At the time this report is being written, new grids have not been installed in the system.

In the previous two Progress Reports, references have been made to calculations done with regard to the retarding analyzer. These were numerical calculations of trajectories of particles traveling through the analyzer, and, although they yielded some useful results, they were considered too time consuming to pursue further. While doing these calculations, however, it appeared that a reasonably quantitative theoretical model[7] of the analyzer could be obtained through calculations involving only the potential distribution of the grid system and some simple dynamic assumptions. Although the validity of these calculations has not been tested experimentally, they did, at least indirectly, suggest a hypothesis to explain the structured peaks (Fig. 1.2). The final cutoff voltage (that grid voltage for which all electrons of a specific energy are incapable of reaching the collector electrode) becomes more sensitive to errors in the grid-wire spacing as the ratio of grid-wire spacing to retarding-electrode spacing increases. If the beam spot size is large enough for the beam to pass through a large area of the grid, or if capacitive 60-Hz noise is large enough to cause the beam to become defocused, thus enlarging the spot size, or if 60-Hz magnetic fields are

[7]The model is not quite complete and will be reported in detail at a later date.

present which are sufficiently large to deflect the beam over a large area of the grid, errors in grid-wire spacing could produce structure. This structure would probably be amplified by the negative-derivative effect.

The wire mesh in the system shown in Fig. 1.3 was examined, and errors up to 50% in wire spacing were found. It was already known that the error in the grid-wire spacing for the collector in the other test system was about 20%, but when the grid and screen were removed it was found that they had been damaged and that errors in wire spacing existed as high as 70%.

1.3.3. The Grid Winder.

The grids consist of a set of equally-spaced wires fastened to a grid plate. Figure 1.4 shows a grid plate, winding spindle, and clamps. The wire (0.0003 in. diameter tungsten) is wound around the spindle with the desired spacing, and fastened to the grid plate by brazing or some other appropriate method. The wires are then cut along the edges of the grid plate and the finished grid removed. The spring-loaded clamps are used to hold down the grid plate, the starting end of the wire, and the finishing end of the wire. The grid plates are 1/2-in. square, and 0.004 in. to 0.008 in. thick, platinum, molybdenum, or tungsten, with 1/4 in. holes in the center.

The winding device, with the spindle mounted, is illustrated in Fig. 1.5. A motor turns the spindle and, through a train of spur gears, a lead screw. The lead screw drives the spindle carriage along the

(OVERLEAF BLANK)

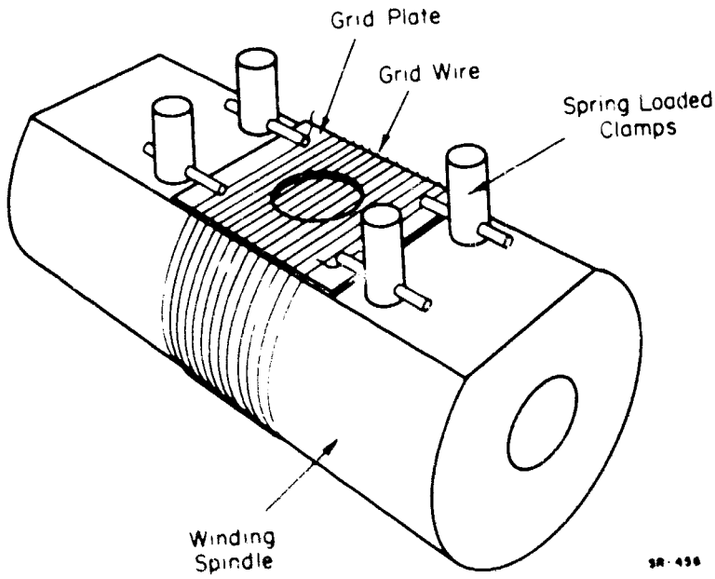

Fig. 1.4. Spindle and grid assembly.

(OVERLEAF BLANK)

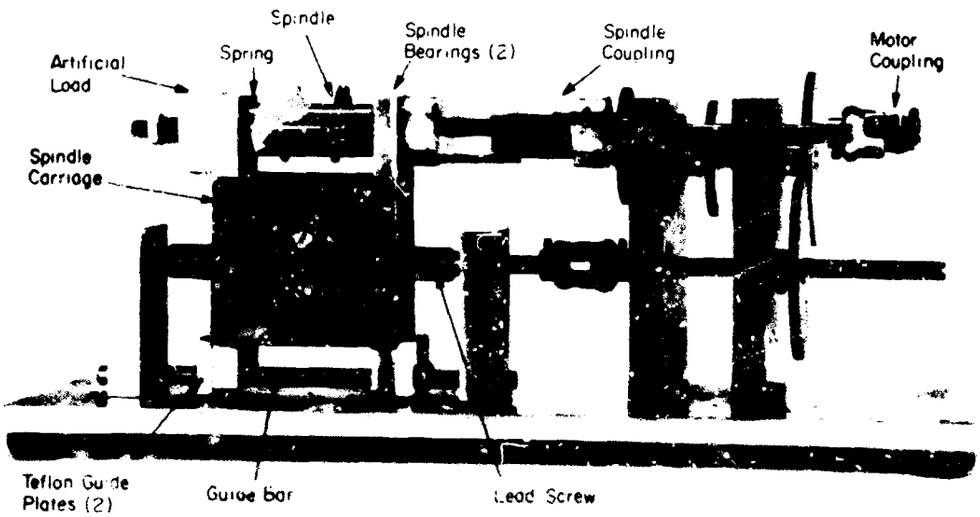

Fig. 1.5. Winding device (second teflon guide not shown).

(OVERLEAF BLANK)

carriage guide bar. The spindle coupling allows the spindle to be rotated while simultaneously translating along its axis of rotation. By selecting the proper gear ratios and lead-screw pitch, the desired wire spacing can be obtained.

Figure 1.5 illustrates the wire-handling mechanism. The wire comes off the spool and passes over the first teflon guide. Between the spool and first guide a weight is hooked to the wire. The weight applies tension to the wire. It is insufficient, however, to cause the wire spool and spool crank to turn. Enough tension must be applied to insure a uniform grid. Too much tension will, of course, cause frequent wire breakage during the winding process. (Too little tension can allow the wire to snag on the spool while it is being unwound. As the wire pulls free the weight drops, and the high acceleration at the end of the drop can cause the wire to break.)

As the winder uses wire, the weight rises. When more wire is needed, it is supplied by turning the spool crank by hand. In this manner the tension is kept nearly constant throughout the winding process.

After passing over the first guide, the wire passes through the second teflon guide which places it on the spindle. The tension on the wire causes it to cut its own groove in the teflon guide, thus almost completely eliminating any error due to a large guide groove. It is important that the second guide be kept as close as possible to the spindle.

In order to wind grids with 0.003 in. spacing with $\pm$ 10% error, the absolute error is $\pm$ .0003 in. This requires that the device be a

(OVERLEAF BLANK)

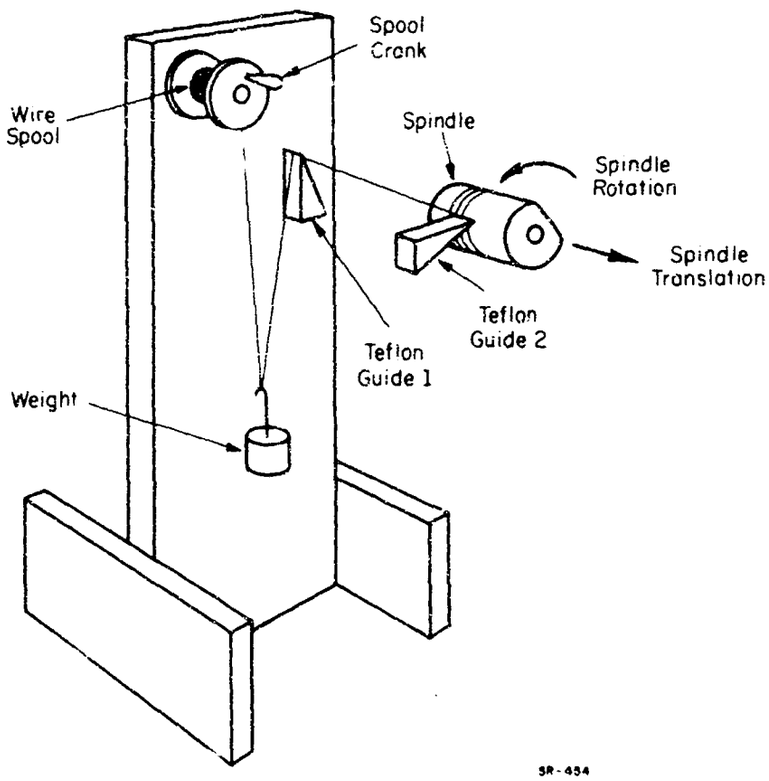

Fig. 1.6. Wire handling and tension mechanism.

(OVERLEAF BLANK)

precision machine. It is absolutely necessary that the lead screw be stra straight and accurate. Commercial screw stock is not good enough. The guide bar is centerless-ground, 1/4-in. diameter stainless steel. It moves through holes in 1/4-in. thick teflon plates fastened to each end of the spindle carriage. The fit between the teflon holes and guide bar is is almost a light press. A spring has been inserted between the one end of the spindle and the spindle bearing in order to eliminate spindle end play. The entire spindle must be artificially loaded in order to take out backlash in the gear train and spindle coupling.

As a matter of practice the motor, winder, wire handling device, and the microscope used for observing the winding process (the wires are only visible to the naked eye under certain lighting conditions) are all mounted on the rigid but separate tables. The finishes on the spindle and grid-plate surfaces and edges are always kept very smooth and clean. Grids have been wound with errors of $\pm$ 0.0003 in. using motor speeds as high as 6 rpm.

Three methods of fastening have been either successfu' or shown promise of being successful. A copper-plating method similar to that described by Bassett and Robertson[8] has been used successfully, although it is a bit messy and the copper-coated platinum plates cannot be spot welded into the analyzer. It is also feared that oxides formed on the plate may give charging problems. The wires can be clamped into the analyzer, and it is hoped that a coating of platinum bright can be applied to cover the oxides. Very strong wire bonds can be formed by this

[8] Basset and Robertson, J. Sci. Instr., 36, 321 (1959).

technique even though copper does not adhere well to the tungsten wires. As the copper begins to plate at high-current-density region around the wires, small points (dendrites) are formed. The high current density in the dendrites causes them to melt, forming small droplets of copper which make a joint considerably stronger than the wire. The spindle used for this method is made from teflon or nylon epoxy. Wire tension for this process is important. If the wires are not sufficiently taut, surface tension of liquid caught between wires due to capillary action can move the wires and change the spacing.

Spot welding the wires in a platinum-foil sandwich also shows great promise. The problems of electrode sticking and making a reliable weld can probably be overcome by the use of a molybednum grid plate instead of a platinum grid plate. The spindle used for this method is made from copper since it is one of the spot welding electrodes.

Hydrogen-furnace brazing is also being attempted. With this process, only materials capable of withstanding the high temperature (about 1000^{o}C) may be used. Further, care must be exercised in choosing materials with the proper expansion coefficients. Enough braze must be used to insure that all the wires are fastened to the grid plate, without braze flowing onto the wires over the hole and fastening them together. Even with these problems, this method looks to be quite promising.

1.4. Study of Ion Ejection by Electron Bombardment.

1.4.1. Introduction.

During the past few years, extensive researches have been carried out to study the interaction of "atomic" particles (electrons,

ions, neutral atoms and molecules, and photons) with solid surfaces. However, very little work has been done on the mechanism of the emission of ions from surfaces by incident electrons. Only recent investigations by R. Gomer[9] and P. A. Redhead[10] have given a partially quantitative explanation of the process. Detailed study of this process can provide:

1. Information on the interaction potential of "atomic" particles with solid surfaces;
2. An advanced technique for the study of adsorption-desorption phenomena;
3. Information for practical application to the design and understanding of the operation of ultrahigh vacuum devices.

The experimental quantities of interest are the species, yield, and energy distribution of ejected ions as a function of coverage and temperature of the surface and the energy of the bombarding electrons.

We have designed a spectrometer for the measurement of ion energy distributions. The instrument has been designed to incorporate the following:

1. High resulution,
2. High sensitivity,
3. Reduced X ray interference,
4. The capability of identifying ion species.

By a suitable choice of the parameters of the instrument, energy resolution of 1% or better can be achieved; an electron multiplier will be used

---

[9] R. Gomer, J. Chem. Phys. 41, 3311 (1964).

[10] P. A. Redhead, Can. J. Phys. 42, 886 (1964).

to increase the sensitivity; X ray interference will be reduced, since there is no direct path between the electron-bombardment region and the collector; and the mass of an ion can be determined by the time of flight method.

1.4.2. Brief Description of the Ion Ejection Process.[10]

Figure 1.7 is a schematic potential-energy diagram of an oxygen atom O and an oxygen ion O^+ near a molybdenum surface. Electrom bombardment can produce transitions, such that the kinetic energy E_k of the ion after escape is greater than zero, in the region where the value of the potential energy of the $O^+ + M_o + e$ system is greater than the value when the oxygen ion is at infinite distance from the surface, and where the wave function of the oxygen atom in the ground state has finite value. If all the ions escape from the surface, the shape of the observed ion-energy distribution is determined by the reflection of the probability density distribution of the atom in the ground state through the potential-energy curve of the ion. This reflection method is illustrated in Fig. 1.8.

It is known that all transitions to the ionic state do not produce free ions, but that there is a high probability that an ion will be neutralized by an Auger process before the ion can escape from the surface. Thus the ion-energy distribution is determined by the wave function of the atom in the ground state, the interaction potential for the ion, and the neutralization probability of the ion. Analysis of the experimental data can give information about each of these quantities.

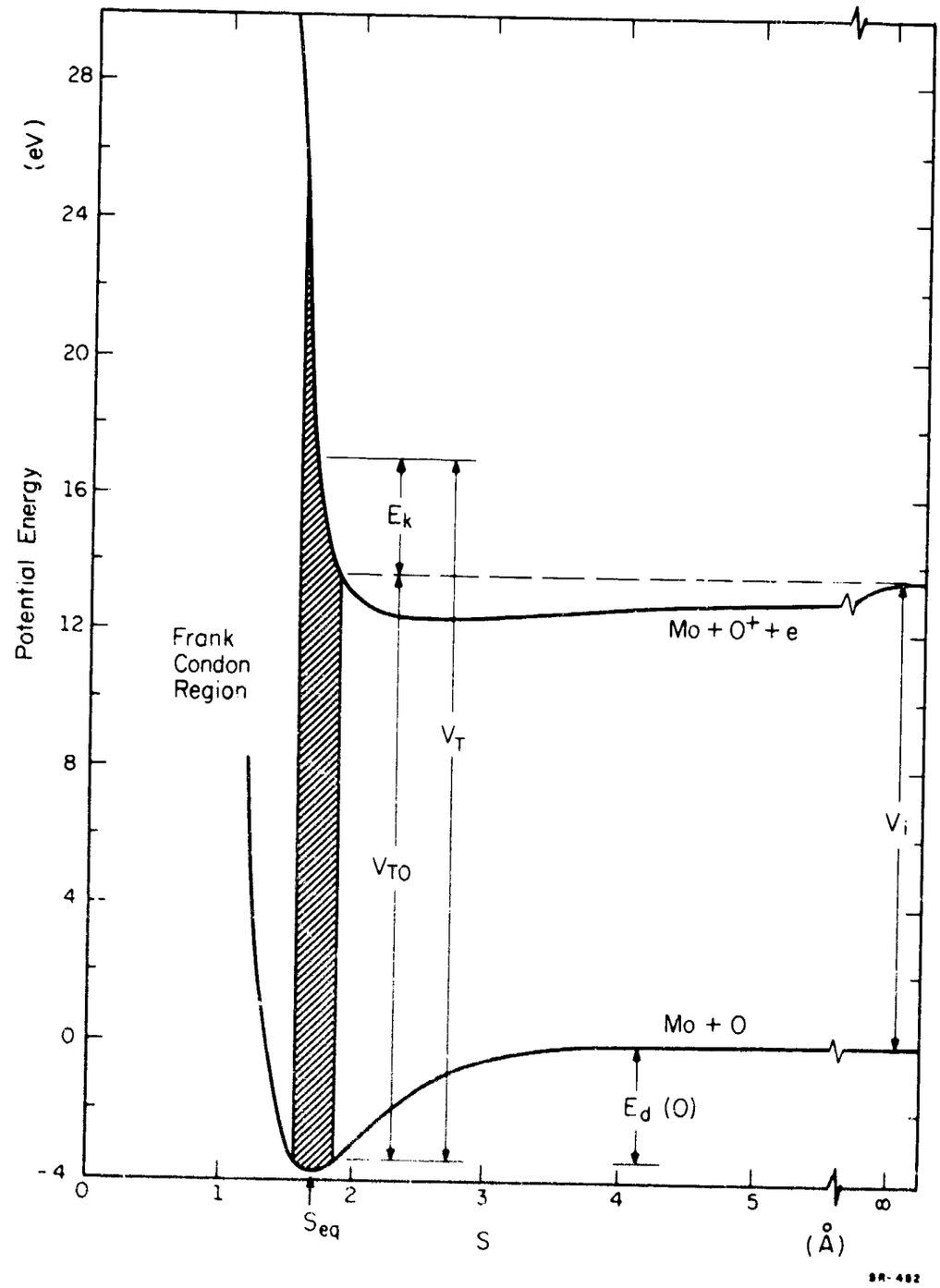

Fig. 1.7. Schematic potential energy diagram for oxygen atom and oxygen ion near a molybdenum surface.

(OVERLEAF BLANK)

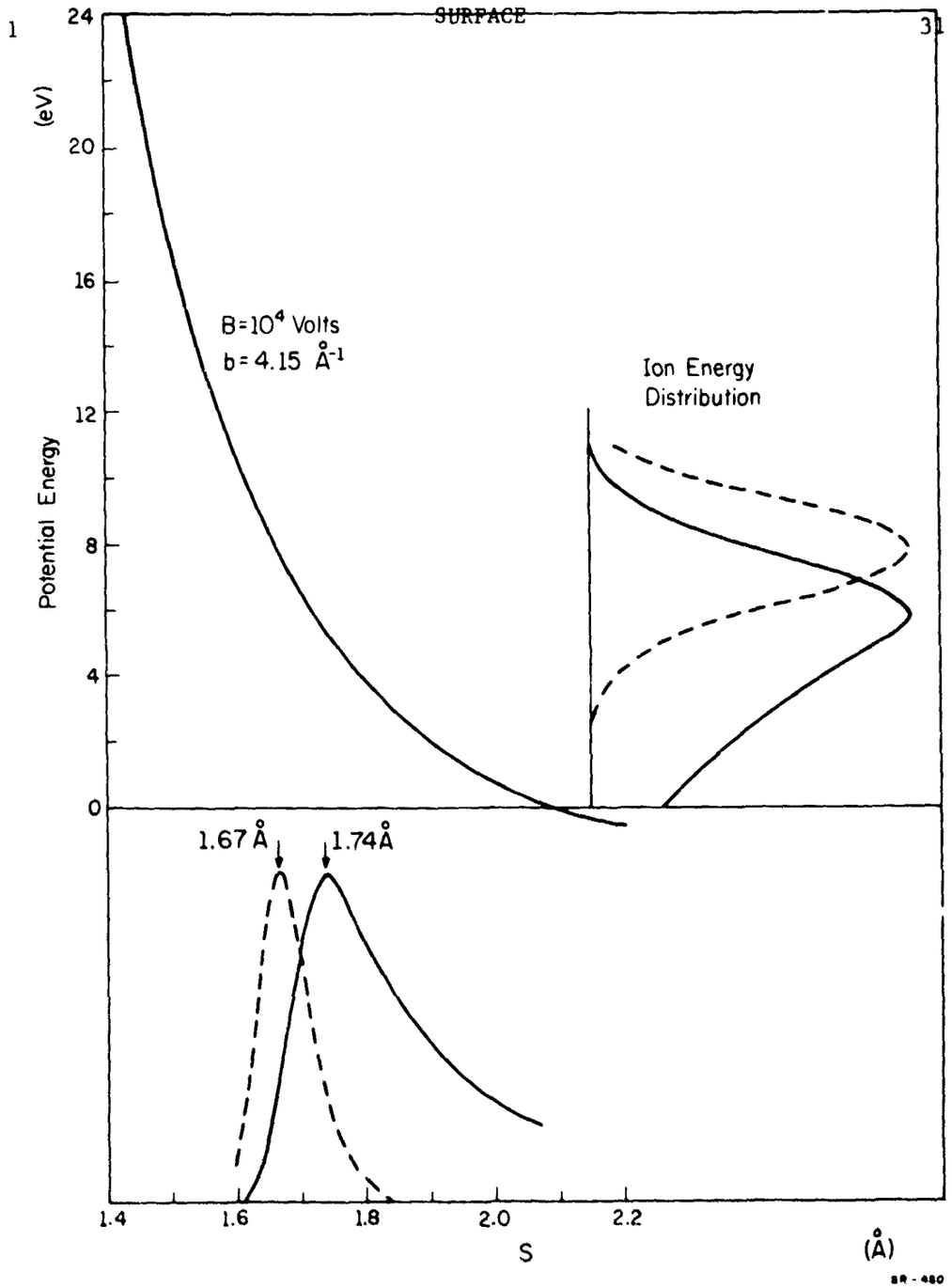

Fig. 1.8. Schematic illustrating the reflection of the probability density distribution through the ion potential energy curve to obtain ion energy distribution.

(OVERLEAF BLANK)

1.4.3. Design of the Apparatus.

The instrument designed for this work (Fig. 1.9) is essentially a small beta-ray spectrometer of the axially-symmetric type. The apparatus, which is housed in an ultrahigh-vacuum system, incorporates an electron gun, a target, angle-resolving apertures, energy-resolving apertures, an electrostatic-lens system, and an electron multiplier (collector). The electron gun delivering primary electrons is placed along the axis of the apparatus. Ions produced at the target follow helical trajectories in the axial magnetic field applied by a solenoid. Only those ions in a particular range of angle and energy pass through the apertures are focused onto an electron multiplier.

The optimum positions of apertures, and the optimum diameter of the electron beam for a given energy resolution are determined on the basis of the theoretical work of J. W. M. DuMond.[11]

Consider a uniform magnetic field B, parallel to the x axis (Fig. 1.10). Suppose a point source is situated on the x axis at x=o, from which ions of homogeneous kinetic energy E emanate with equal probability in all directions. The trajectory of an ion is a helix, whose radial component (projection) is

$$r = \lambda \sin\theta \sin(x/\lambda\cos\theta),$$

in which the length parameter is

$$\lambda = (2/eB)\sqrt{(2mE)},$$

and e is the ionic charge, m is the ionic mass, θ is the take-off angle, and B is the magnetic field.

[11] J. W. M. DuMond, Ann. Phys. 2, 283 (1957).

(OVERLEAF BLANK)

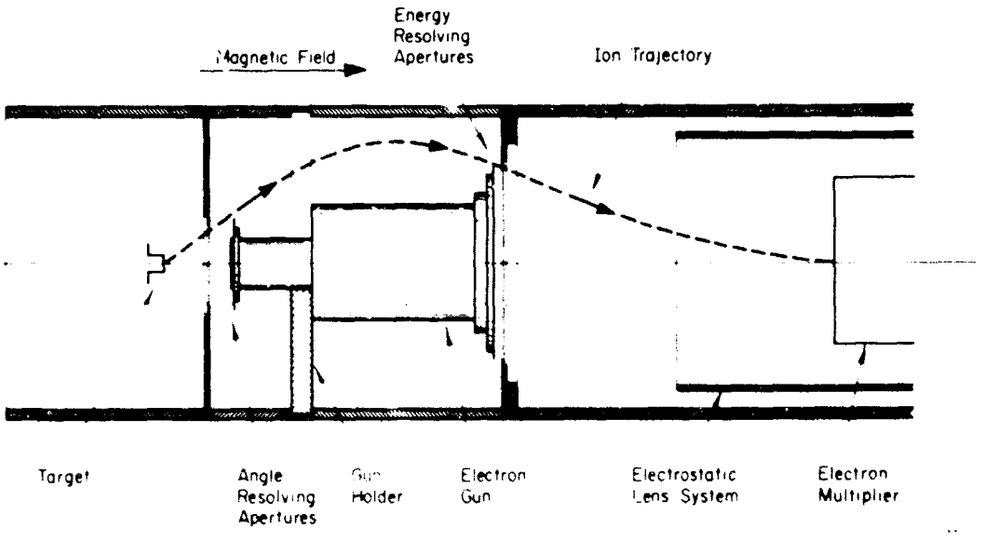

Fig. 1.9. Longitudinal magnetic field spectrometer.

(OVERLEAF BLANK)

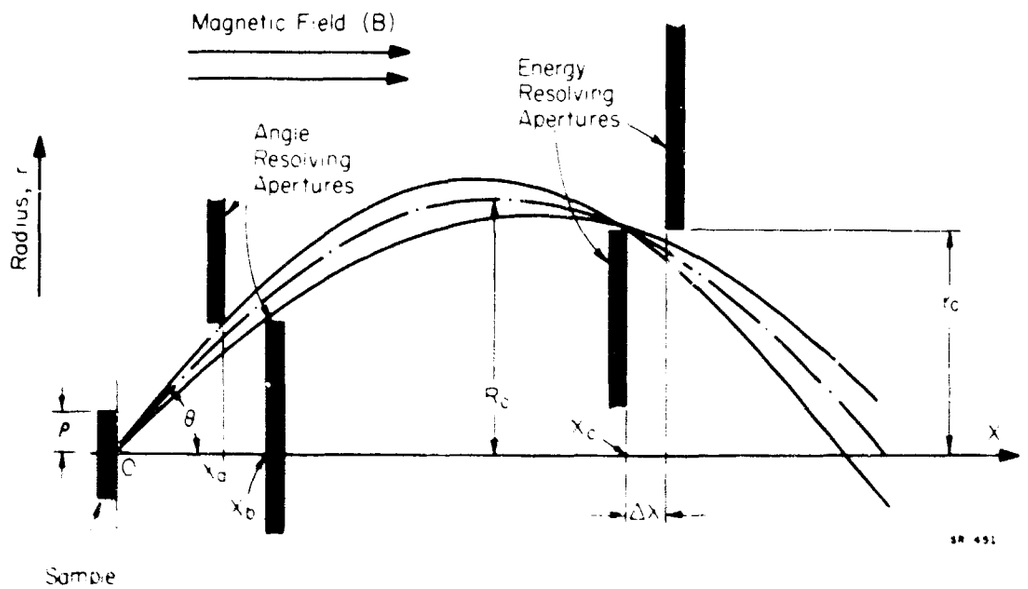

Fig. 1.10. Schematic longitudinal magnetic field spec rometer showing ion trajectory and the pertinent design parameters.

(OVERLEAF BLANK)

The optimum position of the energy resolving apertures is determined by

$$\partial r/\partial\theta|_{B,E} = 0,$$

in which the projections having emission angle between $\theta_c-\Delta\theta$ and $\theta_c+\Delta\theta$ cross each other forming a ring-shaped image. The position of this image is given by

$$X_c = R_c\cdot\Psi\cot\theta_c$$

$$r_c = R_c\cdot\sin\Psi$$

where Ψ is related to θ_c by $\tan^2\theta_c = -(1/\Psi)\tan\Psi$, and $R_c = \lambda\sin\theta_c$.

Line-broadening effects originate from three independent influences: (1) the use of a finite range of take off angle $\theta_c-\Delta\theta<\theta<\theta_c+\Delta\theta$), (2) the finite width of the energy resolving apertures, and (3) the finite radius ρ of the source disk. The optimum conditions which minimize the line broadening while maximizing the transmission rate is given by

$$\Delta\theta = [\Delta E/E)/0.81f(\theta_c]^{1/2}/\sin\theta_c,$$

$$\Delta X = (\Delta E/E)(R_c\Psi/1.62\ \sin2\theta_c),$$

$$\rho = (\Delta E/E)(R_c\sin\Psi/3.24\ \sin^2\theta_c),$$

in which $f(\theta_c) = 6+\cot^2\theta_c+2\Psi^2\tan^2\theta_c$. Table I gives the values of $\Delta\theta$, ΔX, ρ, X_a, X_b, X_c, and r_c for various values of the energy resolution $\Delta E/E$ at the central angle $\theta_c = 38^\circ$.

Table I. Optimum Condition ($\theta_c = 38^o$)

$\Delta E/E$	$\Delta\theta$ (degree)	Δx (inch)	ρ (inch)	x_a (inch)	x_b (inch)	x_c (inch)	r_c (inch)
0.01	2.21641	0.02063	0.00960	0.60307	0.80445	4.15432	1.17709
0.02	3.13448	0.04125	0.01920	0.58343	0.83346	4.15432	1.17709
0.03	3.83893	0.06188	0.02880	0.56886	0.85673	4.15432	1.17709
0.04	4.43282	0.08251	0.03840	0.55690	0.87709	4.15432	1.17709

Deleterious effects due to any asymmetry of the system (stray electric or magnetic fields), scattering of ions, and X ray interference have to be minimized. This will be accomplished by:

1. Shielding all leads from the ion-trajectory region,
2. Using a modulation for the cathode-heating current and making measurements while the heater current is off,
3. Using a Helmholtz coil to cancel the earth's magnetic field,
4. Thinning the edges of the apertures which are close to the ion trajectory,
5. Eliminating contact-potential differences by biasing the target.

Apertures prevent the X rays produced at the target by electron bombardment from reaching the collector.

We shall discuss the present state of our experiment components below.

1.4.3.1. Vacuum System.

The stainless steel, breakable, ultrahigh-vacuum system has been purchased. The system includes a 400-liter-per-second sputter-ion pump and a titanium-sublimation pump. It has been found that a total pressure of 4.7×10^{-11} Torr can be achieved in 21 hours. This vacuum system is sufficient for our purpose.

1.4.3.2. Solenoid.

The solenoid has been constructed by Ogallala Electronics Mfg., Inc. All materials are nonmagnetic. The case is made of stainless steel and hermetically sealed for ultrahigh-vacuum application. The maximum magnetic field obtainable is 1000 gauss, and the field is designed to be

homogeneous within ±3% in the ion trajectory region. The field is designed to decay as rapidly as possible outside the region of homogeneity. The solenoid is cooled by liquid nitrogen.

1.4.3.3. Electron Gun.

An electron gun similar to the one described in a previous Progress Report[12] has been constructed. The electrodes are made of 304 stainless steel and have been hydrogen fired and vacuum fired to reduce the residual magnetization to the order of a milligauss. Electrodes are separated from each other by ceramic disks for insulation and alignment. A low-temperature oxide cathode is used. The dimensions of the heater is 0.1875 in. by 0.02 in. by 0.002 in. Tests indicate that the gun has a capacity of delivering a current of a few microamperes with a spot size of less than 1/16 in. diameter over an energy range from about 30eV to 500 eV. Satisfactory operation of the gun is achieved in the presence of large, axial, magnetic field. Details of these measurements will be reported in the next Progress Report.

1.4.3.4. Target Assembly.

The target assembly consists of a target, a liquid-nitrogen reservoir for cooling the target, and an electron gun to heat the target by electron bombardment. The design of every part has been studied in detail. This and the way to control the temperature of a target will be described later.

---

[12] Progress Report for March-August, 1966, Coordinated Science Laboratory, University of Illinois.

In summary, the vacuum system has been tested, the solenoid has been constructed, the electron gun has been made and tested, and the final design of the target assembly will be completed soon. The detection problem, i.e., the most efficient method of focusing ions exiting from the spectometer into an electron multiplier, will be considered next.

1.5. Photon Emission from Solid Surfaces Under Low Energy Ion Bombardment.

1.5.1. Discussion.

The experiment was continued from the previous period. A new diffusion-pumped system was built to allow experiments with helium ions. Previously, argon gas was used and pumped with a high-speed cryopump. Since a cryopump cannot be used with helium, it was necessary to change to a diffusion pump. Pressures around 1×10^{-10} Torr were desired and obtained.

The main effort during the past consisted in improving the signal to background ratio. The background is due to transition radiation or bremsstrahlung produced by electron impact on parts of the ion source, and to optical excitation of the gas by electron impact. The background was reduced in three ways. (a) An optical filter was put in front of the photon detector to pass the radiation of interest but not charged or neutral particles. For argon ions neutralized on molybdenum, lithium fluoride windows have the desired properties, and for helium ions, very thin, unbacked aluminum films[13] are best suited as optical windows. (b) Two grids with high transparency were mounted in front of the window.

[13] See Thin Film Section, "Fabrication of Very Thin Unbacked Aluminum Films."

They were biased so that no ions or electrons could reach the window. It was observed that lithium fluoride and aluminum show strong luminescence when hit by electrons of energy less than 100eV. (c) The target was rotated so that no photons from the ion source region, after being specularly reflected from the target, could reach the photon detector.

With the improvement of signal-to-background ratio by a factor of a few hundred, the first preliminary data were obtained. The effect which was observed was clearly due to ions hitting the target: it was proportional to the ion current for widely different electron-bombardment energies in the ion source, and independent of the bias voltages applied to the grids in front of the photon detector as long as no charged particles could reach the window in front of the detectors. The desired effect shows as a difference in photon count rate when ions strike the target and when they do not. For the second condition, the ions were either deflected sideways before reaching the target area, or they were repelled by biasing the target. Both methods gave essentially the same results. The background count rate was about a factor of 10 higher than the signal count rate. Long counting times are therefore necessary to get statistically significant results.

1.5.2. Results.

1.5.2.1. Argon.

The yield for 15-eV argon ions neutralized on clean polycrystalline molybdenum was about 5×10^{-8} photons/ion. The uncertainty is about a factor of three, mainly due to the unknown photoelectric yield of the photomultiplier and to the uncertainty in the area "seen" by the

multiplier due to imperfect optical imaging by the mirror. The mirror images photons coming from the target onto the photomultiplier entrance.[14] The angular distribution of the emitted radiation is supposed to be that of pure dipole radiation. No theoretical predictions for the yield are available for comparison. Due to the low signal strength, no measurements of photon yield vs ion energy could be made.

1.5.2.2. Helium.

The yield was about 8×10^{-6} photons/ion for 15-eV helium ions, with an uncertainty of about a factor of four. The increase in uncertainty compared to the argon measurements comes from the uncertainty in the transmission of the aluminum window. Calculations by Sternberg[15] indicated that the yield will be not more than 10^{-4} photons/ion for 10-eV helium ions, and this under the assumption that no other processes intervene. Most ions, however, are neutralized by an Auger process at a distance of a few angstroms from the surface. Therefore, the photon yield is expected to be less than 10^{-4}. The experimental result confirms the theoretical prediction.

The photon yield vs ion energy was measured in the range from 15eV to 110eV. The results show that the yield is, within error limits, proportional to $1/v_i$, with v_i the ion velocity ($v_i\alpha/E_i$, with E_i the kinetic energy of ion). This is predicted by the theory, but in contradiction to the experimental results of Böhmer and Lüscher.[16] It was also

---

[14] See Progress Report for March-August 1966, Coordinated Science Laboratory, University of Illinois, p. 45.

[15] D. Sternberg, Ph.D. Thesis, Columbia University (unpublished) 1957.

[16] H. Böhmer and E. Lüscher, Phys. Letters 5, 240 (1963).

observed that the yield decreased by about a factor of two when the target was covered with gas (about one monolayer of CO, H_2 or both). At this stage, it seems to be desirable to improve the signal-to-background situation by magnetically deflecting the ions coming from the ion source. An improved system which will have a second differential pumping stage is being built. Added pumping will reduce the partial pressures of adsorbable gases in the target region. It will also permit exposing the target to a known amount of an adsorbable gas and measure the photon yield as a function of gas coverage.

R. C. Birtcher
D. E. Coad
J. W. Culton
J. T. Jacobs
N. Maeda
R. N. Peacock
O. G. Reilly
F. Steinrisser

2.1. Gauge Studies in Low Pressure Atmospheres.

Sensitivities of NASA flight-type gauges, commercial B-A gauges, and Schuemann-type gauges are to be evaluated in low-pressure mixed and pure atmospheres. The experiment employs a monoenergetic ionization device (omegatron) as a secondary standard in relating partial pressures. With bias to achieve total ion collection and a monoenergetic electron beam, the omegatron or a similar device should display sensitivities to gases that are in the same ratio as the ionization cross sections for those gases. To illustrate this, an I^+/I^- versus electron-beam-energy plot (holding constant pressure in a pure atmosphere with constant ionization path length and constant ion-collection efficiency) would be a relative-ionization cross-section curve.

Secondary electrons emitted from metal surfaces such as the electron collector increase the ion yield, shift the electron-energy scale, and thus distort the cross-section (sensitivity) curve. Figure 2.1 illustrates data taken at constant filament emission using 200-V electrons in argon. As the electron-collector potential approaches that of the preceding element, secondary electrons from the collector proceed back along the beam path (confined by a strong magnetic field) causing additional ionization. The bottom curve shows the effective decrease in electron current to the electron collector. This is accompanied by increases in electron current to elements further back down the beam path.

(OVERLEAF BLANK)

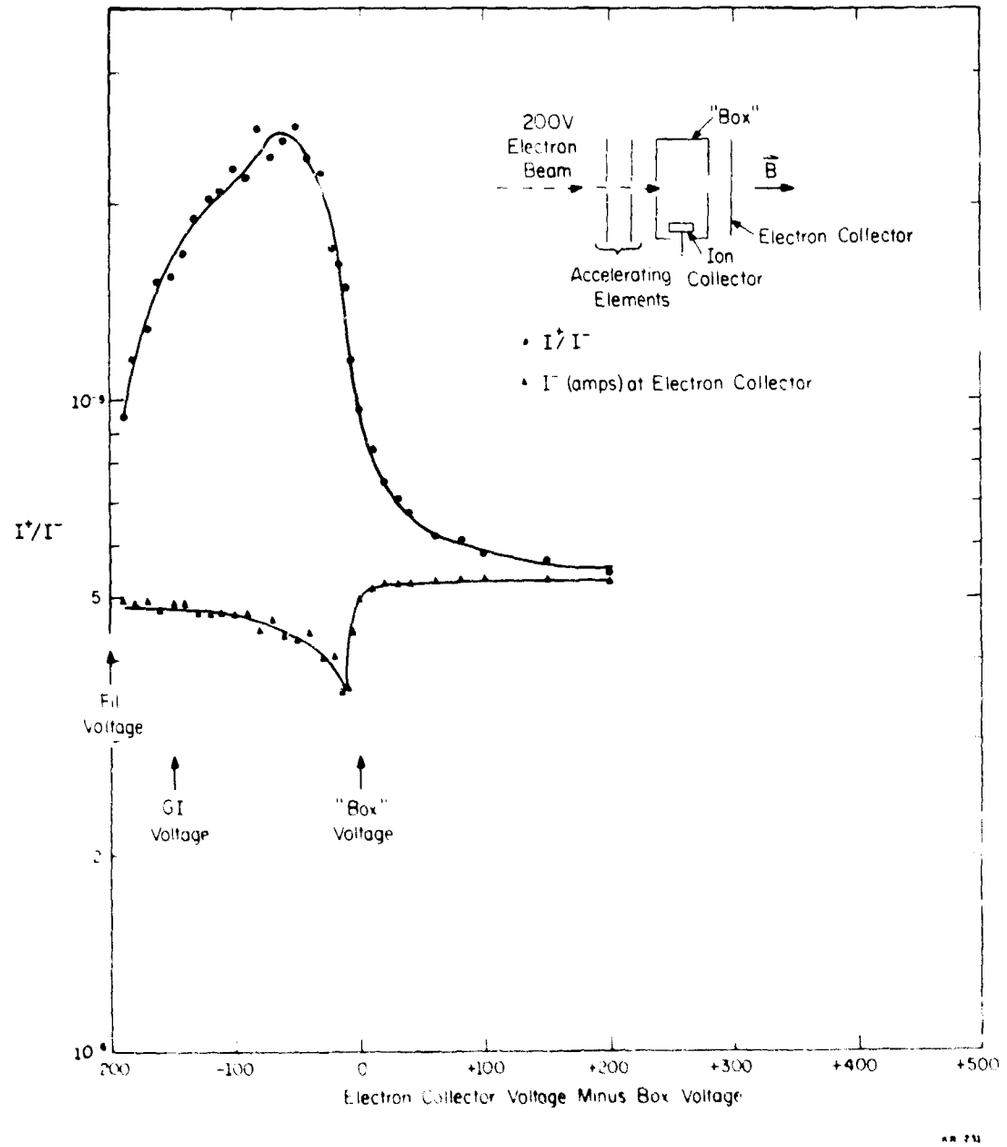

Fig. 2.1. The effect of secondary electron emission upon megatron behavior.

(OVERLEAF BLANK)

The top curve, in effect, shows the variation in sensitivity as a function of electron-collector voltage. This could account for omegatron sensitivity variation with electron-collector potential and reported sensitivity ratios differing from ionization cross-section ratios.

J. W. Culton

2.2. Size Effects in Thin Films.

2.2.1. Introduction.

The non-specular scattering of conduction electrons from the surface of a metal increases the apparent resistivity of the material. This effect is emphasized when the mean free path of the conduction electrons is large compared to the thickness of the material. This phenomenon is called the "size effect." Preliminary size-effect experiments are reported below.

2.2.2. Size-Effect Experiments.

Thin films of gold were evaporated on mica substrates in a Varian VI-4 vacuum system. The vacuum during evaporation was between 7×10^{-7} and 1×10^{-6} Torr. The resistivity ratios of these films were measured. A technique was developed which allowed the preparation of 2000-5000 Å films with a resistivity ratio of 50. This high resistivity ratio indicates that the effect of non-specular scattering from the surface was small.

In order to make accurate measurements of the degree of specular scattering, a high-speed, data-acquisition system was assembled. This consisted of a Vidar 510 digital voltmeter, a Vidar coupler, and a Tally paper-tape punch. These instruments were borrowed from the

Aerospace Group at CSL. A switching system was developed in our electronics shop. This allowed us to make four-point measurements of resistance of both a gold film and a germanium thermometer. It also switched current polarities and thus eliminated the effect of thermal emf's. All four readings are made to 0.1% full scale accuracy in 11 sec.

In order to make plots of temperature vs resistance, a liquid-helium dewar with a thermal leak was used. With this equipment, we were able to make measurements of temperature vs resistance between $4.2^{\circ}K$ and $100^{\circ}K$. The data acquired in one run consist of several-thousand measurements.

Much of our effort during this period has been directed towards computerized data reduction. Mrs. V. Metz wrote a machine-language program which translated the code from the Tally punch to the code of the Laboratory CDC-1604 computer. This program also checks the tape for punching errors. The development of this program was the key to our whole data-acquisition and reduction scheme.

In addition to the above computer program, several other programs were necessary to aid in the analysis of the size-effect problem. A numerical-integration program was used to solve the Sondheimer equation for large p. A large table of values was computed for various large values of p, i.e., $0.8<p<1.0$. This table can now be used to obtain estimates of the degree of specular reflection from our experiments. Preliminary estimates indicate $0.25<p<0.9$ for gold on mica.

A program was written to obtain an analytic expression for the temperature of a germanium thermometer as a function of its resistance.

It was found that seven terms were required in order that 0.5% accuracy be obtained over the range 4.2 to 100°K. A third program was written which interpreted the data so that we could plot the resistivity ratio vs temperature using the Calcomp plotter. With these routines, it is now feasible to handle the thousands of data points taken in each experiment with little effort.

The size-effect tunneling experiments initiated during the last reporting period were continued in collaboration with Dr. E. L. Wolf. The results are not highly reproducible and hence are not conclusive. Efforts will be made during the next period to obtain reproducible results from these tunneling measurements.

2.2.3. Cryopump Tests.

A UHV cryopumped system was completed during the period covered by this report. The system was built in order to eliminate the effects of contamination in studies of thin films. This system should reduce contamination problems in two ways. The first is to provide very high pumping speed during preparation of thin films. This is necessary in order to grow the films slowly without including residual-gas contaminants while still achieving large single-crystal growth. The second is to supply a suitable vacuum to reduce surface contaminants. At 10^{-10} Torr, the lifetime of a clean surface is of the order of a day. Thus at 10^{-10} Torr, we could perform measurements which take several hours on films of active metals without fear of surface contamination. Preliminary tests on this system are reported below.

The repaired cryopump was installed on the UHV system described in previous reports. A 32-hour bakeout of the system at 350°C resulted

in a system pressure of 1.8×10^{-9} Torr. Liquid nitrogen was put in the shroud. The total pressure dropped slowly to 5.5×10^{-10} Torr. Next, liquid helium was transferred into the dewar. The B-A gauge read a total pressure of 2.8×10^{-11} Torr. (This value has not been corrected for the x-ray limit of the gauge.) The partial pressure of hydrogen was 3×10^{-11} Torr. The disparity in these readings is likely due to the fact that the B-A gauge was nude and near the cryopump, while the PPG (Varian Assoc.) was off to one side of the system and connected to it by 1½" diameter stainless-steel tubing.

Another test similar to the above was made. The essential difference was that the system was unbaked. The system pressure with liquid nitrogen in the shroud was 7×10^{-10} Torr. This was decreased to 1×10^{-10} Torr by putting liquid helium in the cryopump.

Initial experiments to test the cryopump's ability to maintain UHV conditions during evaporation of gold from a tungsten boat were somewhat disappointing. The pressure rose to 2×10^{-7} Torr during outgassing of the charge. The pressure was 2×10^{-8} during evaporation.

The filament support was hydrogen brazed. Since this support was heated during the evaporation, it is possible that it is the main source of gas in the system. A new support system which is to be welded in inert atmosphere may alleviate this problem.

In conclusion, it is evident that the effectiveness of the cryopump system for our application is limited only by its inability to pump hydrogen effectively. The addition of a supplemental titanium-sublimation pump is being considered.

2.2.4. Electron Microscopy.

A Varian Associates EM-20 electrostatically-focused electron microscope was received as a gift during the past semester. It was felt that information about the surface texture of thin films could be obtained by examining replicas of film surface. Under the direction of Mr. F. Luehrs of the Materials Research Laboratory, replicas of the surface of epitaxial gold films were made. When these replicas were examined in the electron microscope it was found that it could not be sharply focused. This fault should be remedied soon and the study continued. In the meantime several replicas were studied with an Hitachi HU11C electron microscope by Mr. F. Luehrs. The results are reported in Report R-364.

J. T. Jacobs
R. C. Birtcher
N. Maeda

2.3. Evaporation of Insulating Films.

The ability to grow thin, pinhole-free insulating films is necessary for the success of tunneling experiments. These films must be less than 100 Å thick. A substantial problem is the monitoring of this thickness as the film is deposited.

A considerable effort was made to investigate the use of a double-ionization-gauge technique[1] to measure the pressure of the evaporation beam. The entire system included a feedback network, a differential-pressure measurement, and a resistance-heated Drumheller source. The initial tests indicated that 100-Å films could be grown from an evaporated beam of SiO at a constant pressure in a period as long as 5 min. The

[1] W. P. Bleha, CSL Report, June-August 1965, p. 102.

long-term regulation was better than 1%. The system seems to be an excellent one with which to control the rate of evaporation for a wide range of rates. Two new ionization gauges, each with improved geometry, have been built and tested. Versions easier to insert, remove, and handle in the vacuum system are under design.

J. T. Jacobs
O. G. Reilly

2.4. Radiation from Silver Films Due to Electron Bombardment.

A study was made to determine whether it is feasible and useful to investigate the properties of thin films by studying the emitted radiation under electron bombardment. This radiation has three components: transition radiation, bremsstrahling and plasma radiation. It has received increasing interest in recent years. The main centers of activity are H. Boersch's group at the Technische Universität in Berlin[2,3] and R. H. Ritchie et al.[4,5,6] at ORNL, Oak Ridge, Tennessee.

For simplicity, the same experimental approach as shown in Ref. 1 was chosen (see Fig. 2.2): a field-emission tip was the electron source in front of a thin tungsten anode. Tip and foil could be outgassed by passing current through them. The film to be investigated was evaporated from a source which delivered a collimated beam of the film material onto the anode. This way, the tungsten foil was coated but not the quartz bulb.

---

[2] H. Boersch et al., Z. Physik 165, 464 (1961).

[3] H. Boersch et al., Z. Physik 187, 97 (1965).

[4] R. H. Ritchie et al., Phys. Rev. 126, 1935 (1962).

[5] K. L. Frank et al., Phys. Rev. 126, 1947 (1962).

[6] E. T. Arakawa et al., Phys. Rev. Letters 12, 319 (1964).

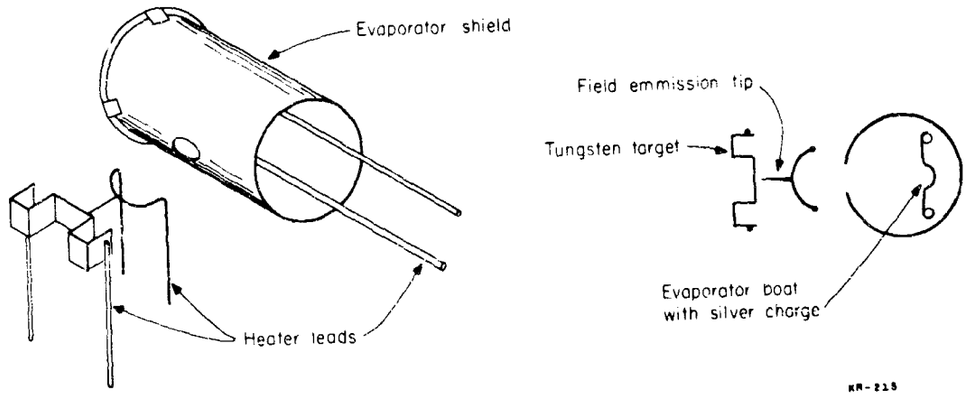

Fig. 2 2. The field emission tub ..h tungsten target and silver evaporation sources.

(OVERLEAF BLANK)

The field-emission tip was made by electrolytic deplating of a 0.004" tungsten wire in a 1% NaOH solution. The wire was first spot-welded so that the tip barely touched the anode. It was then deplated to the desired sharpness. Frequent checks under a micrscope were necessary. The procedure was repeated many times and gave reproducible results. A current of 100μA could be drawn at less than 2 kV. A vacuum of 10^{-9} Torr is necessary to prevent destruction of the tip by ion bombardment.

The intensity of the radiation from silver films produced by such a current was sufficient to be observable by eye in the dark. A spectrograph (0.5m Bausch and Lomb, 16 Å/mm, 1mm slit width) equipped with a photomultiplier with quartz window recorded a spectrum with a signal-to-noise ratio of more than 10 for the peak intensity. Figure 2.3 shows a spectrogram for an angle of observation of 20° with respect to the foil normal. Corrections were made for the photomultiplier response but not for the spectrograph response. The spectrum is in good agreement with published results.

From literature studies and experience it was concluded that it would be difficult to draw conclusions about thin-film properties from the radiation emitted under electron bombardment. There are several reasons. It is difficult to decompose the observed radiation into the three components mentioned above. For most materials, the interesting features appear only in the far ultraviolet around the plasmon energy. The complex dielectric constant of the film and the observed radiation are related in a rather complicated way. These studies were therefore abandoned.

F. Steinrisser

(OVERLEAF BLANK

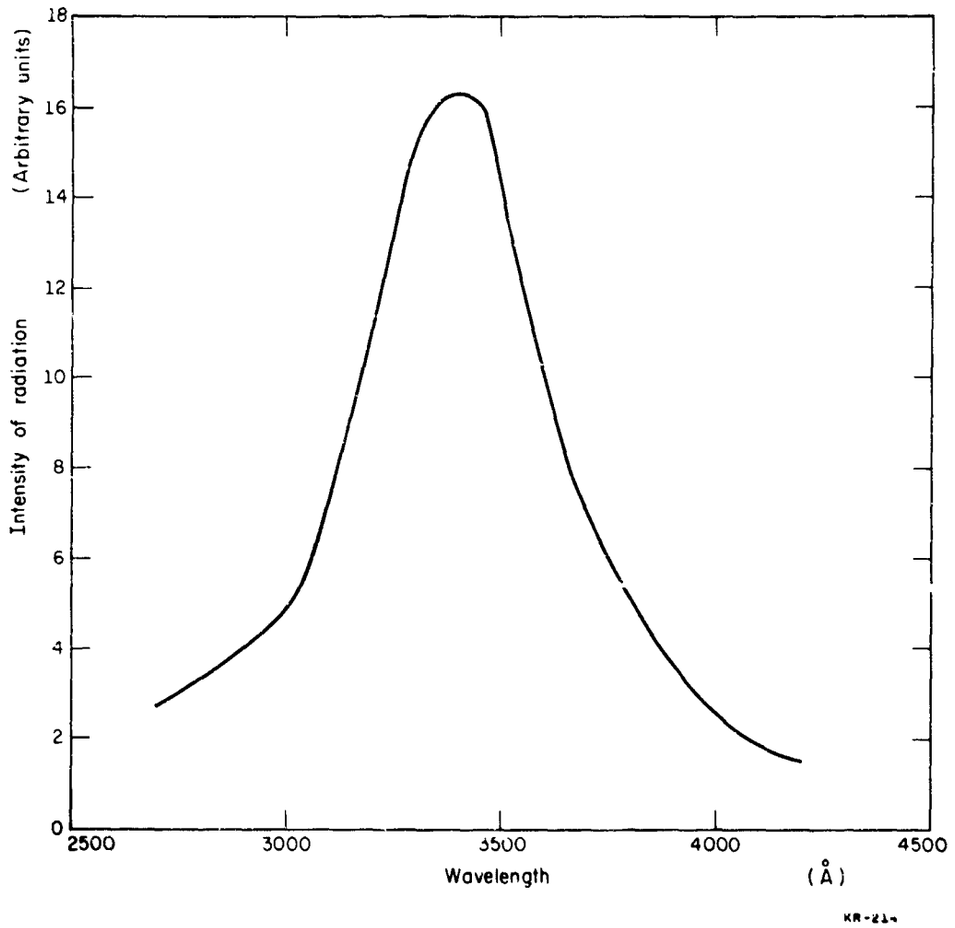

Fig. 2.3. The radiation spectrum of a silver film bombarded by 1.5-keV electrons. The angle of observation was about 20° with respect to the target normal.

(OVERLEAF BLANK)

2.5. Fabrication of Very Thin Unbacked Aluminum Films.

For the experiment described in the Surface Physics section, it was necessary to make an optical filter which would pass photons of energy greater than 15 eV with little attenuation. This filter had to have a size of about 3/4" in diameter. No cracks or pin holes could be tolerated, because it had to shield a photomultiplier against neutral and charged particles. Aluminum filters of 800 Å thickness transmit more than 10% of this radiation.[7] Aluminum is also a fairly-good vacuum material. There are several ways to make such films; one method is the deposition on a cleaved surface of NaCl with subsequent solution of the NaCl in water. Another method is to coat a glass slide with a parting agent, deposit the film on top of it, and float it off in water. Several parting agents were tried; NaCl, evaporated to 1000 Å thickness, could easily be dissolved. The Al films, however, showed many pinholes due to the crystal structure of the NaCl. The next detergent tried was fuchsin, an organic dye.[7] It was evaporated from a Ta boat at about 400°C. It was easily dissolved in water, and the Al films were smooth and showed no pinholes. It was found, however, that the Ta boat had to be recharged every time after the heated fuchsin was exposed to air. Otherwise, a tar-like deposit occurred which would not come off in water. The glass slide with the fuchsin coat alone also couldn't be exposed to air without showing the same effect. Fuchsin is an extremely powerful red dye. After everybody in the laboratory got red hands, faces, etc., after touching parts of the evaporator system, still another parting agent was tried: A sugar-Aerosol solution (15 g. cane sugar in 75 ml of a 1% Aerosol-water

[7] W. R Hunter et al., Appl. Optics 4, 89 (1965).

solution) as used by Carpenter and Curcio[8] proved to be the solution. It is also supposed to work for indium films as mentioned in Ref. 7. After dipping the slide in such a solution, it has to dry very slowly to keep the sugar concentration uniform across the slide. The slides were left in small beakers which may be covered if necessary to get a drying time of about 15 minutes. With this sugar coating, the Al films came off much slower than with the other parting agents mentioned above. The slides are put at an angle into a small container. Water is added until it touches the film on one side. The water dissolves the sugar slowly, and the film starts to float. After about 15 minutes, the film is completely loose, floats, and can be picked up with a wire mesh or a photochemically etched grid. Before the water dries, the underside of the film must be rinsed gently in absolute alcohol to remove the water. Otherwise, the film is likely to break when the water dries.

Films of 600-800 Å thickness and 3/4" diameter were made this way. They not only staved free of pinholes, but they also survived repeated bakeouts to 400°C in vacuum without breaking or showing pinholes.* The support was a 304-stainless-steel etched grid with 0.040" wire spacing and about 70% transparency. It is worth mentioning (but not understood) that the transparency of these Al films in the visible decreases after taking the glass slide from the vacuum into air and again after floating the film off in water.

F. Steinrisser

---

[8] F. E. Carpenter and J. A. Curcio, Rev. Sci. Instr. 21, 675 (1950).

*No indication was found in the literature that unbacked Al-films were successfully subjected to such a thermal treatment.

M. Raether
H. Böhmer
L. D. Bollinger
W. E. Carr
J. Chang
R. W. Hosken
T. Lie

3.1. Beam-Plasma Interaction.

We have investigated the high frequency instability in a beam-plasma system under conditions where Coulomb collisions have a crucial effect on the growth rate of the instability.

The interaction of a monoenergetic electron beam with a collisionless, cold plasma is described by the dispersion relation[1,2,3,4]

$$1 = \frac{\omega_p^2}{\omega^2} + \frac{\omega_B^2}{(\omega - kv_o)^2} \qquad (1)$$

where ω_p is the plasma frequency, ω_B the beam plasma frequency and v_o the beam velocity. The system is unstable for wavenumbers less than

$$k_{max} = (\omega_p/v_o)(1+\alpha^{1/3})^{1/2}, \qquad (2)$$

where $\alpha = n_B/n_p$ is the ratio of beam to plasma density. The maximum growth rate occurs for

$$k_{opt} = (\omega_p/v_o)[1+(3/2)(\alpha/2)^{2/3}] \qquad (3)$$

[†]Supported in part by the University of Illinois.

[1]Akhiezer, A. I. and Fainberg, Ya. B., Doklady Acad. Nauk. SSR 69, 55 (1949).

[2]Bohm, D. and Gross, E., Phys. Rev. 75, 1864 (1949).

[3]Bludman, S. A., Watson, K. M. and Rosenbluth, M. N., Phys. of Fluids 3, 747 (1960).

[4]Imshennik, V. S. and Morozov, Yu. I., Sov. Phys.-Tech. Phys. 6, 464 (1961).

and the frequency and growth rate for this value are given by

$$\mathrm{Re}\{\omega\} = \omega_p\left[1-\tfrac{1}{2}(\alpha/2)^{2/3}\right],$$

$$\gamma = \tfrac{1}{2}\sqrt{3}(\alpha/2)^{1/3}. \qquad (4)$$

Here it is assumed that $\alpha \ll 1$, a condition that is almost always satisfied. In the present experiment α is in the range 10^{-2} to 10^{-5}.

The influence of collisions on the instability is readily discussed through the inclusion of a relaxation-type collision frequency in the equation of motion for the plasma electrons. Collision of beam particles with either neutral atoms or ions can usually be neglected on account of their high velocity. The dispersion relation (1) then takes the form

$$1 = \frac{\omega_p^2}{\omega(\omega+i\nu_c)} + \frac{\omega_B^2}{(\omega-kv_o)^2} \qquad (5)$$

where ν_c is the collision frequency for momentum transfer. This equation has been discussed by Bludman, Watson and Rosenbluth.[3]

For the most unstable mode, one may write

$$\frac{\omega}{\omega_p} = \frac{kv_o}{\omega_p} + \epsilon \qquad \epsilon \ll 1$$

to obtain to first order

$$\epsilon^3 + i(\nu_c/2\omega_p)\epsilon^2 = \alpha/2.$$

The growth rate γ is then given by $\gamma = \omega_p \mathrm{Im}\{\epsilon\}$. In the limiting cases $\gamma \gg \nu_c$ and $\gamma \ll \nu_c$ one finds

$$\nu = \nu_o[1-(2/\alpha)^{1/3}(\nu_c/\omega_p)/\sqrt{27}] \quad (6)$$

$$\nu = \nu_o\sqrt{(2^{5/3}\alpha^{1/3}\omega_p/3\nu_c)} \quad (7)$$

respectively, where ν_o is the collisionless growth rate as defined in Eq. (4). In the intermediate region $\mathrm{Im}\{\varepsilon\}$ is the most conveniently found numerically.

In the experiments described here, only Coulomb collisions are important; collisions of plasma electrons with Ne atoms can be neglected because of their small cross section and the low gas pressure. For the electron-ion collision frequency we take the experimental value of Chen,[5]

$$\nu_c = 3.6(n_p/T_e^{3/2})\ln(2\times10^4 T_e^{3/2}/n_p^{1/2}),$$

where T_e is the electron temperature and allow for electron-electron-collisions by multiplying this expression by a factor 2.4.[6] Within the limits of the experimental solution ($T_e \sim 300^\circ K$, $10^{10} < n_p < 10^{13}$ cm^{-3}) the logarithm remains almost constant and its value is approximately 5. It follows that in the low density region the growth rate increases as $n_p^{1/6}$ whereas in the high density region it decreases as $n_p^{-1/4}$. There exists, therefore, a critical electron density n_{max} for which the growth rate has a maximum.

---

[5]Chen, C. L., Phys. Rev. 135, A627 (1964).

[6]Comisar, G. G., Phys. of Fluids 6, 76 (1963).

3.2. Description of the Experiment.

The experimental arrangement was the same as described in previous Progress Reports. The electron beam is injected into the afterglow of a low pressure discharge in Neon. This way, the plasma density is independent of the beam current.

Figure 3.1 shows a schematic of the experiment. The electron beam is generated by a Pierce type electron gun. It has a 3/4"-diameter, Lanthanum-Boride-covered, Molybdenum cathode of concave shape and is capable of delivering a beam current up to 3 amperes. A focusing magnet whose field is carefully shielded from the plasma generates a parallel electron beam of about 1 cm diameter. The hard-tube beam pulser can deliver a 20-kV pulse of 1 to 50 μsec duration into a 4-KΩ load. The rise time is 0.25 μsec and the pulse voltage remains constant within 0.3% for a 10-μsec pulse.

The plasma section is a thin wall Pyrex glass tube of 4-cm diameter, 30 cm long. The gas pressure in the discharge tube is typically 4×10^{-2} Torr Neon. Breakdown of the gas is effected by applying a high-voltage pulse (10-15 kV) to a hot cathode. The electron density is initially several times 10^{13} cm^{-3} and decays with a time constant that varies from 100 to 200 μsec in the pressure range between 2.5×10^{-2} to 5×10^{-2} Torr. The beam duration in the present experiment is 1.5 μsec so that the plasma density can be taken as constant during this time. In the density range of interest ($n_p < 2\times10^{13}$ cm^{-3}) the plasma is at room temperature as inferred from the ambipolar diffusion coefficient and the time dependence of the recombination light. Additional ionization from the beam -- either by direct ionization by beam electrons, or by plasma electrons accelerated in the

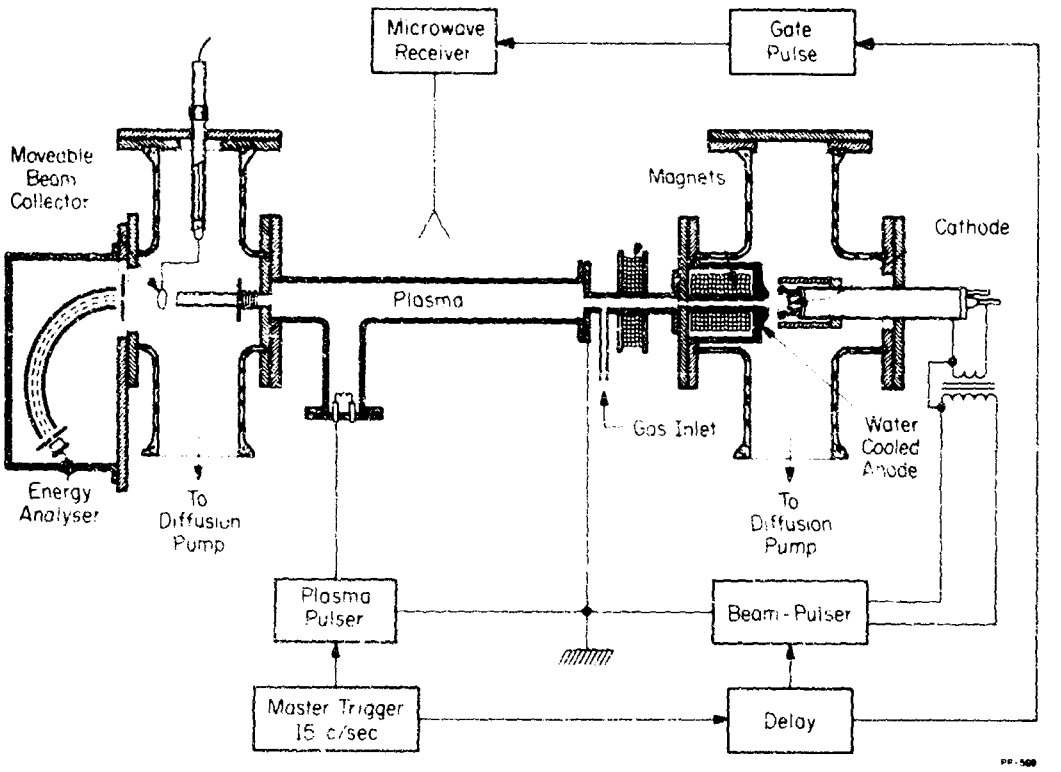

Fig. 3.1. Schematic of the experiment.

(OVERLEAF BLANK)

fields of the instability -- is negligible under the experimental conditions considered here.

The plasma as well as the beam are pulsed with a repetition frequency of 15 Hz. With a delay line the time elasping between the plasma and the beam pulse and therefore the plasma density can be varied continuously.

A fraction of the total beam current is used to measure the energy distribution of the beam with a 127° deflection electrostatic analyzer.

3.3. Results.

The instability resulting from the electron beam-plasma interaction can be detected in a variety of ways, for example, by monitoring the radiation from the unstable waves, or by observing how the energy distribution function of the beam changes due to its interaction with the plasma. From these two possibilities, the energy distribution has the advantage of being easily observable over a wide plasma-density range.

Figure 3.2 shows examples of the measured beam-electron-velocity distribution function, after a beam of 10 μsec duration has passed through plasmas of different densities. One can see immediately that the energy loss and the smearing of the distribution function is largest at medium densities. The fact that the distribution function is narrow for $n_p = 2.2 \times 10^{13}$ cm^{-3} compared to lower densities shows already the influence of the collisional damping.

No attempt will be made in the present report to discuss the shape of the distribution function, which contains very detailed

(OVERLEAF BLANK)

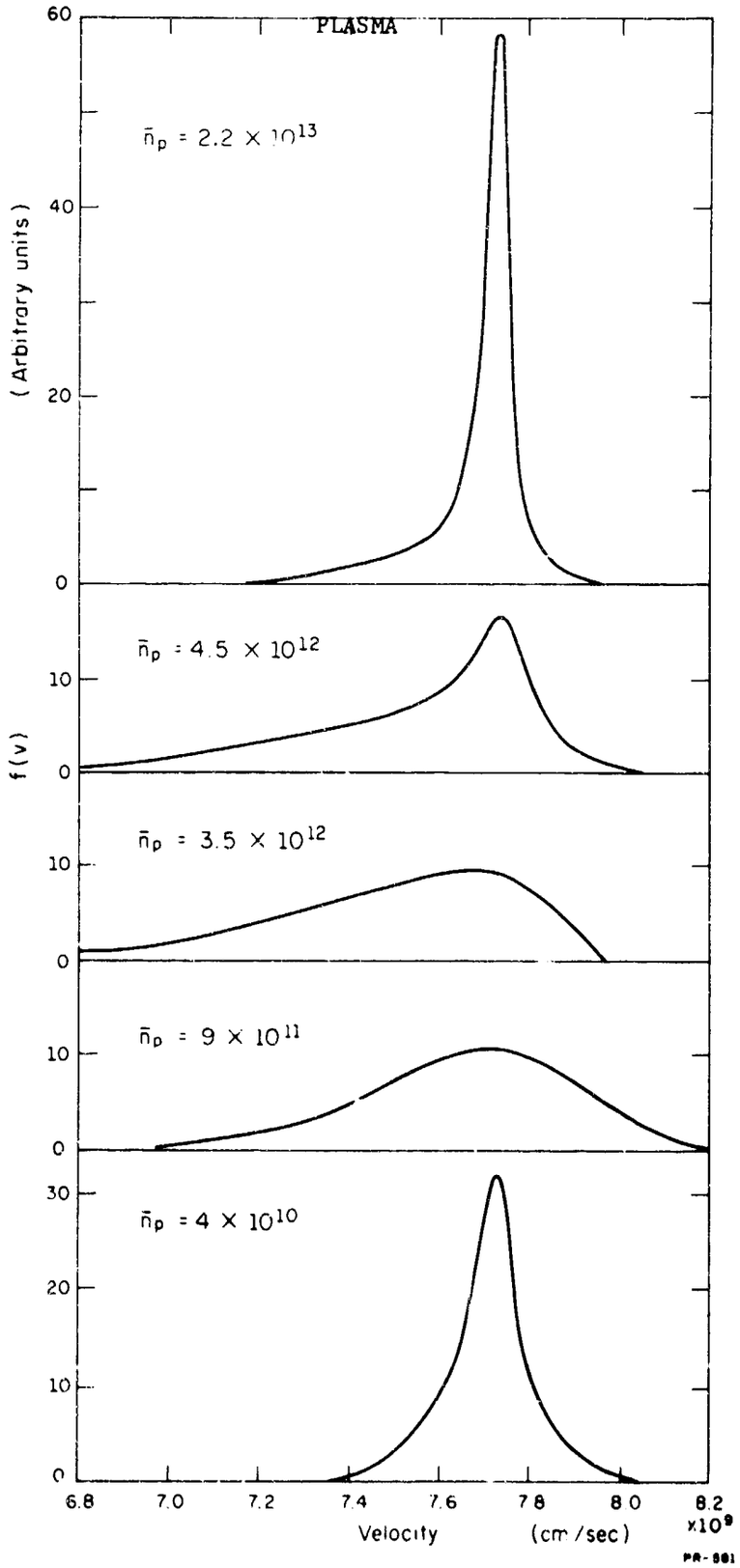

Fig. 3.2. Electron-beam velocity distribution function after interaction with plasmas of different densities. The distribution functions are normalized to equal areas. Beam parameters: current 500 ma, voltage 17 kV, pulse length 10 μsec.

(OVERLEAF BLANK)

information about the instability; in the present context is is sufficient to characterize the distribution function by a single parameter like energy loss or half width.

In the following experiments the beam pulse length is only 1.5 μsec to avoid heating of the plasma. Under this condition the energy loss especially for small beam currents becomes so small that its value, calculated from the observed energy distribution, lies within the error bar of the measurement. Therefore the half width of the energy distribution is used as a parameter indicating the degree of instability.

Figure 3.3 shows how for a certain beam current (350 mA) the half width of the energy distribution function changes with plasma density. One can attempt to correlate this with the theoretical considerations given in the introduction by assuming that half width will be proportional to the energy in the most unstable mode, which can be written as

$$E_k^2 = E_o^2 \exp(2\gamma t)$$

or in the spatial domain

$$E_k^2 = E_o^2 \exp(2\gamma z/v_g)$$

where $v_g = 2v_o/3$ is the group velocity. This can be normalized for the maximum growth rate to obtain

$$I(n_p) = (E_k^2/E_{kmax}^2) = \exp\{(2z/v_g)[\gamma_{max} - \gamma(n_p)]\}$$

where n_p is the electron density. This curve is compared with the experimental data in Fig. 3.3. One sees that the instability grows

(OVERLEAF BLANK)

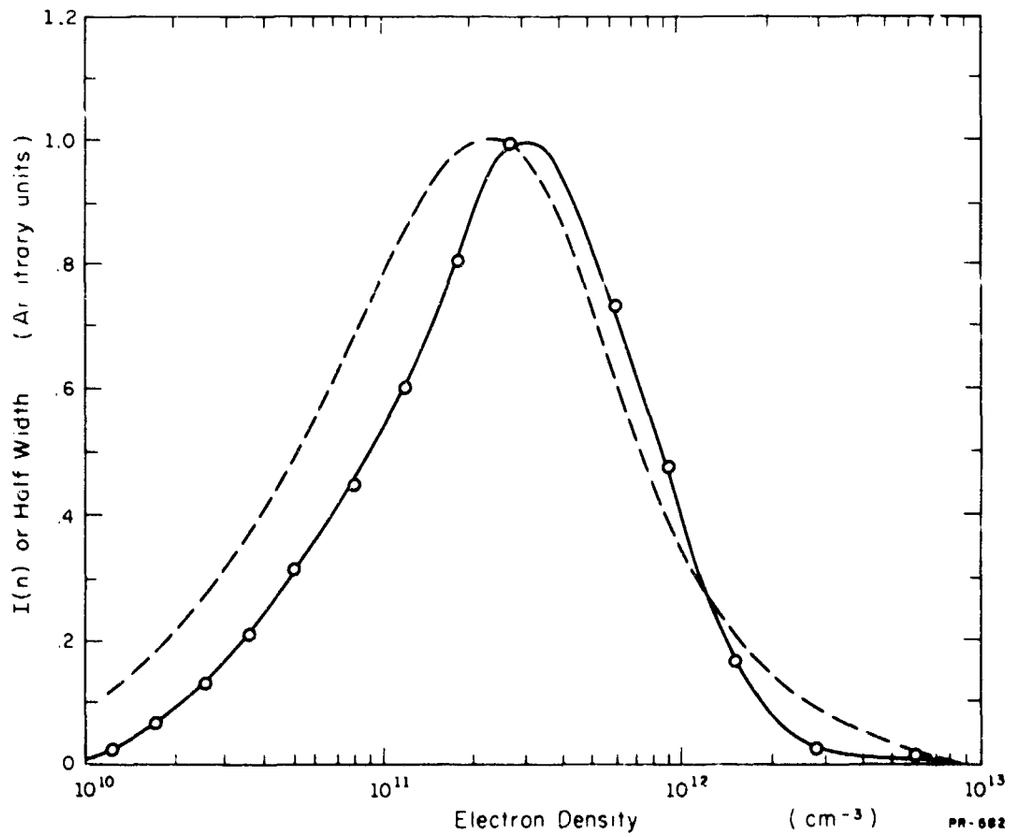

Fig. 3.3. Half width of the beam energy distribution function (solid curve) and calculated intensity ratio (dashed curve) as a function of plasma density. Beam parameters: current 350 ma, density 1.8×10^{8} cm^{-3}, voltage 16 kV, pulse length 1.5 μsec.

(OVERLEAF BLANK)

with increasing density up to a certain point, and that at high densities collisional damping takes over. From the good agreement of both curves one can conclude that the treatment of Sec. 3.1 indeed describes the collisional damping correctly. It should be pointed out, however, that the exponential growth does not persist over the whole interaction distance. Measurements of the spatial growth of the instability show a saturation of the oscillation amplitude in the last quarter of the interaction region, which saturation must be attributed to nonlinear effects.

The plasma densities at which maximum instability occurs for a given beam density are plotted in Fig. 3.4 together with the theoretical curves for 300° K and 400° K.

The collisional damping reacts quite sensitively to the temperature of the plasma. No attempt is made to heat the plasma externally. The instability, itself, however, can raise the plasma temperature, an effect which is demonstrated in Fig. 3.5. Here a 500 mA beam of 10 μsec duration traverses the plasma. The plasma is heated by the instability during the beam pulse and the instability grows to a large level in the initially collision dominated regime. As a result the density for maximum stability is shifted to higher values. Obviously, the level of the instability must be large to heat the plasma effectively. As a consequence, no heating is observed in the highly damped regime ($n_p > 2\times10^{13}$ cm^{-3}). Furthermore, the heating should depend on the beam density. To check this, the plasma density for maximum instability is measured for various beam currents (i.e. beam densities) at constant beam duration (10 μsec). The results are plotted

(OVERLEAF BLANK)

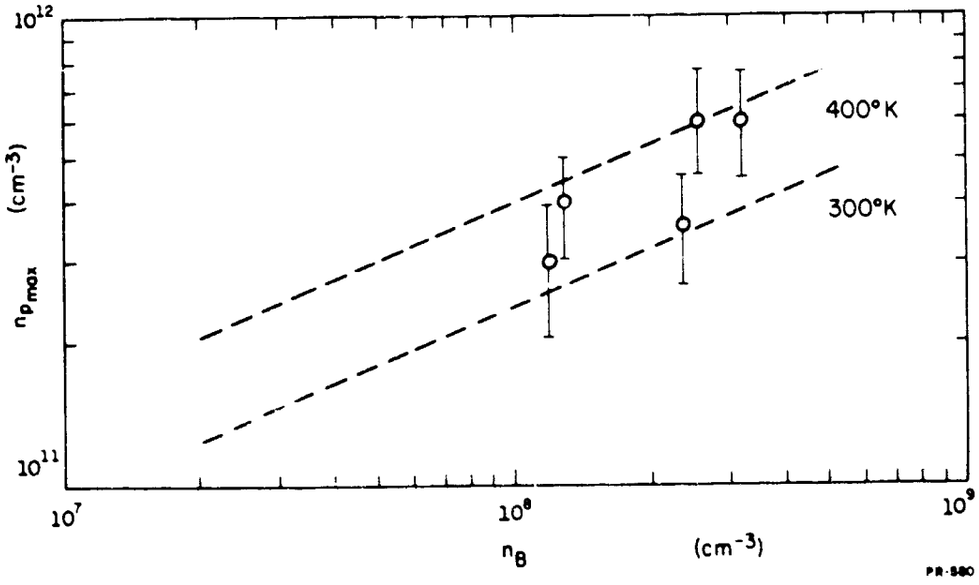

Fig. 3.4. Plasma density of maximum instability as a function of beam density. The dashed lines are calculated for two different temperatures. The points are experimental results for electron beams of 1.5-μsec pulse length.

(OVERLEAF BLANK)

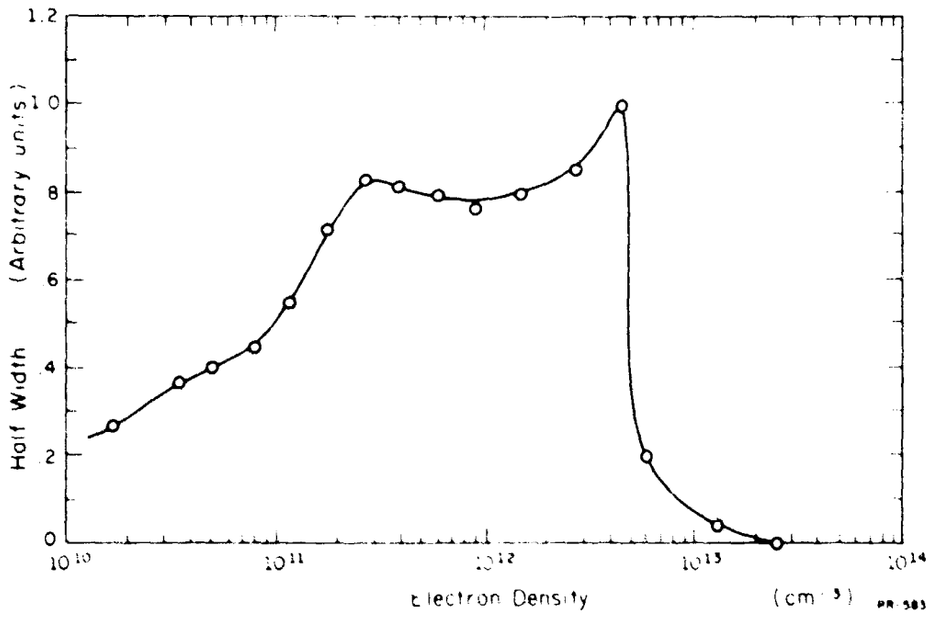

Fig. 3.5. Half width of the beam energy distribution function as a function of plasma density. Beam parameters: current 500 ma, density 2.1×10^{8} cm^{-3}, voltage 17 kV, pulse length 10 μsec.

(OVERLEAF BLANK)

in Fig. 3.6 together with curves calculated for various plasma temperatures. As expected, the change in plasma temperature is smallest for small beam densities, whereas one can deduce from the intersection of the experimental and the theoretical curves that, for example, for a beam density of 2×10^{8} cm^{-3} the plasma is heated from room temperature to $1500^{\circ}K$.

The heating effect can even more clearly be shown by receiving the radiation of the instability as a function of time. To this end a microwave receiver (frequency 28 GHz, sensitivity 100 dbm) is used. Three stages of its if amplifier are biased negatively so that the total gain is zero. The bias then is gated to zero voltage during a short time (0.3 μsec) and the power received during this interval is monitored with a phase-sensitive detector. The position of the gate pulse can be varied continuously with respect to the beam pluse. In Fig. 3.7 which shows the radiated power as a function of time, a beam of only 150 mA and 6-μsec duration is injected into the plasma at a constant density of 9.7×10^{12} cm^{-3}. The radiated power starts out fairly constant in time but rises later on over more than an order of magnitude. Since the growth rate of the instability for the conditions of Fig. 3.7 is (including collisional damping) of the order of 5×10^{8} sec^{-1}, the growth of the oscillation amplitude can only be explained by heating the subsequent decrease of the collisional damping.

H. Böhmer
J. Chang
M. Raether

(OVERLEAF BLANK)

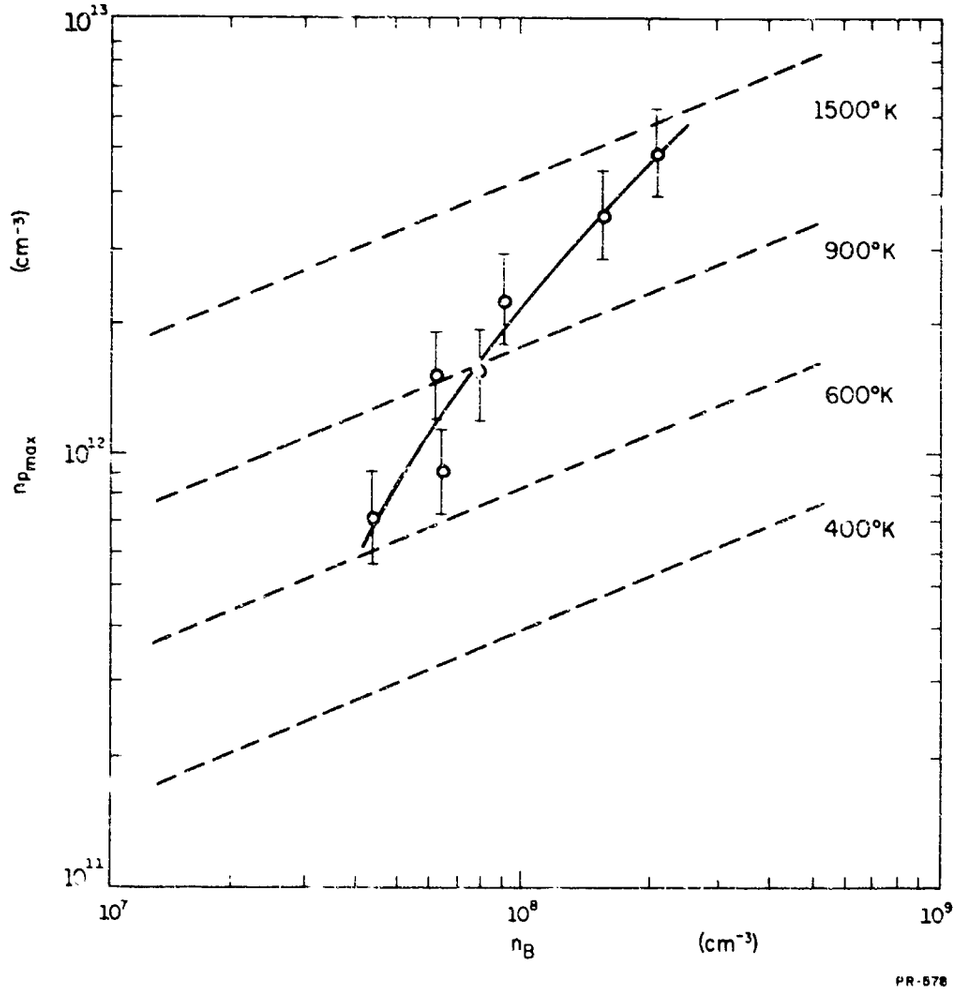

Fig. 3.6. Plasma density of maximum instability as a function of beam density. The solid curve is an average of experimental points for beams of 10 μsec pulse length. The dashed lines are calculated for different plasma temperatures.

(OVERLEAF BLANK)

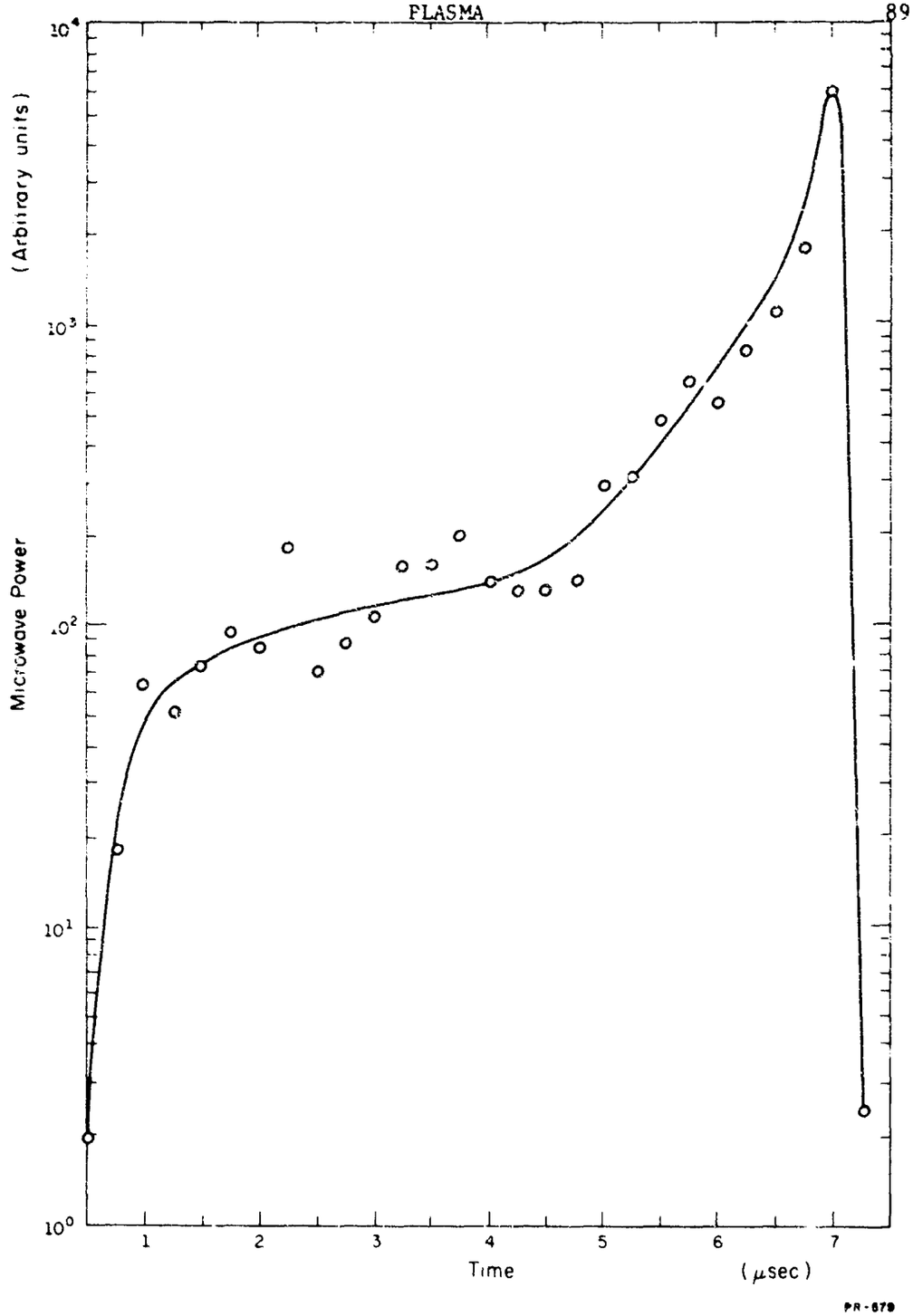

Fig. 3.7. Received microwave power as a function of time. The receiver frequency is 28 GHz. Beam parameters: current 150 ma, voltage 12 kV, pulse length 6 μsec.

(OVERLEAF BLANK)

4. RAREFIED GAS DYNAMICS[†]

B. L. Hicks
B. J. Reilly
H. J. Schmidt
M. A. Smith
Y. Wu
S. M. Yen

4.1. Boltzmann Shock Wave.

Solution of the Boltzmann equation for a shock wave has now been calculated for a second Mach number, namely, $M_1 = 4$ and runs have been started for $M_1 = 1.4$. We have made further analyses of the $M_1 = 2.5$ solution, especially with regard to systematic errors in the calculated values of eleven moments of the velocity distribution function f and of the collision integral a-bf. These results are being interpreted with the help of the new AVERR program described below. Our present program will make calculations of shock structure up to $M_1 = 10$.

In the past eighteen months we have made about fifty runs for different values of M_1, of the number of stations in the shock wave, and of the number of collisions in the Monte Carlo sample. The only one of these runs that diverged was for one very small sample containing 1/16 the number of collisions used for our final calculations.

With the help of our programmer, Mrs. Barbara Reilly, and our consultant, Mrs. Margaret Smith, we have made a number of valuable changes in the main Boltzmann program. Some of these facilitate use of the program for a variety of kinetic-theory problems. One change makes it possible to calculate directly certain important macroscopic

[†]Supported in part by the Office of Naval Research under Contract No. ONR N00014-66-C0010-A01.

quantities used in Navier-Stokes theory and will therefore permit more thorough interpretation of our results.

A new Fortran averaging program, AVERR, has been finished and put to use. This program makes it possible to calculate easily, for each station in the shock wave, the mean value and probable error of each of some eighty moments and related functions of physical interest derived from the velocity distribution functions and the collision integrals that are computed by our Monte-Carlo methods. Some of these functions are: partial heat fluxes, viscous stress, two translational temperatures and gradients, and the effective values of the Prandtl number, coefficient of viscosity, and coefficient of heat conduction. We will thus know for every one of these functions, for each station and Mach number, what contribution to the error is made by the Monte-Carlo method. These Monte-Carlo errors appear to be small.

A companion Fortran program, written by Mrs. Reilly, can be used for calculation of the values and maximum errors of some of these quantities, derived from moments of velocity distribution function and of the collision interval, for any theory, not just those derived from our Monte-Carlo calculations.

4.2. Krook Shock Wave.

We have obtained solutions of the Krook equation for the shock wave for M_1 = 1.4, 2.5, 5, and 10. The number of stations chosen was 9. The average collision frequency used corresponds to that for the collision law of rigid elastic spheres. The initial f was the Mott-Smith distribution function. In other runs, additional

solutions were obtained for M_1 = 1.4 and 2.5 by using the Navier-Stokes distribution function as the initial f. We have made studies of the characteristics of the convergence of our iterative method by monitoring the change in the distribution f, in some of the significant moments of f and in the collision integral, from one iteration to the next. The solutions for M_1 of 2.5 have been studied in detail. Both the distribution function and the moments have been compared with those of the Monte-Carlo and the Navier-Stokes solutions. We have been making similar studies for the solutions of three other Mach numbers. The uniqueness of the solutions for M_1 = 1.4 and 2.5 has been studied by comparing solutions with the two different initial distribution functions.

4.3. Heat Transfer in Rarefied Gases.

Since 1964 we have solved the nonlinear Boltzmann equation for two classes of problems, the pseudo-shock and the shock wave. During the past half year, solution of the nonlinear Boltzmann equation for a new and richer class of problems has been started, the problems of heat transfer in a rarefied gas.

The Boltzmann program has been slightly modified by Mr. H. J. Schmidt so that it can be applied to heat transfer problems (heat transfer between two plates at different temperature). The boundary conditions prescribe the distribution function to be half-range Maxwellian, representing complete energy accommodation and isotropic emission. Computer runs have been made for Knudsen number Kn (mean free path divided by distance between plates) of 0.5 and 10 and for a temperature ratio T_1/T_2 of 0.7. Calculations will also be made for

Kn of 0.5 to 100 and T_1/T_2 of 0.5 to 0.9. The solutions obtained will be compared with the corresponding Krook solutions obtained by Schmidt and others.

D. Alpert
G. Arndt
T. C. Casale
D. Eisenman
S. Y. Ettinger
J. Hanson
D. A. Lee
E. M. Lyman
D. Turner

5.1. Broad-Area, Single-Crystal Copper Electrodes.

As a continuation of previously-reported experiments with single-crystal tungsten electrodes, the breakdown voltages and volt-ampere characteristics of single-crystal, electropolished copper electrodes of 3 cm diameter at a pressure of 10^{-9} Torr have been studied at four gap spacings. In order to increase the breakdown voltages characteristic of untreated surfaces, Argon gas was admitted to a pressure of 10^{-4} Torr in order to blunt the cathode whiskers by selective sputtering. The sputtering was done with a steady field-emission current of about 100 μA. After evacuation of the gas, the voltampere data and the breakdown voltages were obtained as shown Table I. Column 1 describes the experimental condition of the electrodes; column 2 gives the voltage for a visible spark; column 3, the field-enhancement factor β, at the tips of whiskers on the cathode, as obtained from the Fowler-Nordheim plots of log $1/V^2$ vs I/V; column 4, the field at the whisker tips at the breakdown voltage and column 5, the average field in the gap.

Data in Table I were taken with the anode at liquid nitrogen temperature and the cathode at room temperature. The pressure was 10^{-9} Torr. The runs are shown in sequence. (A number of intermediate runs are not included.) From this table it may be concluded for the copper electrodes that

1) Gas conditioning of the electrodes results in an improvement of about 3 in the voltage-holding capability.

Table I. Vacuum-insulation properties of flat single-crystal copper electrodes 3 cm in diameter.

	(1)	(2) V_{BD} kV	(3) β	(4) F_{crit} MV/cm	(5) F_{ave} MV/cm
Gap = 0.51 mm					
1.	New, baked out, first breakdown	24	-	-	-
2.	After a few sparks	39	108	85	0.76
3.	After gas conditioning	80	40	62	1.57
4.	Ratio: Row 3/Row 1	3.3	-	-	-
Gap = 0.71 mm					
5.	After gas conditioning	88	42	52	1.24
6.	After touching electrodes together	30	196	79	0.42
7.	After gas conditioning to 136kV at 2.03 mm gap	29	277	114	0.41
8.	After gas conditioning at 0.71 mm gap	82	52	60	1.15
9.	After 10 days at high vac, without conditioning	24.5	260	89	0.35
10.	After gas conditioning at 0.71 mm	75	-	-	-
Gap = 0.25 mm					
11.	After gas conditioning	46	27	50	1.81
Gap = 2.03 mm					
12.	After touching electrodes together	36	-	-	-
13.	After gas conditioning	150	88-100	65-74	0.74
14.	Ratio: Row 13/Row 12	2.8	-	-	-

2) Touching the electrodes together seriously lowers the breakdown voltage (row 6), but gas conditioning restores it (row 8).

3) Gas conditioning at a larger gap spacing (2.03 mm, row 7) is not effective in improving the breakdown threshold for a smaller gap (0.71 mm).

4) In all instances, gas conditioning at a given gap spacing restores the breakdown voltage to about the same value regardless of the cause of the previous deconditioning (touching, breakdown, long-term storage, or conditioning at a different gap spacing).

The behavior of the copper electrodes was much the same as for the tungsten electrodes except that for W, the ultimate breakdown voltage was somewhat higher than for copper (for example, at 0.71 mm, after anode outgassing and gas conditioning, V_{BD} = 116kV, β = 26). The copper anode was not outgassed, yet reached a higher value of V_{BD} (88kV) than did the baked, but unoutgassed W(59kV).

The critical field at the tips of the emitting whiskers on the copper cathode as determined by the Fowler-Nordheim plots, varies from 11.4 to 5.0×10^7 volts/cm with a mean value of 7.2×10^7 volts/cm. Thus it is of the order of a volt per angstrom, as for tungsten.

The observations are consistent with the picture of initiation of electrical breakdown by the joule heating and subsequent explosion of one or more whiskers on the cathode. The data have not yet been analyzed to see if anode spot heating could explain the initiation at low values of β, as predicted by Chatterton, and Charbonnier et al.

5.2. Beta 3--A Program for Plotting the Fowler-Nordheim Curve and Calculating β.

A program has been developed which computes from current-voltage, field-emission data, the enhancement factor β and the critical field at the emitter tips. The I-V data are plotted in the form log I/V^2 vs $1/V$. It is assumed on the basis of the Fowler-Nordheim theory that ideal data should lie on a straight line, the slope of which is used in computing β. The computer finds a line using a least-squares fit of the observed data. For experimental situations, however, data do not lie on a straight line, but instead curve up at the higher values of 1/V due to instrumental difficulties. The program must, therefore, eliminate those points which lie in this region of curving up in order to obtain a line representative of the emitter characteristics. The program does this by successively computing lines and standard deviations of the points used in calculating these lines then eliminating all points beyond 1.7 times the standard deviation. The program continues to do this until a single iteration produces a change in the slope of the line less than .5%. It then replaces all points within 3 times the current standard deviation to ensure that there are enough points used in computing the line and that the line is representative of the bulk of the data. To prevent the replacement of too many points, the slope of this new line must not deviate more than 1.5% from the last one computed, otherwise no points are replaced.

In the second part of the program, β and the critical field are calculated. In the final portion of the program the data, along with a heading and the final computed line are displayed on a CRT display unit

for an immediate visual check on resonableness of the computer's selection of a representative line through the data.

5.3. Study of Whisker Formation With the Field-Emission Microscope.

Using high-purity-tungsten tips, we have looked for the growth of whiskers at high fields and ultrahigh vacuum, as indicated by changes in the patterns appearing on the screen of the field-emission microscope. For a clean tungsten tip at room temperature, we have not yet seen a case of whisker formation at pressures of 10^{-10} Torr and fields up to 7×10^{7} volts/cm. On the other hand, on tips on which there is adsorbed gas or some other form of impurity, the patterns show flicker spots and occasional flashes, often accompanied by gross changes in the patterns. The new patterns (whose features are revealed by cleaning the tip by heating) may be interpreted as arising from new whiskers. The field-emission current in the above case is highly erratic. More investigation will be required to relate the effects observed with their causes.

For all the tips, both clean and contaminated, observed in this set of experiments, the Fowler-Nordheim plots are straight lines with no evidence of sharp bends as reported by some other investigators. An interesting and as yet unexplained instability in the field-emission current from a tip has been observed; for applied fields less than about 5×10^{7} volts/cm (measured on a clean tungsten tip), the emission current drifts downward toward an asymptote as small as 10% of the initial current. The time constant is of the order of tens of minutes. For applied fields greater than 5×10^{7} volts/cm the current rises. This affect occurs at room temperature, at 10^{-10} Torr, for both clean and contaminated tips.

5.4. Cylindrical Field-Emission Microscope for Studying Whisker Formation.

A cylindrical field-emission tube having special features which will permit an interaction between the cathode and anode at high fields is under construction. The fine tungsten center wire is surrounded by a small moveable cylindrical anode, so that, after the interactions have taken place, the tube can be moved aside to permit the field-emission pattern of whiskers on the wire to be observed on the fluorescent screen.

5.5. Apparatus for Direct Observation of Whisker Formation in an Electron Microscope.

Our first attempt to observe whisker formation under high fields on electrodes placed directly in the specimen chamber of an electron microscope was not successful, because the EMU-2 microscope then available to us had insufficient resolution. The experiment will be repeated using a Mikros EM-20 electron microscope. The new apparatus to be inserted into the specimen chamber is under construction.

5.6. A Cryogenic High-Voltage Breakdown Experiment.

A high-voltage breakdown experiment between broad-area and electrodes at liquid-helium temperatures is in the initial design stage.

W. J. Bouknight
E Brachhausen
D. H. Cooper
J. D. Gooch
K. Hasz
L. Hickok
J. Hsu
G. R. Karr
B. D. Kirkwood
H. W. Knoebel
H. V. Krone
N. Mehta
J. L. Myers, Jr.
D. O. Skaperdas

6.1. Accuracy Considerations in the Relativity Experiment[†].

6.1.1. General Requirements.

Recent discussions with Prof. R. H. Dicke have lead to a reappraisal of the accuracy requirements of the relativity experiment, to suggest that the goal ought to be one of achieving an accuracy at least comparable to that of the observation of the relativistic precession of the orbit of the planet Mercury, namely an accuracy of about 1%.

Of all the prior tests of the theory of relativity that give information about the space-like part of the theory (space-like part of a Schwarzschild-like metric), the Mercury precession provides the most accurate data. The only other experiments which are of comparable accuracy are principle-of-equivalence or red-shift tests, but these test only the time-like aspects. Actually, the Mercury-precession observations test a certain combination of time-like and space-like aspects, but the time-like aspects of the theory have been sufficiently accurately confirmed by the red-shift experiments, that is reasonable to take the view that a need for independent tests of the space-like aspects now commands a high priority. The spin-axis precession of the orbiting gyro provides the opportunity for just such an independent test of the purely space-like aspects of Einstein's general theory of relativity.

[†]This work was supported in part by the National Aeronautics and Space Administration under Grant NsG 443.

The need for such an independent test has been heightened by the development of new experimental evidence showing that the nonrelativistic part of Mercury's orbital precession may be greater than hitherto believed, leaving a relativistic part which is smaller by some 8% than that predicted by Einstein's theory. The experimental evidence is a new measurement of the oblateness of the sun (formerly thought not to be significantly oblate) sufficient to account, on classical grounds, for the mentioned increase in the nonrelativistic part of the precession. These measurements were directed by Dicke,[1] who argues that the result suggests that the theory may need to be modified by including a scalar term along with the present tensor terms in the theory. Such a modification would also result in a nearly 8% shift in the theoretical prediction of the spin-axis precession of the orbiting gyro. Whatever the exact theoretical interpretation such a discrepancy, if real, may require, the challenge to the Einstein theory would be serious and would demand independent testing.

Prior to the present reporting period, the studies of feasibility for the orbiting-gyro experiment have been aimed at showing that the naked-gyro version using passive readout could achieve a 10% accuracy. This figure had been chosen for the sake of definiteness as one that seemed achievable on the basis of preliminary estimates. The individual parts of these studies, however, have not been so sharply constrained by this figure. Indeed, it appears possible to interpret the results as bearing on the feasibility of a much more ambitious accuracy figure, such as 2% or even 1%. In the present terminal phases of the feasibility study,

---

[1] R. H. Dicke and H. M. Goldenberg, "Solar Oblateness and General Relativity," Phys. Rev. Letters, 18, 313 (27 Feb 1967).

these more-demanding interpretations will be made, to determine the feasibility of an experiment sufficiently accurate to measure a possible 8% departure from the Einstein prediction.

D. H. Cooper

6.1.2. Error Propagation During the Experiment.

As an example of the extended interpretations cited above, consider the effect of various running times for the experiment in relation to random observation errors for the spin-axis position. Roughly speaking, the experimental error decreases with increasing running time because of two factors. One is that the time base for measuring the rate of change in spin-axis position becomes longer, decreasing the effect of errors in position measurement, and the other is that the number of position measurements that may be made increases. The two factors combine to make the rate error vary as the inverse three-halves power of the running time.

The exact numerical relationship for a hypothetical model of data-reduction procedures is shown in Fig. 6.1. In this consideration, the expected spin-axis precession rate, about 5 seconds of arc per year, is denoted by ω, to be measured with an error ϵ_ω, from position measurements each having an error ϵ_θ. It is assumed that the position measurements are made each week as a compil[illegible]he observational data collected during that week. This is a reasonable assumption, since the angular position would change by only 2% of its annual motion during such an interval, while the random error inherent in a week's data might run to 10% of the annual motion. Thus a data interval of one week would be an essentially stationary interval. In any case, the model is that of a position measurement with error ϵ_θ made once per week with a probability p.

(OVERLEAF BLANK)

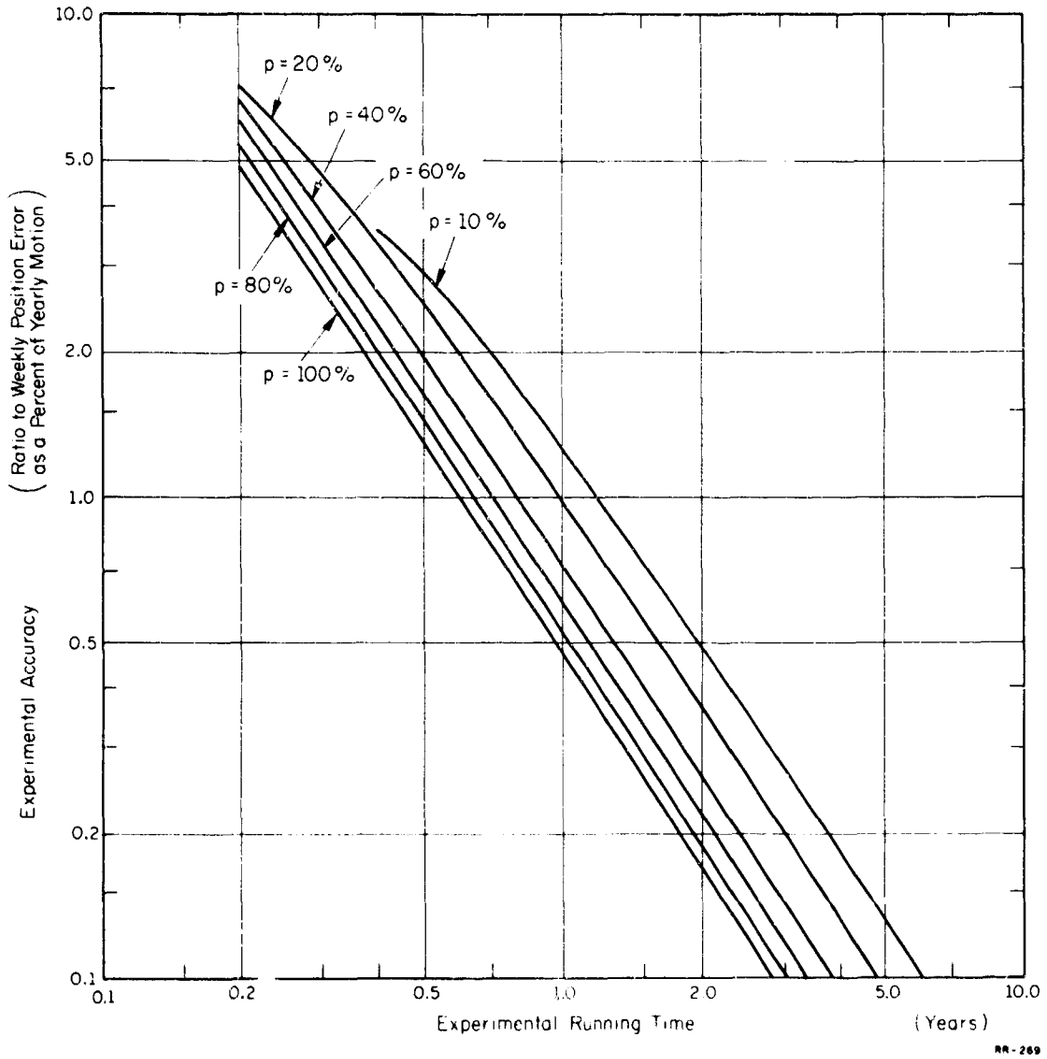

Fig. 6.1. Percent error in the experimental value of the relativistic precession as a function of the running time in years and of the probability p of each week's position data reaching a certain standard of accuracy. The percent error in the precession is given as the ratio to the standard of accuracy for the week's position data expressed as a percent of the yearly motion. Logarithmic scales are used (the tic mark between 0.5 and 1.0 is placed at 0.7).

(OVERLEAF BLANK)

The probability p that a measurement with error ϵ_θ would be made is introduced to make allowance for the possibility that not all weeks will produce data with such a small error. What should be done with the data from the poorer weeks is the combining of them with the rest of the data using weights that are inversely proportioned to the errors for each datum, so that all of the data would be used in a statistical-fitting procedure. In the actual experiment this would be done, but the model is simplified here to assume that the "bad" data are simply discarded, and that the "good" data, obtainable with probability p, are given equal weight in the fitting procedure.

Such a model is easily analyzed, and the results of the analysis is presented in Fig. 6.1. Plotted versus the experimental running time in years, the rate error ϵ_ω is given in units of the weekly position error ϵ_θ for various values of p. For example, if 100% of the weeks give position data with an error ϵ_θ which is 10% of the yearly motion, then the rate error ϵ_ω will also be 10% of the expected rate for a running time of 0.6 year. On the other hand, if the rate error is to be 2% for the same quality of weekly data, the experiment would have to run for 1.8 years. Again, if only 10% of the data were usable, and a 1% experiment were to be done, 6 years would be required. A likely condition, however, is that the weekly data will be accurate to about 10% of the yearly motion, with a probability near 70% and that a two-year run will seem reasonable; then the rate determination would be accurate to about 2%.

D. H. Cooper

6.1.3. Estimator Trials of Spin-Axis Readout Accuracy.

The computer-based simulation of procedures for estimating the center of noisy photographic images, as described in the preceding report,[2] has been exercised with realistic data during the present reporting period. The noise standard-deviation data, reported previously,[3] as measured for red-extended Royal-X Pan photographic film, were used in conjunction with density-vs-exposure data, supplied by the Smithsonian Astrophysical Observatory and representing standard processing conditions; see Fig. 6.2.

Starting from a night-sky density value of 0.305, as representing a zero-signal condition, the program interpolated in the data of Fig. 6.2 to convert exposure values, throughout the image, to density values to follow the semicircular exposure curve and to achieve specified density values at the center. Then, for each point along the programmed exposure curve, the previously reported data[3] were used to determine the mean and standard deviation in opacity, so that random values of opacity, obeying the previously described distributions[4] fitting these means and standard deviations could be generated. The noisy image so constructed was then convolved with the weighting function of the center estimator to find the center, to complete one trial. A large number of statistically independent trials were made to collect data on the mean value of the estimated center in addition to its root-mean-square value (standard deviation). The means were always negligibly small, as to be expected

---

[2] Progress Report for Sept. 1966-Feb. 1967, Coordinated Science Laboratory, University of Illinois, pp. 93-108.

[3] Ibid., Figs. 6.5 and 6.6.

[4] Ibid., pp. 95-99.

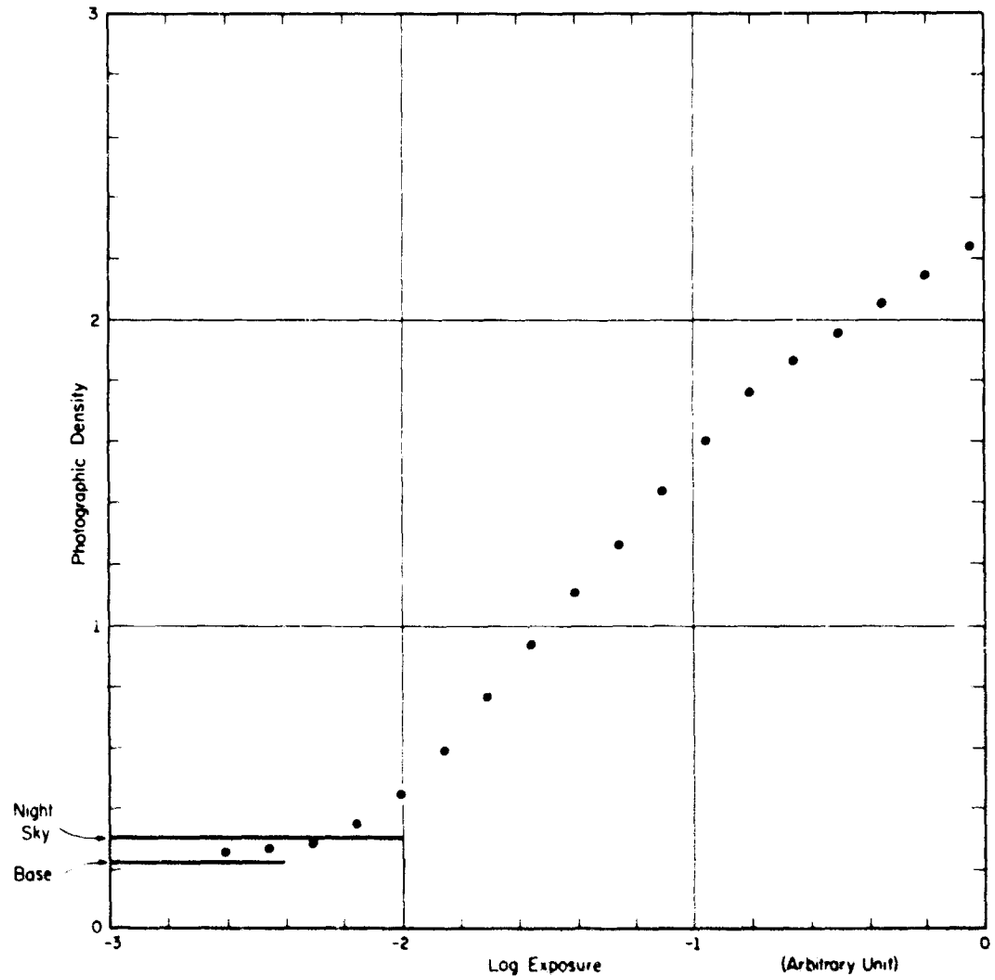

Fig. 6.2. Density-vs-exposure data for Royal-X Pan photographic film. These data, supplied by the Smithsonian Astrophysical Observatory characterize the standard film and processing conditions for use with the Baker-Nunn cameras in the St Satellite Observing Net. The exposure scale is in arbitrary units which may be calibrated by reference to the night-sky density, since the camera sensitivity is known as producing a 0.3-to-0.4 density increment above night sky for an input at its aperture of 8×10^{-11} lumen sec m^{-2}.

(OVERLEAF BLANK)

with unbiased estimators, so that such data provide only a kind of a check on the procedures, the principal accuracy data being the standard deviation of the estimations.

Various estimators, represented by various weighting curves, were tried, starting with a truncated center-of-gravity estimator. For each estimator, statistics on 100 trials were collected for central densities 0.30, 0.35, 0.40, 0.45, 0.50, 0.55, and 0.60 density units above "night sky," as defined above. The results may be seen plotted in Fig. 6.3, in which the abscissa is the central exposure value, relative to an exposure giving a 0.3 density increment above night sky. The ordinate shows the rms accuracy as a percentage of the whole image width.

The results of different kinds of departures from center-of-gravity weighting may be seen, principally those resulting from assigning zero weight to the central interval, and those which result from "peaking-up" the edges of the weighting pattern. Generally, the suppression of the central interval is beneficial, especially if it is accompanied by edge peaking. For example, the poorest estimator supresses the central interval but gives uniform weight in the edge intervals, whereas one which also suppresses the central interval, but gives a linearly increasing weight to the edge, is better than the center-of-gravity estimator. Of those tried, the ones peaking the edges with second-order curvature are the best. The introduction of curvature in this manner, combined with central-interval suppression, provides improvements which are slight enough, however, to suggest that further adjustments will prove marginal and that further explorations probably need not be undertaken.

(OVERLEAF BLANK)

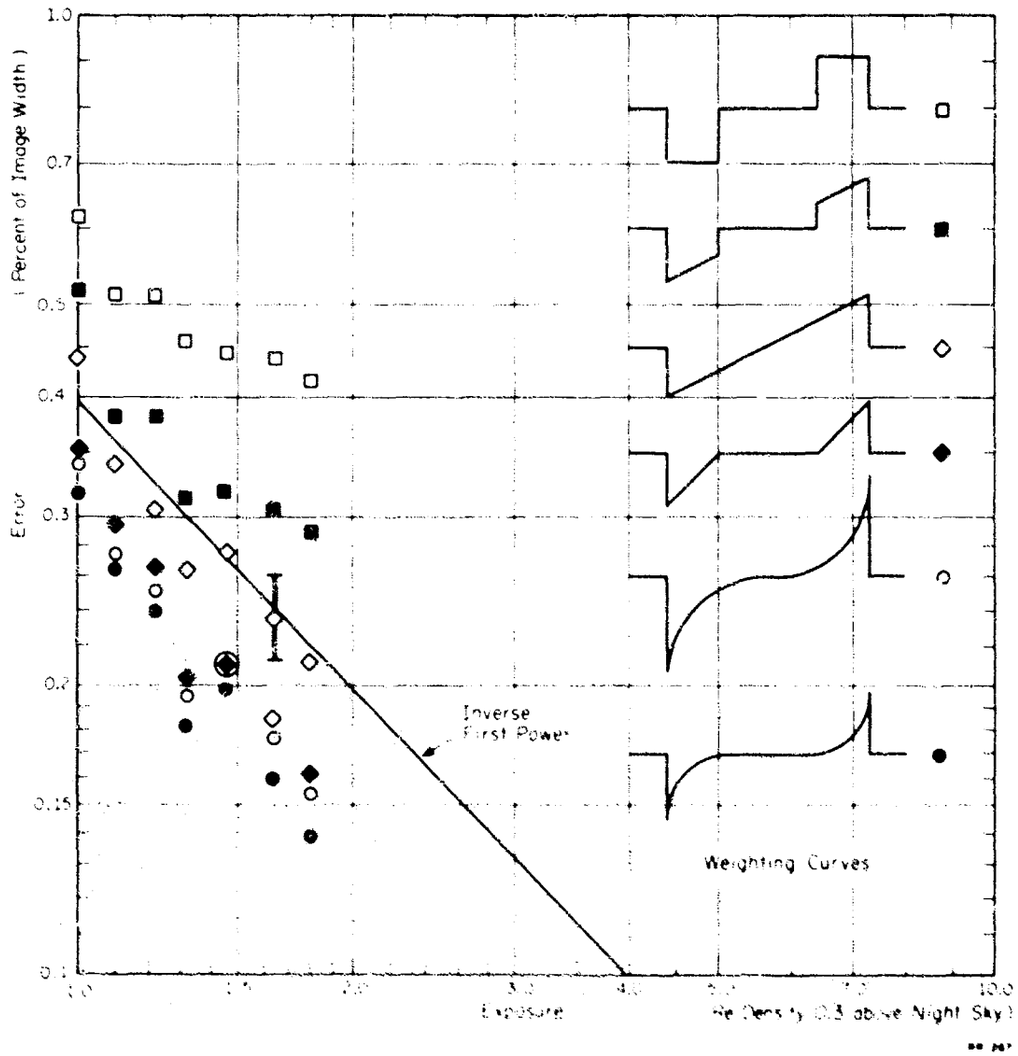

Fig. 6.3. Error in estimating center as a function of exposure at the center for various weighting functions used in the estimator. It is seen that the departure from the center-of-gravity estimator (open diamond) that suppresses a central interval and provides a second order edge peaking is the most effective. The error symbol shown for one of the points has the same size, on these logarithmic scales, for all the points and represents the statistical uncertainty associated with 100 trials for each point.

(OVERLEAF BLANK)

Studies with improved statistics (1000 trials for each point) were undertaken to explore the consequences of reduced flash rate. For this simulation, the best estimator of Fig. 6.3 was used, and the program was asked to delete half the points uniformly throughout the image, so that the accuracy data could be compared with that for no such deletion. The comparison is shown in Fig. 6.4. The results agree so well with the expected square-root-of-two loss that no further studies of this factor need be made.

Also from Fig. 6.4, it may be seen that the accuracy improves more rapidly than linearly with exposure, for these small exposures, but the improvement with exposure tends to be slower at the higher exposures. This last point requires further exploration. In preparation for this, film-noise statistics corresponding to greater densities are being obtained.

D. H. Cooper
W. J. Bouknight

6.1.4. Overall Readout Accuracy.

The data of the preceding section may be used to estimate the overall readout accuracy. In keeping with tightened demands for precision, the following discussion will be based on an assumed satellite diameter of 0.6 m. This is twice that formerly considered, so that the assumed spin rate will necessarily be 50 Hz, or half the former rate, and the facet areas will be 944 cm^2 each, or quadruple the former areas. Further, the exposure time for photographing each flash will be 14 μsec, or twice the former time, because of the reduced spin rate. On the same

(OVERLEAF BLANK)

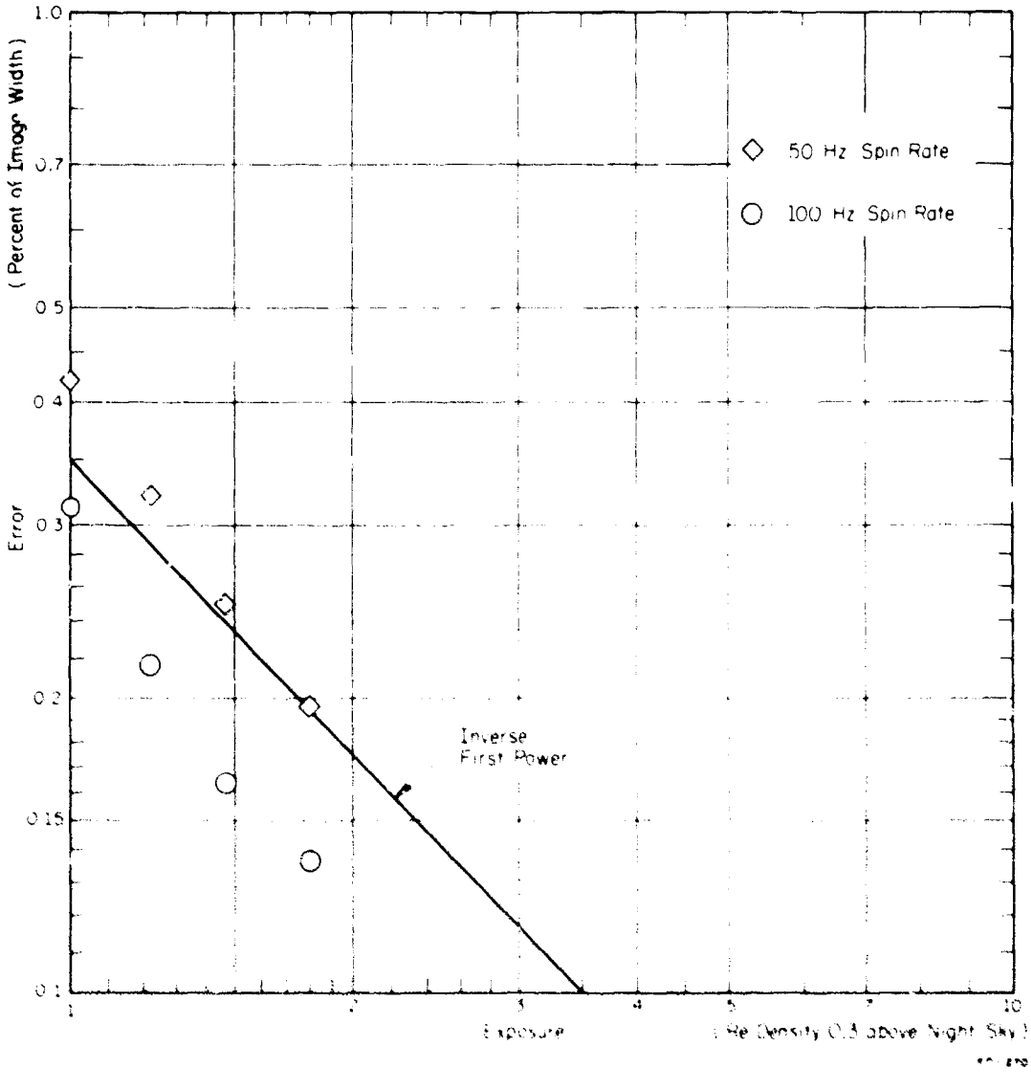

Fig. 6.4. Effect of reduced flash rate. The open circles represent data for the conditions obtaining for the lowest-lying points of Fig. 6.3, but based on 1000 trials. The number of flashes in the image corresponds to a flash spacing equal to the resolution of the camera, a spacing corresponding to a 100-Hz spin rate and a slant range of 2500 km. Deleting half the points (open diamonds) simulates the reduction of spin rate to 50 Hz. The size of the plotting symbols represents the statistical uncertainty.

(OVERLEAF BLANK)

basis of calculation reported previously,[5] the photographic-exposure value corresponding to a slant range of 2500 km, and using the full mirror aperture, would be 4×10^{-10} lumen-sec/m^2 at the lens of the Baker-Nunn cameras. This value is five-fold greater than the "threshold value" capable of producing a density increment of 0.3 to 0.4 above "night sky."

The data of Fig. 6.4 corresponding, for the lowest set, to a flash spacing at 2500 km corresponding to a 100-Hz spin rate, while the upper set would be for 50 Hz. The upper set indicate an inverse first-power dependence of error upon exposure as the trend at the higher exposure values, the error 0.1% being for an exposure 3.5 times as great as that needed to achieve a density 0.3 units above "night sky." Further extrapolation to the factor 5 would bring the error to 0.07%. These percentages are based on the full image width of some 1800 seconds of arc, so that the corresponding angular rms error is about 1.3 seconds corresponding to a probable error of 0.85 second.

For a given error in estimating the center of an image, the error in estimating the mirror-normal orientation is only half as great. On the other hand, three independent measurements of a mirror normal are needed to locate the spin axis. These combine in such a way that the probable-error circle has a radius which is twice the error for locating a mirror normal, for normal locations that are widely spaced. Thus, it would appear that a single triad of observations would locate the spin axis with a probable error of 0.85 second of arc. If in a week's time, 9 such triads may be obtained (27 observations), the accuracy corresponding to a week's data would be about 0.3 second of arc.

---

[5] Progress Report for March-August, 1966, Coordinated Science Laboratory, University of Illinois, p. 108.

6.2. Observability of Relativity Satellite†.

6.2.1. Effects of Orbit Inclination.

In the previous Progress Report[7] a digital-computer simulation which predicts possible flash-angle distributions for a gyroscope satellite in earth orbit was described. This satellite-observation program (SATOBS) produces flash-angle information as shown in Fig. 6.1 of ref. 7 and reproduced here in Fig. 6.5(a) for convenience. In this figure, each vertical line represents a pass of the satellite over the observing station, and the length and vertical position of the line indicates the range of mirror-normal angles on the satellite which would reflect sunlight to the station. As seen in the figure, the length and position of the vertical lines change as a function of time. It is also evident that the pattern falls within two envelopes, one for morning and one for evening observations. At the times of the equinoxes, day 81 and day 265, the two envelopes overlap.

Figure 6.5(a) is for a zero-inclination (equatorial) orbit. The effects of inclining the orbit with respect to the equator are shown in Fig. 6.5(b) and (c), which are for orbital inclinations of five and ten degrees, respectively. As seen in the figure, the regression of the orbit line of nodes modulates the flash-angle envelope at the nodal regression frequency of about six cycles per year. The amount of modulation depends on the sum of the station latitude and the orbit inclination. For example, in the case of a 1000-km orbit altitude, the maximum

---

†This work was supported in part by the National Aeronautics and Space Administration under Grant NsG 443.

[7]Progress Report for Sept. 1966-Feb. 1967, Coordinated Science Laboratory, University of Illinois, pp. 81-87.

(OVERLEAF BLANK)

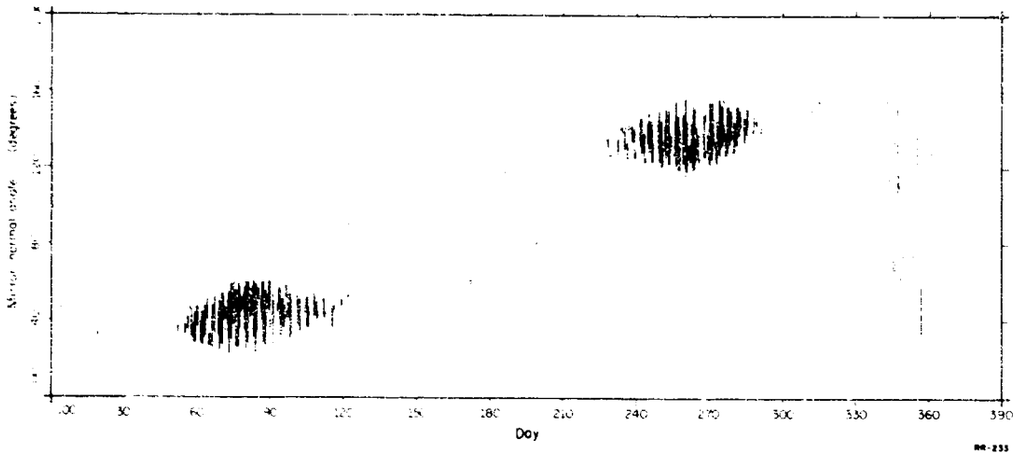

(a) Orbit inclination = 0°

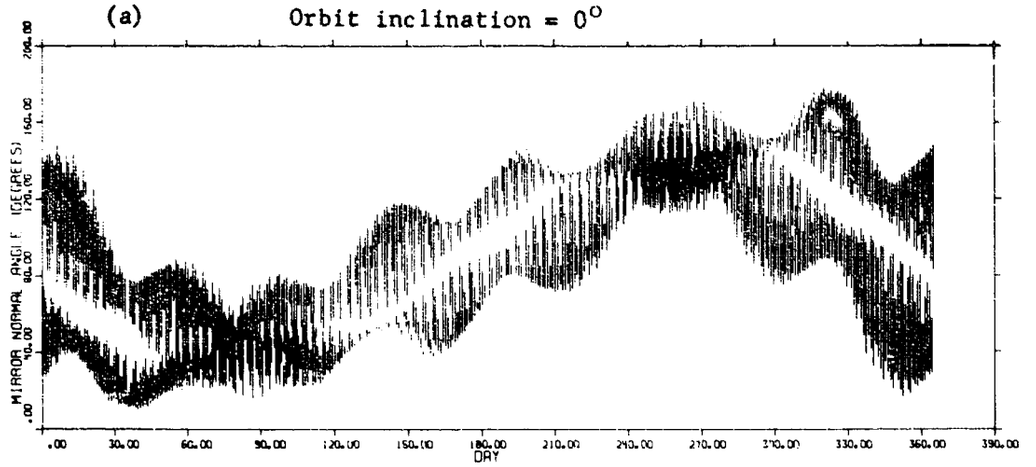

(b) Orbit inclination = 5°

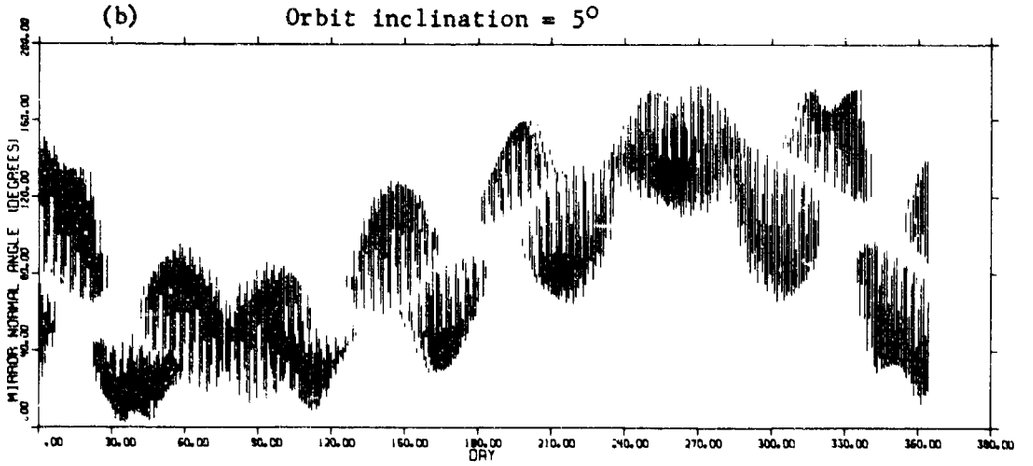

(c) Orbit inclination = 10°

Fig. 6.5. Flash angle distributions for tracking station Curacao, position 12°N, 291°E. The data are for circular orbits of 1000-km altitude, satellite spin axis along the vernal-equinox line.

(OVERLEAF BLANK)

allowable angle between the earth-station vector and satellite vector is 18.4° assuming a 15° lower limit on the elevation of the Baker-Nunn tracking camera. This means that whenever the angular distance between the earth station and satellite is greater than 18.4°, no observation is possible. Therefore, given the station at Curacao, latitude 12°, an orbit inclination of 6.4° would give "100-percent modulation." The modulation is less than 100 percent for inclinations of 0° and 5° as seen in Fig. 6.5(a) and (b), and for the 10° case, Fig. 6.1(c), the modulation is "greater than 100 percent" and the flash-angle envelope exhibits gaps at periodic intervals.

From the above discussion, it is evident that tracking stations having latitudes in excess of 18.4° are useless for tracking a satellite in a 1000-km equatorial orbit. Of course, these stations can be used for inclined orbits or orbits of higher altitude. Figure 6.6(a) and (b) show flash-angle distributions for a station in Hawaii, latitude 20.7°, orbit inclinations 5° and 10° respectively. It is seen that for this station, the observing frequency increases with orbital inclination.

Program SATOBS was also run for non-circular orbits with low eccentricity. As could be expected, eccentricities of .01 and .02 produced very small changes in the flash angle distributions. Since these values of eccentricity are easily attainable with present launching techniques, all future discussions of the relativity satellite will assume circular orbits.

6.2.2. Envelope of Observability.

An inspection of Figs. 6.5 and 6.6 shows that the flash angle distribution patterns are bounded by envelopes. The boundaries may be

(OVERLEAF BLANK)

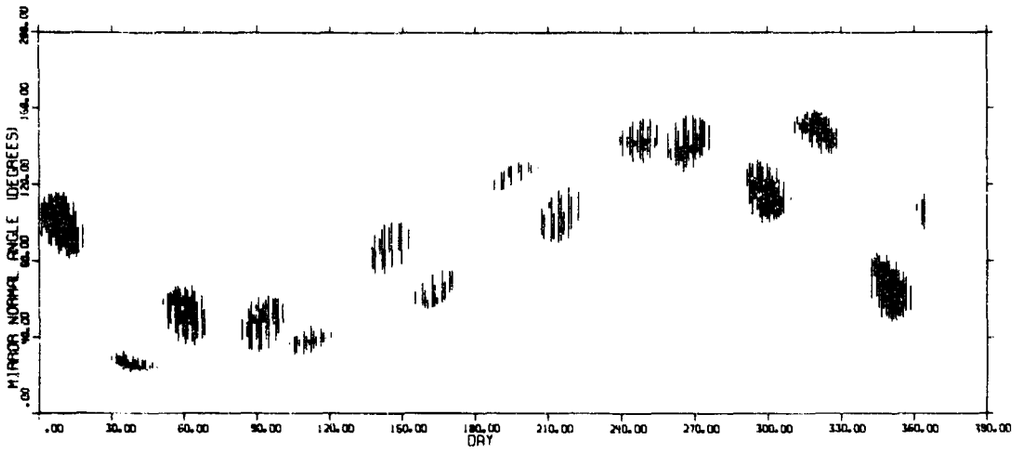

(a) Orbit inclination = 5°

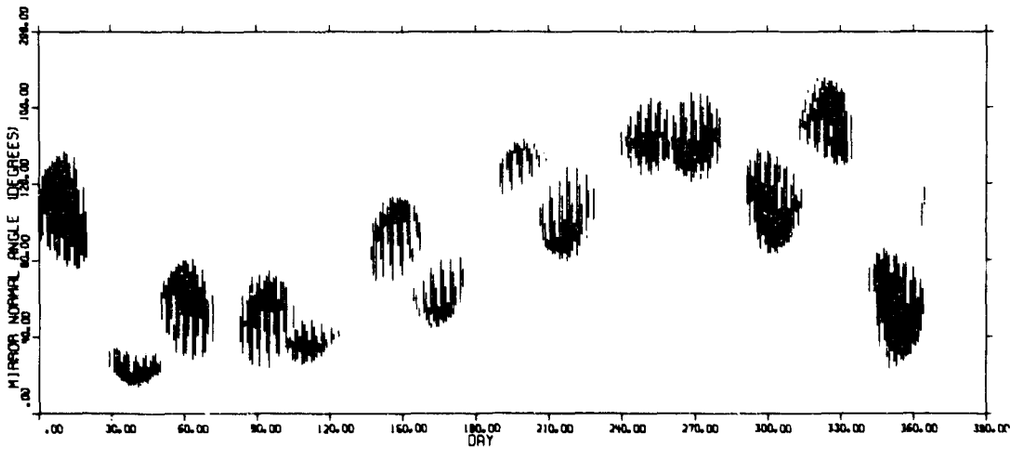

(b) Orbit inclination = 10°

Fig. 6.6. Flash angle distributions for tracking station Maui, Hawaii, position 20.7°N, 203.7°E. Data are for circular orbits of 1000-km altitude, satellite spin axis along the vernal-equinox line.

(OVERLEAF BLANK)

determined by finding the maximum and minimum values of the flash angle as a function of time. The resulting envelope is called the envelope of observability (EO) because observations giving spin-axis data are possible only from mirrors whose normal angles lie inside the envelope. A digital computer program, ENVO, has been developed to find the EO for any given orbit and station conditions. The program takes about five minutes to run a complete case on a CDC-1604 computer at CSL, compared to 30-40 minutes for program SATOBS to run the same case. The EO is computed in the following manner: given the station latitude and longitude, satellite orbit altitude, inclination, initial right assension, spin-axis direction, and time, radius vectors are computed from the center of the earth to the sun, satellite, and earth station. The cosine of the flash angle is computed and maximized with respect to two angles, x_1, the station longitude measured from the vernal equinox line and x_2, the argument of the satellite, measured in the orbital plane from the line of nodes. All other angles are fixed by the initial conditions and time. At the same instant of time, the minimum of the cosine is also determined. These two extremes give the minimum and maximum of the flash angle.

Of course, the optimization of the cosine function is constrained by the same three conditions necessary for an observation as were used in SATOBS,[7] namely, earth station in darkness, satellite in sunlight and station-to-satellite line of sight more than 15° above the horizon. In ENVO, these three constraints are based on angles y_1, y_2 and are formulated as penalty functions which are added to the authentic trigonometric expression whenever one or more of the constraint angles are outside the prescribed limits.

In general, observations are possible in the morning and evening of each day and thus two envelopes are produced. The initial conditions on x_1 and x_2 determine which of the two envelopes is to be followed. Figure 6.7 is an EO produced by ENVO, with points computed about four times a month, or every 7.5 days. These envelopes compare reasonably well with the SATOBS output in Fig. 6.5(a).

Either the flash angle distribution of Figs. 6.5 and 6.6 or the EO of Fig. 6.7 may be used to determine the effectiveness of a particular mirror mounted on a spinning satellite. In the former case one simply counts the number of vertical lines intersected in a year's time by the chosen flash angle. This is accomplished very rapidly by another computer program, COUNT. The same results can be obtained by counting the number of days the particular flash angle is within the EO and multiplying by the average number of passes per day. As stated earlier, ENVO runs nearly 10 times as fast as SATOBS, so the EO method will be pursued in the optimization of orbital parameters for the relativity satellite.

J. L. Myers, Jr.

6.3. Solar Radiation-Pressure Torque[†].

The work reported in the previous Progress Report included results for the precession of the CSL relativity satellite in an equatorial, nonregressing orbit. During this period, the computer program used to calculate the solar-radiation-pressure-induced precession has been extended to include the effects of orbital regression and advance of perigee for arbitrary values of orbital inclination. These correction

[†]This work was supported in part by the National Aeronautics and Space Administration under Grant NsG 443.

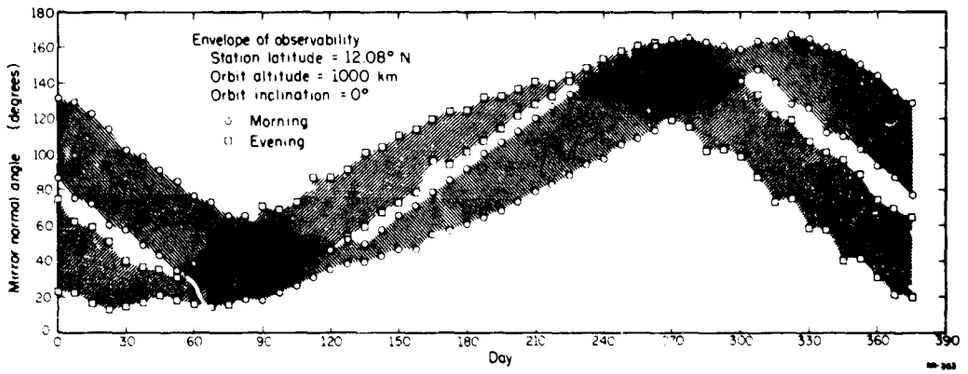

Fig. 6.7. Envelope of observability for station at Curacao, position 12°N, 291°E. Satellite spin axis along vernal-equinox line.

(OVERLEAF BLANK)

terms are, for advance of perigee

$$\Delta\omega = 3\pi J_2 (R/P)^2 (2-5/2\sin^2 i),$$

and, for orbital regression,

$$\Delta\Omega = -3\pi J_2 (R/P)^2 \cos i,$$

in units of radian per second, where R is the radius of the earth, P is the semilatus rectum, i is the orbital inclination, and J_2 is the second coefficient of the potential function. The principal effect of the introduction of these rates is to change the amount of time the satellite is in the earth's shadow.

Since the orbit is regressing, the angular movement of the satellite spin axis is now to be referred to an earth-fixed inertial set of coordinates. Although the computer program is now working correctly, complete results are not yet available for publication. Preliminary results, however, indicate that the magnitude of the satellite precession is approximately the same as for the nonregressing case. This is to be expected since the percent of time in sunlight is essentially all that is changed from the nonregressing case.

Some differences from the nonregressing case are expected for inclined orbits because the satellite spin-axis orientation with respect to the sun will then be changed.

G. R. Karr

6.4. Infrared Absorption of Atmospheric Trace Constituents.

A series of balloon-borne experiments for measuring the amounts of various upper-atmosphere trace constituents, with special emphasis on nitric oxide, is being proposed. In order to determine the

absorption sensitivity of the proposed system for NO, a laboratory experiment was performed to measure infrared absorption of its individual rotation-vibration lines in the 5.3-micron region. The results of this measurement were compared with those of a very-high-resolution experiment conducted with larger concentrations of NO.[8]

The total IR absorbance A of an absorption line for a small quantity of gas can be calculated from the Beer-Lambert relation,

$$A = (S/2\gamma)bc = (bc/2\gamma)\int_{band} k(\nu)\, d\nu, \qquad (1)$$

where $k(\nu)$ is the absorption coefficient of the line of strength S, b is the gas path length, c is its concentration and γ is the line half width. The function $k(\nu)$ can be accurately represented by a Lorentz curve whose width γ is a function of pressure and temperature. The equation was used to calculate the expected IR absorption under the conditions of the laboratory and proposed balloon experiment. The quantity of gas involved in both experiments is small enough to satisfy conditions where Eq. (1) is valid.[9]

The NO diatomic molecule is unique in that it has a Q-branch or central absorption line which is stronger than its other lines. The line spacings are about 3.6 cm^{-1}, the half widths γ are about 0.05 cm^{-1} atm^{-1} and the strength S of the combined Q-branches is about 3 cm^{-2} atm^{-1} (Ref. 8). In order to obtain a correct value of a line absorbance A, the spectral slit width $\Delta\nu$ of the IR spectrometer must be smaller than the line half width γ, which is shown as follows.

---

[8] L. L. Abels and J. H. Shaw, Journ. Molec. Spectrosc. 20, 11-28 (1966).

[9] W. M. Elsasser, "Heat Transfer by Infrared Radiation in the Atmosphere," Harvard University Press, 1942.

The transmission T is defined by

$$A = \mathrm{Log}_{10}(1/T)$$

from which one obtains

$$T = \exp(-2.3A),$$

so that from Eq. (1) there results

$$T = \exp(-2.3\ Sbc/\gamma) \quad . \qquad (2)$$

The slit function of a spectrometer with equal entrance and exit slits and set at a fixed frequency ν_o is ideally triangular in shape and actually very closely approximates the Gaussian function

$$P(\nu) = P_o \exp[-(\nu-\nu_o)^2/\Delta\nu^2], \qquad (3)$$

where $P(\nu)$ is the spectrometer output power at ν, P_o is the output power at frequency ν_o, and $\Delta\nu$ is the spectral slit width, which equals the product of the spectrometer dispersion and slit width.

The total radiant power that reaches the detector when a spectrometer with a finite spectral slit width $\Delta\nu$ is set at ν and a sample having a Lorentz-shaped absorption at ν_o is placed in the beam, is the integral of the product of Eqs. (2) and (3) evaluated over the frequency range in which the detectable level of this power is larger than the noise level. The transmission T measured by the spectrometer set at ν_o is the above integral divided by the total power that would reach the detector if the absorbing material were removed from the beam. The result is

$$T = \int P_o \exp\{-[(\nu-\nu_o)/\Delta\nu]^2 - 2.3Sbc/\nu\}d\nu \Big/ \int P_o \exp\{-[(\nu-\nu_o)/\Delta\nu]^2\}d\nu. \qquad (4)$$

Equation (4) has been evaluated numerically[10] as a function of $A = \text{Log}_{10}(1/T)$ versus the product of concentration c and path length b for various values of $\Delta\nu/\gamma < 1.0$ (see Fig. 8). This clearly shows that unless $\Delta\nu/\gamma < 1$, the measured value of absorbance A must be corrected according to Fig. 6.8. A Beckman IR-9 spectrometer was used to corroborate and extrapolate the curves of Fig. 6.8 to $\Delta\nu/\gamma = 20$ for small initial values of A.

The spectral slit width for "state-of-the-art" spectrometers is approximately 0.1 cm^{-1}. The half-width γ of NO lines below one atmosphere pressure is not accurately known; however, even at one atmosphere, where $\gamma = .05\ cm^{-1}$, absorbance corrections according to Fig. 6.8 would be necessary. The half width γ is not well known for the low-pressure conditions of the laboratory or for the proposed balloon experiments. An approximate value was obtained, however, from the results of the laboratory experiments with low pressure cell.

The laboratory experiment used a Spex model 1700, 3/4-meter, f/6.8 Czerny-Turner-type spectrometer modified to operate in either the normal (integral) or derivative mode. A block diagram of the system is shown in Fig. 6.9. A blackbody source consisting of conically-wound nichrome wire within a cavity was operated at a temperature of 900°C over the face of the 3/8" aperture. A CaF_2 lens, L1, collimates the radiant flux which passes through a gas cell with sapphire windows. The gas cell is connected to a source of NO, a vacuum pump and a Pirani gauge, so that any pressure of NO could be adjusted within the cell. An f/6.8 CaF_2 lens, L2, focuses the blackbody aperture on the entrance slit, S1. When operated in the integral mode a piezoelectric chopper C is placed before S1.

---

[10] W. J. Potts, "Chemical Infrared Spectroscopy," Vol. 1, J. Wiley and Sons, 1963.

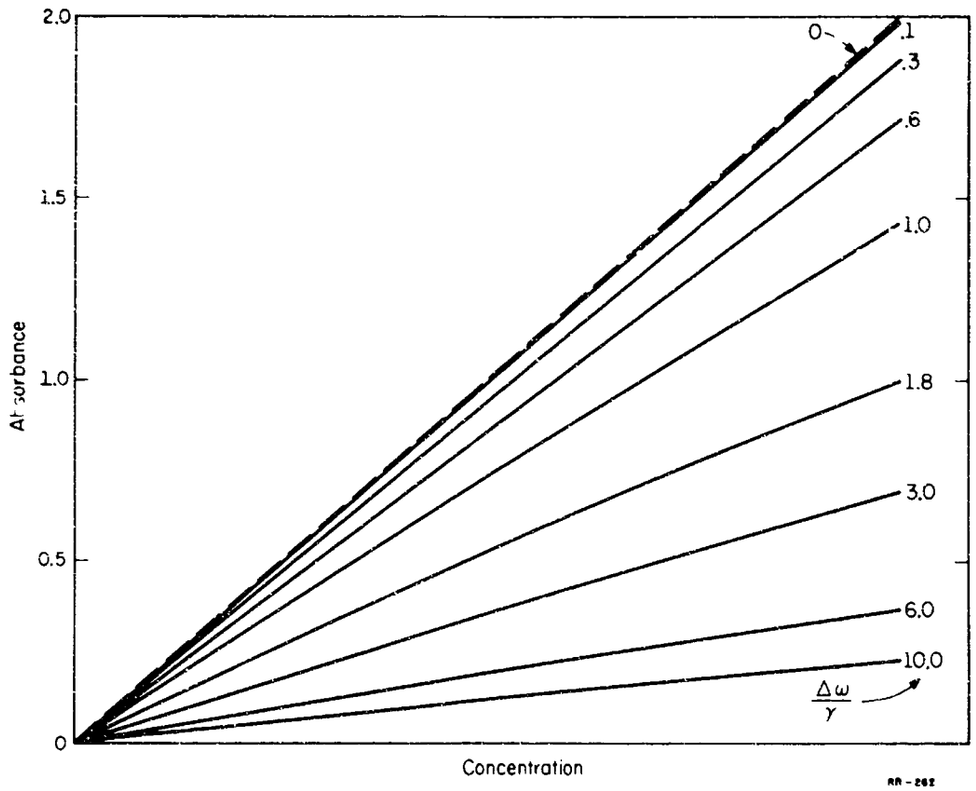

Fig. 6.8. Absorbance versus concentration for various values of $\Delta\nu/\gamma$.

(OVERLEAF BLANK)

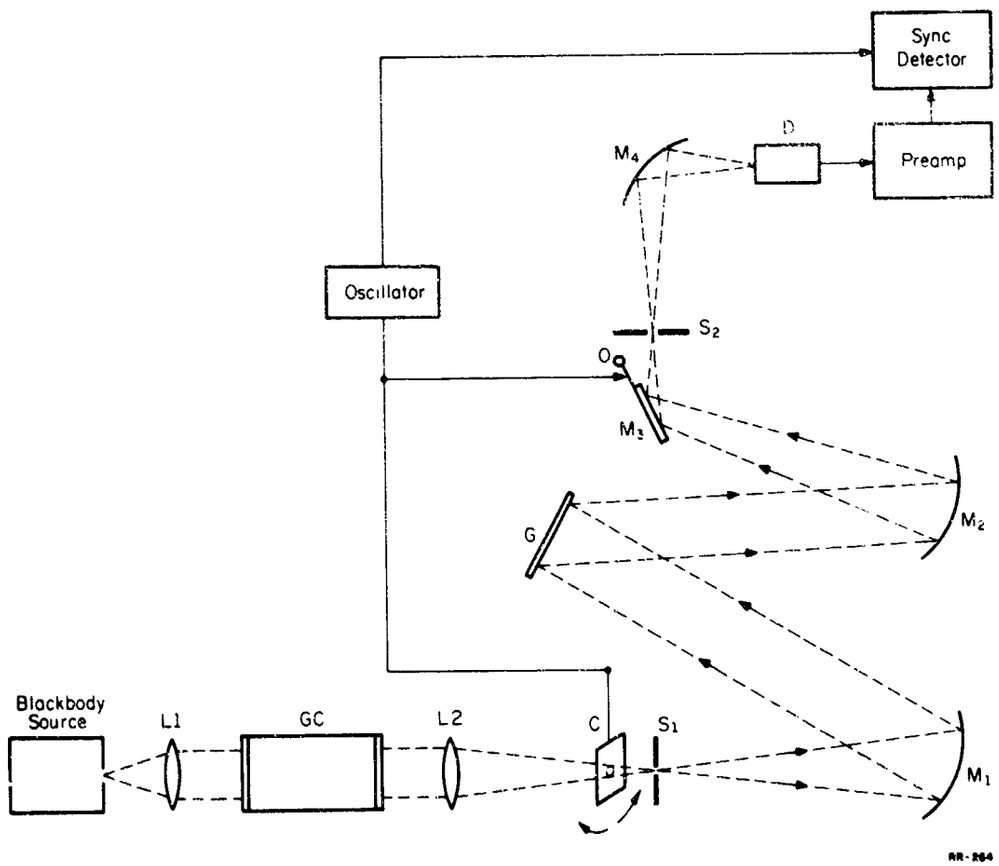

Fig. 6.9. Block diagram of laboratory experiment.

(OVERLEAF BLANK)

Grating G has 150 lines/mm, is 105mm×105mm, and is blazed at 4μ. Its dispersion is 2.85 cm^{-1}/mm so that for 0.2mm entrance and exit slits, the spectral slit width is 0.28 cm^{-1}. Instead of passing through the exit slit provided by Spex, the diffracted beam focused by mirror M2 is intercepted by a mirror fastened to a cantilever-mounted piezoelectric device (bimorph) placed close to the focus. When operation is in derivative mode, chopper C is removed, and the bimorph oscillates at a frequency and angular displacement determined by the oscillator frequency and voltage amplitude. The intercepted beam leaves the spectrometer sideways and is periodically swept across the exit slits S2, placed at the focus of the entrance-slit image. An ellipsoidal mirror is used to focus and reduce the entrance-slit image onto the sensitive area of the detector. This is a Texas-Instruments, indium-antimonide, photovoltaic detector with a non-cooled, narrow-bandpass, IR filter centered at 5.3μ attached to it for removing the higher-order diffracted terms. The specific detectivity $D^*(\lambda, 1000, 1)$ of the detector when operated at 77°K is 9×10^{10} cm $cps^{\frac{1}{2}}$ $watt^{-1}$, sured at λ = 5.3μ with the radiation chopped at 1000 cps and a noise bandwidth Δf = 1 cps. The output of the detector is fed to a PAR type-HR-8 synchronous detector with the Type-A preamplifier selected to match the detector output impedance. A portion of the oscillator output is used as a reference for the synchronous detector. The system was enclosed in a plexiglass box and purged with dry air in order to remove the large H_2O absorption band in the 5.3μ region.

With the system operating in the integral mode, enough NO was let into the gas cell to make an absorbance measurement at a reasonable S/N value. At a measured pressure P = 10 Torr the absorbance A = 0.15

was measured with S/N $\approx$ 40, an integration time τ = 3 sec and spectral slit width $\Delta\nu$ = 0.28 cm^{-1}. A Beckman IR-9 spectrometer with $\Delta\nu$ = 0.28 cm^{-1} was also used with another NO gas cell at 10 Torr to measure absorbance. The agreement with the Spex instrument was within 15%.

In order to make the data of Ref. 8 fit the conditions of the lab experiment, the Q-line half-width γ at 10 Torr and lower must be about .014 cm^{-1}, since this value of γ and the above experimental conditions substituted into Eq. (1) approximately equals the measured absorption corrected for the finite slit width $\Delta\nu$ = 0.28 cm^{-1}.

With the system operating in the derivative mode, the NO gas cell pressure was varied until the Q-line signal was barely detected with an integration time τ = 10 sec and an observation time of several minutes. Detection was made with S/N $\approx$ 1 and an NO pressure of 0.25 Torr. If the half width γ remained constant, the absorbance of A = 0.15 measured in the integral mode with S/N $\approx$ 40 and P = 10 Torr corresponds within a factor of two to the observed signal in the derivative mode, a reasonable discrepancy considering the approximate values of the observed S/N values. Hence, it is assumed that γ gets no smaller than .014 cm^{-1} under the conditions of the proposed experiment.

Barth's value[11] of the NO column density for a 35-km Zenith path at 85km is 1.1×10^{14} molec/cm^2, which is equivalent to a density of 3.2×10^{7} molec/cm^3 or a partial pressure of 8.9×10^{-10} Torr. For a balloon altitude of 40km, the slant path would be 255km. Taking the total Q-branch line strength at 3.1 $cm^{-2}atm^{-1}$ from Ref. 8, γ as .014 cm^{-1}, b as 255km and c as 8.9×10^{-10}/760atm., the calculated absorbance from Eq. (1)

[11] C. A. Barth, J. Geophys. Res., 69, 3301 (1964).

becomes $A = 3.0 \times 10^{-3}$. To prevent a very low value of measured absorbance, the value of $\Delta\nu/\gamma$ should not be too high (see Fig. 6.8).

The spectrometer of Ref. 8 has a value of $\Delta\nu = 0.1\ cm^{-1}$, which represents the state of the art at 5μ. The value of $\Delta\nu$ used in the Spex instrument is 0.28, which, if double-passed would be about 0.14. This type of instrument is proposed for the balloon experiment. Hence, $\Delta\nu/\gamma = 10$, and from Fig. 6.8 we would expect a measured $A = (3.0 \times 10^{-3})/8 \approx 4 \times 10^{-4}$. This means that the proposed balloon system S/N should be greater than 2,500.

The experimentally observed $S/N \approx 40$ was obtained with a weak IR source, an integration time $\tau = 3$ sec and poor radiant flux collection efficiency due to the use of lenses, windows and apertures. In a balloon experiment where the sun is used as a source and for $\tau = 10$ sec, an extrapolation predicts a system $S/N \approx 25{,}000$. A servo-actuated device, described below, would be used for locking on the sun. Hence, it is estimated that a single absorption line can be observed with an effective $S/N \approx 10$. For such small absorbances the derivative mode of operation overcomes the severe dynamic-range problem and allows small absorptions to be observed. Additionally if three absorption lines are scanned, one on either side of the Q-branch, cross correlating the synchronous detector output with the expected signal will enhance the effective S/N by a factor of about 3. Such a scan would take about 7 minutes.

D. Skaperdas

6.5. Sun-Seeker.

There are many existing schemes[12,13,14] for sensing the direction of, and pointing apparatus toward, the sun, stars, and planets. These find use in earth-bound laboratories, in rockets, or balloons that carry scientific experiments. During the past few months, an experimental two-axis sun-seeker was designed and constructed at CSL for the purpose of evaluating the various schemes for sun pointing in a balloon-borne experiment. The design requirements are as follows:

(1) Acquire the sun over 360 degrees in azimuth and approximately 90 degrees in elevation.

(2) Track in elevation and azimuth with an accuracy of a small fraction of a degree.

The system consists of a coarse and a fine sensor for each axis. The coarse sensors perform the initial acquisition of the sun and align the system to an accuracy of one or two degrees. They are then disconnected, and the fine sensors take control of the tracking and maintain the required accuracy of pointing. The coarse sensors consist of two silicon photovoltaic cells mounted on a sunshade in such a manner that equal shadowing of the cells occurs when the sunshade is pointed directly at the sun. Each cell is connected directly to one coil of a two-coil, three-position relay which is held in the off position when the

---

[12] R. A. Nidey, "Stabilization and Orientation of the Payload," Kitt Peak National Observatory Space Division Report 010-62, Sept. 1962.

[13] M. L. Shechet, "Lightweight Suntracker for Balloon Applications," Rev. of Sci. Instr., 31, May 1960.

[14] C. Cantor, "Fine Sun Tracker for Advanced Orbiting Solar Observatory," Goddard Space Flight Center Report N66-32060.

illumination of both cells is equal. A differential of illumination of the two cells will close the relay contacts and furnish appropriate voltages to the servo-drive system to correct for the misalignment. For the azimuth axis, a third acquisition cell is added on the rear side of the sunshade and connected in parallel with one of the tracking cells. This allows 360-degree azimuthal acquisition of the sun. Since the elevation axis must acquire the sun over less than 90 degrees, it does not need the third acquisition cell.

Two systems of fine sensing have been constructed as "breadboard" models. The first system, shown in Fig. 6.10, functions by scanning a square aperture (slit) across the sun's image with a sinusoidal motion. This produces a periodically-modulated light beam that falls upon a photomultiplier and produces a pulse-position-modulated signal. This signal is then synchronously demodulated with the slit-driving signal and produces a polarized error signal that is fed to the servo drive and serves to keep the sun's image accurately centered on the vibrating slit. This type of system is capable of detecting tracking errors of a few arc-seconds magnitude.

The second fine sensing system, shown in Fig. 6.11, consists of two small rectangular silicon photovoltaic cells mounted behind a rectangular slit in an enclosure. Except for the slit, the enclosure is light tight. The cells are mounted such that when the sensor is pointed directly at the sun, the beam of light from the slit slightly overlaps both cells. The silicon cells are used as current sources and are connected in opposite polarity to the input of an operational amplifier. In order to obtain the most stable operation, the cells are operated in

(OVERLEAF BLANK)

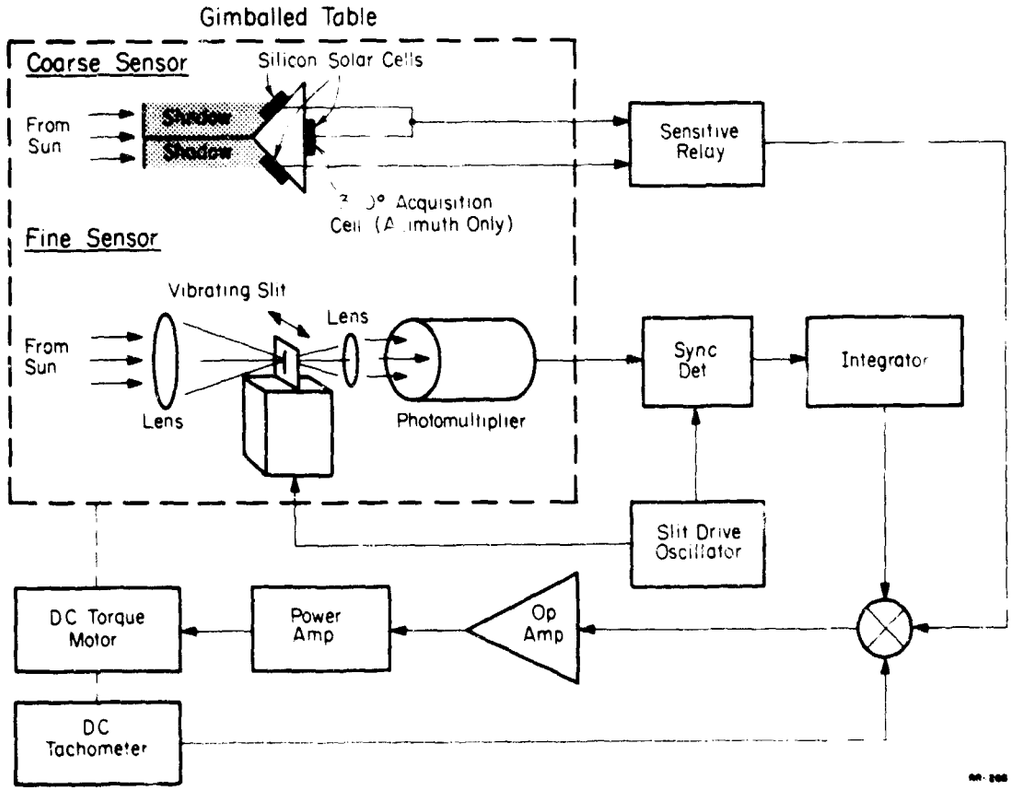

Fig. 6.10. Block diagram of scanning-type fine sensor.

(OVERLEAF BLANK)

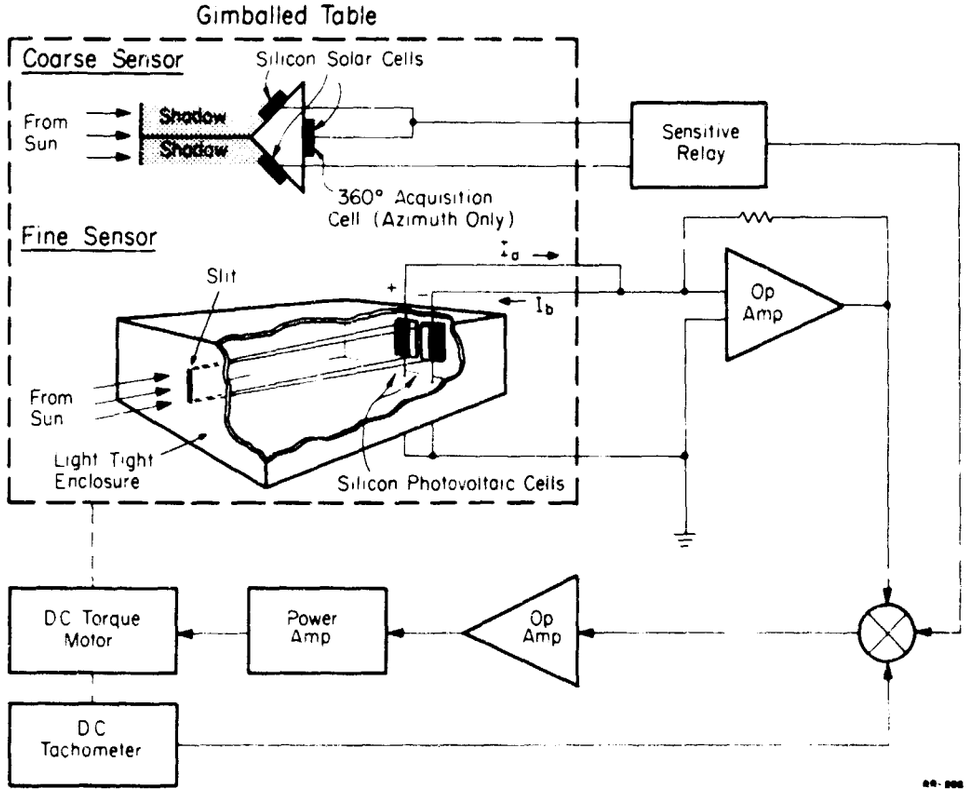

Fig. 6.11. Block diagram of solar cell fine sensor.

(OVERLEAF BLANK)

their short-circuit mode. Any difference in short-circuit current of the two cells is sensed and amplified by the operational amplifier. Since the current of each cell is proportional to the illumination on the cell, an error signal will be present at the output of the amplifier when the light from the slit is not precisely centered on the cells. This error voltage, when fed to the servo amplifier, will cause the servo to drive the system back into alignment.

For maximum accuracy, the silicon cells must be closely matched. The desired field of veiw, detector saturation characteristic, photo-cell linear region, etc., determine the dimensions of the cell, slit, and enclosure.

The accuracy of this system is reported[15] to be a few arc seconds. However, this system is subject to some inaccuracies due to temperature and aging effects of the photovoltaic cells.

Both of the above described fine sensors have been constructed and tested on our experimental sun seeker. For testing the pointing accuracy, a laser beam was reflected from a mirror mounted on the sun seeker to a calibrated scale. The laser and scale were spaced a distance of four meters from the sun seeker. The measurement accuracy of this method was limited by the laser spot size and was of the order of 1 arc minute. Both sensing systems tested in this manner gave pointing accuracies equal to or less than the measuring accuracy. Additional tests will be made with increased measurement accuracy. It would be particularly desirable to make long-term tests under various environmental conditions.

---

[15] C. Cantor, "Fine Sun-Tracker for Advanced Orbiting Solar Observatory," Goddard Space Flight Center Report N66-32060.

If the photovoltaic system does maintain arc-second accuracy over wide ranges of time and temperature, it would, of course, be the most desirable system because of its simplicity and ruggedness.

The coarse acquisition system performed well with no apparent problems. The particular solar cells used (Hoffman N220GG-10L) have sufficient output that they must be masked with neutral-density filters to avoid spurious response from reflected sunlight. The gain can thus be varied by changing filters and the dead zone (zone of control by fine sensors) adjusted as desired.

H. V. Krone

6.6. Fluid Amplifiers.

The use of commercial fluid-amplifier components in low-speed (< 1000 cps) switching and control applications is becoming well established. Expected operating speed is readily obtained in physically small systems. However, in systems employing long pneumatic lines, pulse delay times much longer than indicated by the speed of sound are experienced. This slow response is frequently due mostly to mismatch at the far end of the line and in part to the propagation speed, c, falling off at low frequencies. For a matched transmission line

$$c = c_{max}(1+R^2/\omega^2L^2)^{-1/4}$$

in which L and R are constants dependent respectively on the reciprocal and the reciprocal squared of the tube area.

This equation frequently leads one to employ a modulated carrier system in which the signal information is translated up to frequencies where the propagation speed is near maximum. This is a complicated system

and it is felt that the desired performance could in many cases be achieved by more attention to impedance matching and the proper choice of tube area. A theoretical and experimental investigation is being carried out to determine the optimum tubing diameter and matching termination for good response as a function of transmission-line length. These results will aid in choosing the best technique (simple transmission-line or carrier system) for various fluidic systems employing long lines.

H. W. Knoebel

(OVERLEAF BLANK)

W. D. Compton C. Jones R. Spry
E. Johnson E. L. Wolf

7.1. Introduction.

Semiconductors are particularly sensitive to irradiation with high-energy neutrons, electrons or gamma rays. The fate of vacancies and interstitials that are introduced by the radiation depends upon the temperature of the irradiation and the concentration and type of impurity present in the lattice. Vacancies, in silicon, diffuse easily and combine with interstitial oxygen to produce substitutional oxygen, thereby giving the so-called Si-A center. Other defect centers result from the association of vacancies with the donor or acceptor impurity. The luminescence resulting from the recombination of electrons trapped at these defects with free holes in the valence band gives information about the position of the energy level in the forbidden gap and the interaction of the trapped charge with the lattice.

Semiconducting devices frequently employ materials of quite low resistivities. At high dopant levels, the low-temperature resistivity may be dominated by impurity band effects. Measurements of di/dV and d^2i/dV^2, the first and second derivatives of the current with respect to applied bias as a function of bias, have been made on junctions of highly-doped p-type silicon with indium as the counter electrode. In the ideal case, the depletion layer at the surface of the silicon acts as the tunneling barrier. In less-ideal cases, adsorbed gas and oxides contribute to the barrier. Information concerning the density of states of the

†Supported in part by the National Aeronautics and Space Administration under Grant NsF 228-62.

impurity band has been obtained from a comparison of these results with theoretical predictions based upon the $E^{\frac{1}{2}}$ density of states of a parabolic band. Phonon-assisted tunneling has also been seen with the K = 0 optical phonon of the silicon and the optical phonon associated with the vibration of the boron impurity in the silicon lattice.

7.2. Radiation Effects.

Measurements have continued on the nature of the recombination luminescence arising from electron-hole recombination at defects introduced into silicon by high-energy radiation. Following irradiation with fast neutrons, or high-energy gamma rays, the sample is etched and mounted in a liquid-helium dewar. The recombination luminescence is excited by a filtered, high-intensity mercury arc and observed with a Jarrell-Ash Model-82 Monochromator with a cooled PbS detector.

As was reported previously, the luminescent spectra for n- and p-type material are nearly identical and are the same for irradiations with either neutrons or gamma rays. The luminescence spectra are different, however, for material prepared by Czochralski and by the float-zone technique. Figure 7.1 illustrates the luminescent spectra for an n-type, float-zone sample following irradiation with Co^{60} gamma rays. Table I lists the energy location of the luminescent peaks shown in Fig. 7.1 B. Figure 7.2 illustrates the luminescent spectra for n-type pulled samples following irradiation with Co^{60} gamma rays. Curves A through E represent the changes that occur following annealing at room temperature for the indicated number of days. Table II lists the energy location of the luminescent bands shown in Fig. 7.2, curve B.

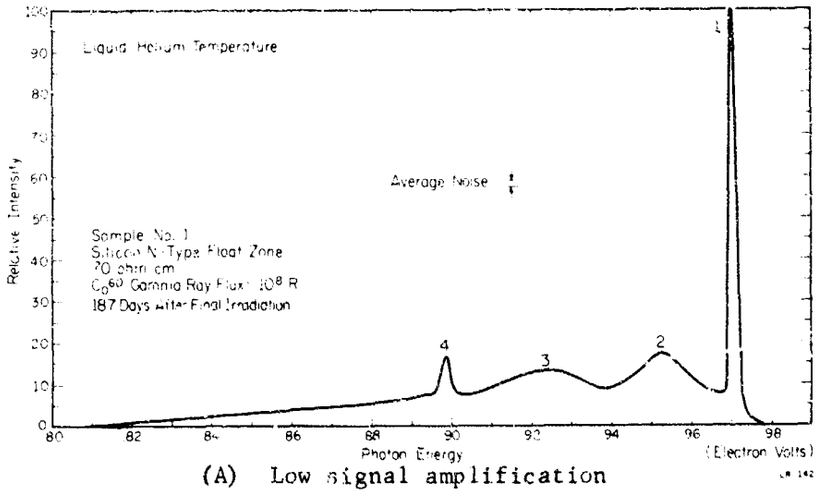

(A) Low signal amplification

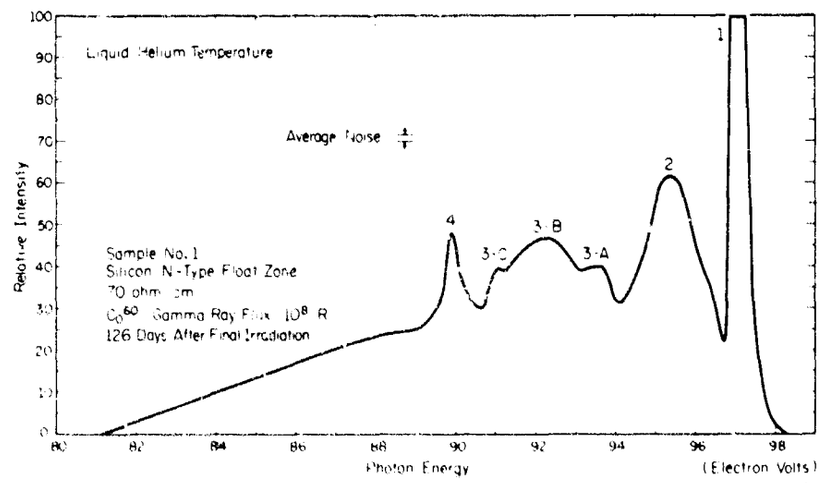

(B) High signal amplification

Fig. 7.1. Liquid-helium-temperature luminescence spectra of gamma-irradiated 70 ohm-cm n-type float zone grown silicon. Spectral resolution 32 Å.

(OVERLEAF BLANK)

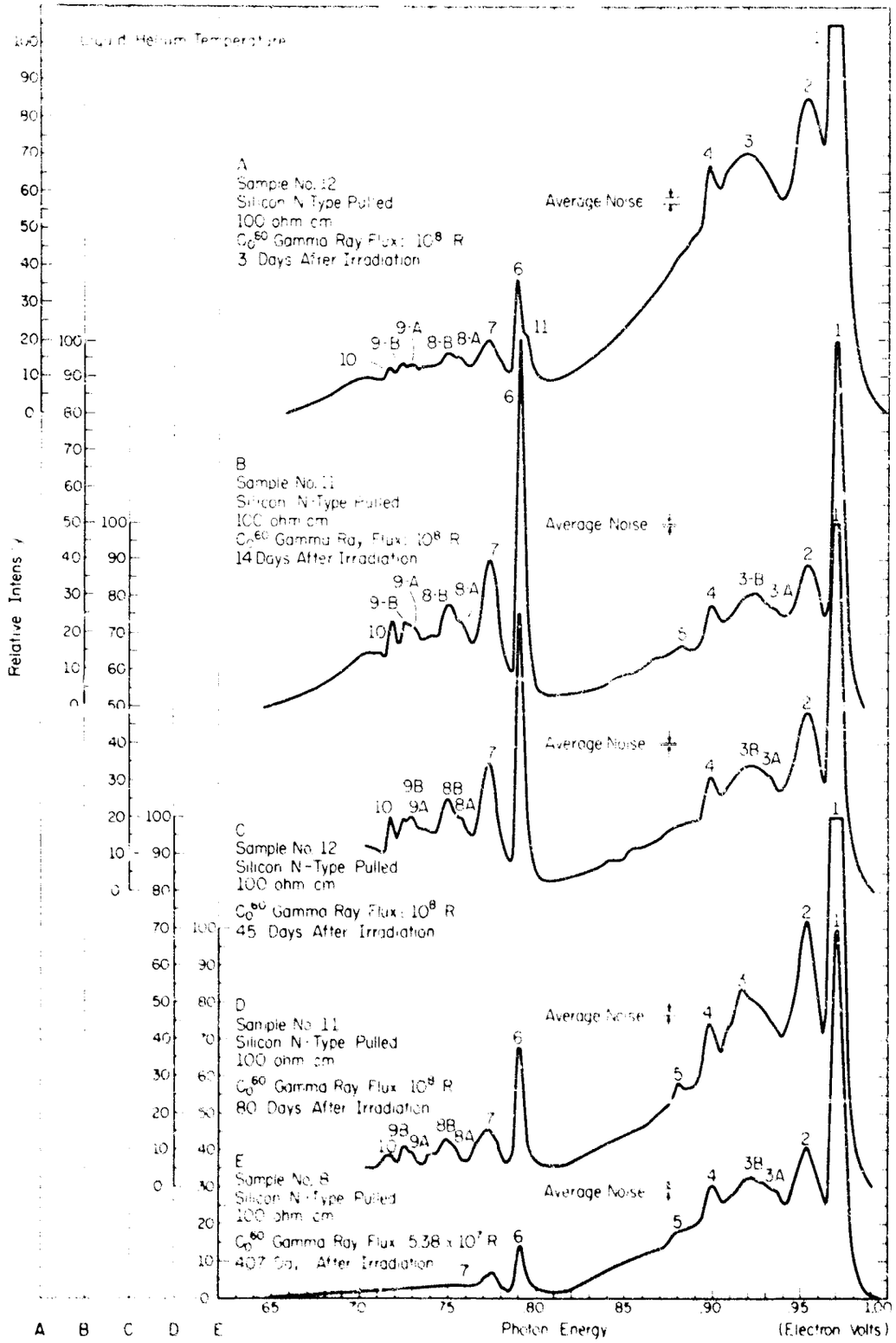

Fig. 7.2. Liquid-helium-temperature luminescence spectra of gamma-irradiated 100 ohm-cm n-type pulled silicon. Spectral resolution 64 Å.

(OVERLEAF BLANK)

Table I

Energy Location of Luminescence Bands

of Fig. 7.1B

Band Number	Peak Location (eV)	Separation from Band no. 1	Phonon Emitted
1	0.971		zero
2	0.954	0.017	TA
3-A	0.935	0.036	2TA
3-B	0.923	0.048	L
3-C	0.911	0.060	TO
4	0.899	0.072	TO+TA

TA: traverse acoustic phonon

L: longitudinal phonon

TO: transv se optical phonon

Table II

Energy Location of Luminescence Bands of Curve B, Fig. 7.2

Band Number	Peak Location (eV)	Separation from Band No. 1 in the High-Energy Pattern (eV)	Separation from Band No.6 in the Low-Energy Pattern (eV)	Corresponding Bands	Separation between Corresponding Bands (eV)	Phonon Emitted
1	0.971			6	0.179	zero
2	0.955	0.016		7	0.180	TA
3-A	0.936	0.035		8-A	0.179	2TA
3-B	0.925	0.046				L
4	0.900	0.071		10	0.181	TO+TA
5	0.883	0.088				TO+2TA
6	0.792			1	0.179	zero
7	0.775		0.017	2	0.180	TA
8-A	0.757		0.035	3-A	0.179	2TA
8-B	0.751		0.041			L
9-A	0.730		0.062			TO
9-B	0.727		0.065			0
10	0.719		0.073	4	0.181	TO+TA

TA: transverse acoustic phonon
L: longitudinal phonon
TO: transverse optical phonon
O: zero wave vector optical phonon

Several features are to be noted from these data. The low-energy spectra seen with the pulled material is absent in the spectra of the float-zone material. Comparison of Tables I and II confirms that the high-energy portion of the spectra are essentially equivalent for the two materials and that much of the low energy portion of the spectra for the pulled crystal is a replication of the high-energy portion of the spectra. The energy separations among various peaks of the spectra are also listed in the tables.

These spectra are believed to result from recombination of free holes with electrons that are bound to defects with energy levels 0.194 eV below the conduction band (Peak 1) and 0.374 eV below the conduction band (Peak 6). Peaks 1 and 6 are believed to result from recombination without the assistance of phonons. Peaks at lower energy than the zero-phonon peaks are believed to correspond to recombination with the emission of one or more phonons, the type of phonon being indicated in the last column of the two tables.

The defect with an energy level located at 0.196 eV below the conduction band is believed to be the Si-A center. The microscopic nature of the defect with an energy level located at 0.374 eV below the conduction band is not known.

An extension of these studies is underway with instrumentation designed to provide higher-resolution spectra and uniaxial stresses for determination of the symmetry of the defects. Measurements of the luminescent spectra of germanium are also underway. A new data-sampling technique is being developed that will allow the CDC-1604 computer to be used on line with the experiment.

7.3. Tunneling Conductance Measurements on p-Type Silicon.

As the concentration of impurities, donors or acceptors, is increased in a semiconductor, the discrete energy levels associated with the impurities broaden and eventually combine to form a band. At these high concentrations, the electrical resistivity becomes "metallic" or independent of temperature. The details of the donor, or acceptor, interaction that leads to the formation of a band are not fully understood. In particular, the nature of the energy spectrum and the density of electronic states in the vicinity of the original impurity level and the density of electron states in the intermediate impurity concentration range[1] are not well established.

Lifshitz[2] has demonstrated theoretically that an "erosion" or sharp minimum can occur in the density of states in the immediate vicinity of the original impurity level if the impurities interact by overlap of their wave functions. The experimentally-observed activation energy, ϵ_2, exists in the concentration range immediately below the concentration required for a temperature independent resistivity. Davis and Compton[1] argue that it arises from a thermal activation of carriers from a non-conductive ground state to a diffuse conducting state.

Tunneling techniques present a particularly sensitive method of examining sharp variations in the density-of-state functions. Conley, et al[3]

---

[1] E. A. Davis and W. D. Compton, Phys. Rev. 140, 483 (1966).

[2] I. M. Lifshitz, Advances in Physics 13, 483 (1966).

[3] J. W. Conley, D. B. Duke, G. D. Mahen, and J. J. Tiemann, Phys. Rev. 150, 466 (1966).

have described the tunneling characteristics of metal-semiconductor contacts in which the tunneling barrier is the depletion layer at the surface of the semiconductor. The calculation assumes that the conduction or valence band in the semiconductor is parabolic and that the extrinsic carriers are not frozen out onto the impurity levels. They show that the differential conductance in this type of contact exhibits a broad minimum centered at a positive bias voltage equal in magnitude to the Fermi degeneracy of the semiconductor. Positive bias here corresponds to a lowering of the Fermi level in the semiconductor relative to the Fermi level in the metal. Deviations from the $E^{\frac{1}{2}}$ density of states inherent in a parabolic band can be expected to arise as a result of the high impurity concentrations, thereby giving deviations from the predictions of this theory.

Differential conductance measurements have been made at $4^{\circ}K$ on tunnel junctions made by evaporating indium onto vacuum-cleaved silicon bars. The silicon employed was p type, containing boron in concentrations ranging from 4.7×10^{18} cm^{-3} to 2×10^{19} cm^{-3}. The electrical properties of the samples employed are listed in Table III. The method of production of these samples insures that they are metal-semiconductor contacts[3] with no intervening insulating layer. The samples are prepared by cutting bars of dimensions 2 by 4 by 10 millimeters with the (111) axis along the long direction of the bar and then nickel plating the entire bar to provide a return contact. The bars were then scratched with a diamond point, mounted in a Varian ion-pump system equipped with a swinging hammer, and cleaved while indium was being evaporated through a mask mounted between the sample and the boat. Separated dots of the metal were produced. During the evaporation of the indium, the pressure in the ion pump was

Table III

(a) Acceptor Concentration (cm^{-3})	(b) $\bar{r}/a_o^*$	Room Temperature Resistivity (ohm-cm)	(d) Shift of $(di/dV)_{min}$ from zero bias (mV)	(d) (e) Impurity band peak from $(di/dV)_{min}$ (mV)	(c) Half of sing-trip splitting at $r=\bar{r}$ (mV)	(d) d^2i/dV^2 p-p width (mV)
4.7×10^{18}	2.96	0.017	+0.2		4.5	4.5
1.1×10^{19}	2.24	0.010	+1.9	7.9		8.3
1.4×10^{19}	2.05	0.008	+1.9	7.0	10.7	8.6
2.3×10^{19}	1.74	0.006	+3.6,4.0		15.2	11.4

(a) Determined from the Hall coef. at room temperature assuming $R = 1/Ne$.

(b) $\bar{r}$ is the mean nearest neighbor distance, measured in effective Bohr radii, a_o^*, assuming a random array.

(c) Assume can scale from data on the hydrogen molecule, using m^*, ϵ. [S. Flügge, Handbuch der Physik, XXXVII/2, Molekul II, p. 21, Fig. 8.]

(d) Measured at 4.2^oK.

(e) Better estimates of this quantity can be obtained from data of d^2i/dV^2, since a steeply varying background is observed in di/dV.

typically 10^{-7} millimeters of mercury. The samples were taken from the vacuum system and mounted in a jig suitable for immersion in liquid helium, the contact to the indium dot being made by an indium pressure contact. The evaporated indium dots were approximately 1000 Å thick and had a diameter of approximately 0.002 in.

Representative data are presented on two samples having room temperature resistivities of 0.017 and 0.010 ohm-cm. The low temperature resistivity of the 0.017-ohm-cm material gives an activation energy of conduction of about 0.1 meV. The resistivity of the 0.010-ohm-cm material exhibits no temperature dependence at low temperatures. The differential conductance of these two samples is shown in Figs. 7.3 and 7.4. Both curves exhibit strong deviations from the broad minimum in conductance predicted by Conley, et al. In Fig. 7.3 there is a pronounced minimum in the differential conductance near zero bias and a partially-resolved shoulder for positive bias of approximately 15 meV. In Fig. 7.4 the minimum is shallower and has shifted to a positive bias of about 2 meV. This trend continues for higher concentrations of impurities.

It is suggested that the sharp features seen in the differential conductance, in a small range of bias near zero bias, can be identified with features of the density of electron states in this range, although it is unlikely that the differential conductance is directly proportional to the electron density of states. Having made this identification, the position of the minimum in the conductance measured from zero bias provides a measure of the Fermi-level position with respect to the minimum in the density of states in the semiconductor. In Fig. 7.3 the Fermi

(OVERLEAF BLANK)

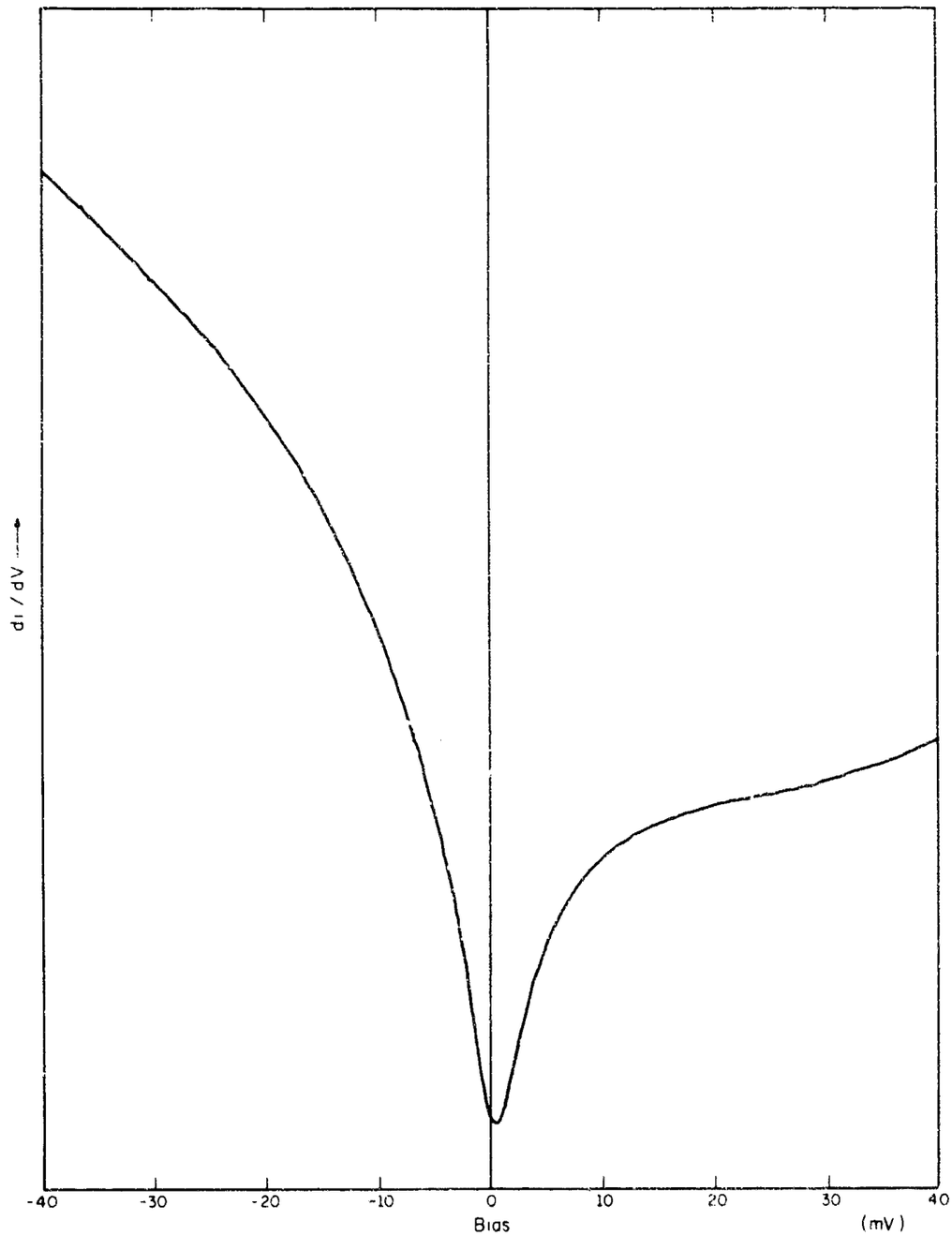

Fig. 7.3. Differential conductance di/dV for indium-silicon tunnel junction at 4.2°K. Silicon contains 4.7×10^{18} cm^{-3} boron-acceptor impurity. Vertical scale and zero are arbitrary. [LR-161]

(OVERLEAF BLANK)

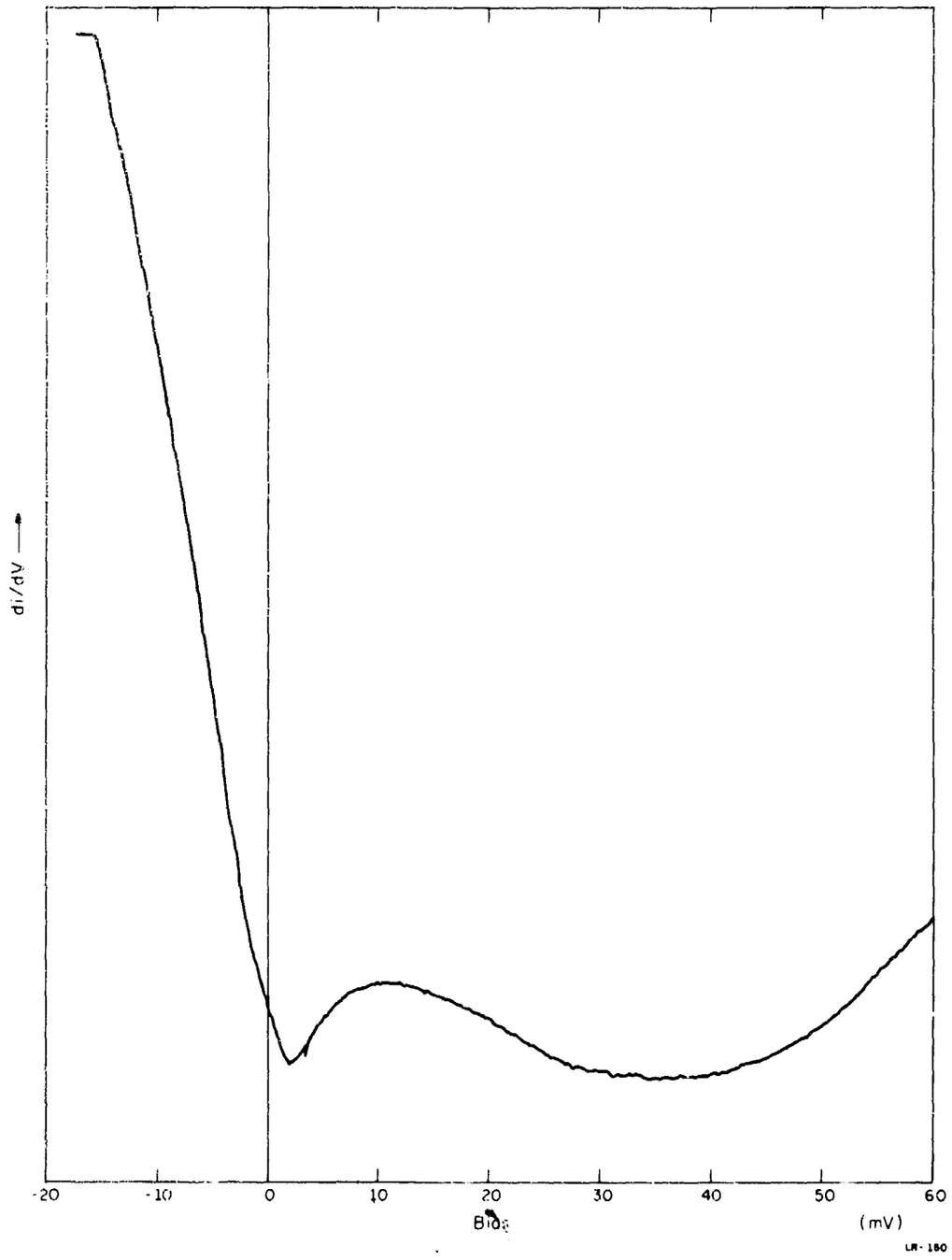

Fig. 7.4. Differential conductance di/dV for indium-silicon tunnel junction at 4.2°K. Silicon contains 1.1×10^{19} cm^{-3} boron-acceptor impurity. Vertical scale and zero are arbitrary.

(OVERLEAF BLANK)

level is centered in the dip, i.. Fig. 7.4 the Fermi level lies deeper in the valence band by approximately 2.0 meV. This trend continues for higher doping as is shown in Table III. Second-derivative, d^2i/dV^2, curves show that a symmetrical aspect of the differential-conductance minimum clearly evident in Fig. 7.3 is actually retained at higher concentration where the minimum is no longer resolved. The minimum has simply been shifted, broadened, and weakened. The fact that the conductance minimum shifts with concentration and does not occur exactly at zero bias strengthe the contention that it is not a zero bias anomaly[4] but is to be identified as a feature of the density of states.

It is suggested that these anomalous features in the differential conductance can be explained on the basis of the theory of Lifshitz.[2] The basic idea can be presented as follows. Suppose one considers the boron acceptors as being hydrogenic and that the overlap of their wavefunctions leads to an interaction of pairs of acceptors. The wavefunctions of these pairs are to be combined in singlet or triplet (bonding or antibonding) combinations in direct analogy with the hydrogen molecule. The singlet- and triplet-state energies are shifted symmetrically with respect to the original ground-state energy, with the singlet state lying below the original ground state. Lifshitz[2] included the interaction of more than two impurities and discusses the broadening of the levels as a result of this greater interaction, important at high concentrations. Neglecting this for the lower concentrations, it is expected that the Fermi level will be quite close to the original ground state of the acceptor and that

---

[4]R. N. Hall, J. H. Racette, and H. Ehrenreich, Phys. Rev. Letters 4, 456 (1960).

this minimum in the density of states corresponds to the minimum in the conductance seen in Fig. 7.3. It is suggested that the activation energy, ϵ_2, can be associated with the thermal activation of carriers across the steep minimum in the density of states.

As the acceptor concentration is increased, an increase in the screening by the free carriers weakens the binding of the holes to the boron ions, thereby shifting the ground-state level of the isolated impurities toward the edge of the band. As the split-off triplet state of the boron pairs begins to strongly overlap the valence band, the Fermi level shifts away from the minimum. It is believed that this effect accounts, in qualitative terms, for the observations and that these data represent the variation in the density of states in the neighborhood of the valence-band edge that results from the high concentration of acceptor impurities.

Measurements of the tunneling characteristics were also made on junctions formed from degenerate silicon containing 5×10^{19} cm^{-3} and 1.3×10^{20} cm^{-3} of boron atoms. The Fermi level is expected to be about 100 meV below the valence-band edge. The tunneling junctions were fabricated in air. A point of indium was pressed onto a freshly-cleaved surface of silicon forming a cold weld. The oxidation, or adsorption, on both of the indium and silicon in the air produces the insulating-tunneling barrier.

Measurements of d^2i/dV^2 vs V were made on these junctions at temperatures between 1.6 and 4.2°K. An example of these data is given in Fig. 7.5. The convention is that positive bias lowers the valence band of the semiconductor relative to the metal Fermi level. For a positive

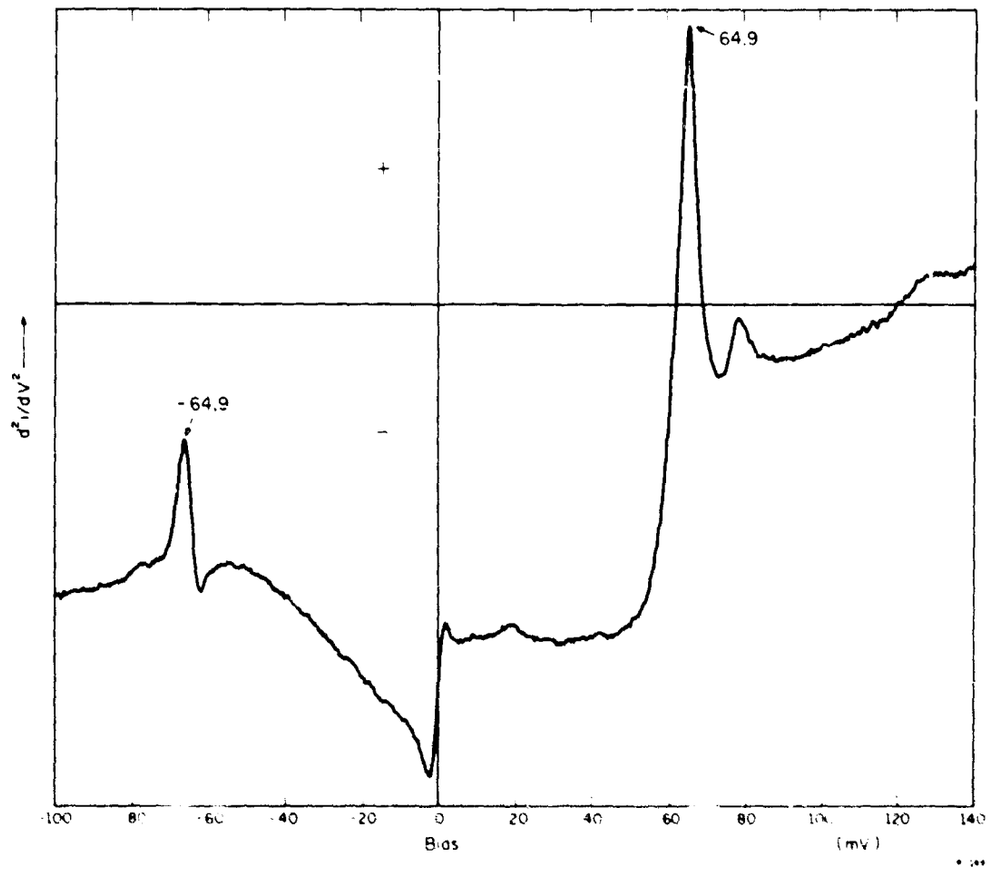

Fig. 7.5. d^2i/dV^2 spectrum for indium-p-type silicon (1.3×10^{20} cm^{-3} boron) tunnel junction at 4.2°K. Modulation level is 3 millivolts. Peaks (left to right) occur at -64.9 (+), -60.7 (-), -2(-), +2(+), +19.5 (+), +64.9 (+), +77.8 (+), and +129 (+), in millivolts.

(OVERLEAF BLANK)

bias equal to the Fermi degeneracy of the semiconductor, the metal Fermi level is opposite the top of the valence band.

Prominent peaks are seen to occur symmetrically for a bias voltage of 64.9 ± 1.2 meV as measured by neutron scattering.[5] The prominent structure at positive and negative bias thus corresponds to the metal Fermi level being located above and below respectively, the semiconductor Fermi level by an amount equal to the K = 0 optical phonon energy of the silicon. It should be noted that owing to the large Fermi degeneracy of the silicon, both the energies $E_F + \hbar\omega$ and $E_F - \hbar\omega$ lie well within the valence band. The secondary peak at 77.8 ± 0.5 meV lies at the energy of the localized vibration in silicon due to boron as measured by Balkanski,[6] with infrared techniques. Other weak but consistently-observed features of the spectrum are the peak at 19.5 meV which corresponds closely to the value of 20 meV of the silicon transverse acoustic phonon at the zone boundary, as measured by Brockhouse, and a broad weak peak approximately twice the K = 0 phonon energy.

The strong peak at positive bias of 64.9 millielectrons volts is clearly visible in a differential conductance plot as an upward step in the conductance. This upward step in conductance at the optical phonon energy is associated with the threshold for an inelastic tunneling process involving emission of an optical phonon. In this process the electron is injected into the silicon valence band at an energy $\hbar\omega$ above the Fermi level. It decays to the Fermi level by emitting the optical

---

[5] Brockhouse, Phys. Rev. Letters 2, 256 (1959).

[6] M. Balkanski, J. Phys. Chem. Solids 27, 671 (1966).

phonon. The phonon couples a lower density of states to a higher density of states, thereby giving an increase in conductance.

A peak in d^2i/dV^2 is quite prominent at negative bias voltages. Actually the structure has a complicated line shape but is predominately an upswing at -64.9 meV. This structure is qualitatively different from the negative bias structure seen in p-n junctions.[7] The upward step in conductance corresponds to a decrease in conductance arising from the coupling of a higher density of states to a lower density of states. The threshold for the process occurs at the same energy as above, the energy of the optical phonon.

---

[7] R. T. Payne, Phys. Rev. 139A, 517 (1965) and Chynoweth, Logan and Thomas, Phys. Rev. 122, 877 (1962).

J. Bouknight
G. Crawford
L. Hedges
J. Knoke
D. Lee
V. Metze
E. Neff
R. Resch
H. G. Slottow
J. Stifle
R. Trogdon

8.1. Introduction.

The computer group is responsible for the management, maintenance, and development of the CSL computer facility.

8.2. CDC 1604 Computer.

Period		March 1 to Aug. 31, 1967
Total Running Time:		2520 hours
Average Per Day (7 day week):		13.7 hours
Operational Time:	97.30%	2452 hours
Preventive Maintenance Time:	2.54%	64 hours
Emergency Maintenance Time:	0.16%	4 hours

E. Neff

8.3. Display System.

Construction of the CRT display unit has been completed, and the system is in operation. A complete description of the display is contained in CSL Report R-357 and therefore only a brief summary will be given here.

The CRT display, shown in Fig. 8.1, has the following specifications:

Display medium

Electrostatically deflected 17-in. CRT

(OVERLEAF BLANK)

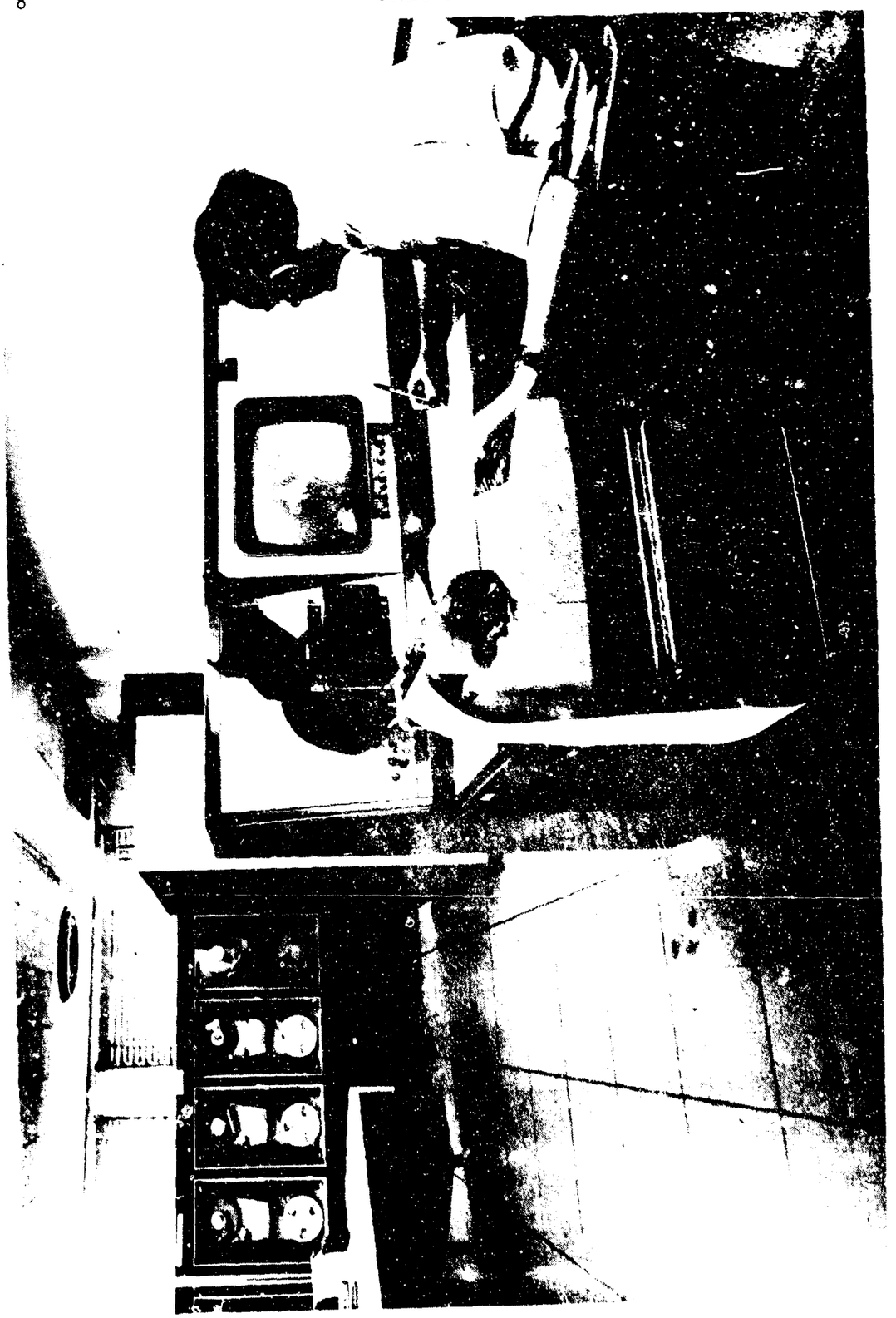

Fig. 8.1. CRT display console.

(OVERLEAF BLANK)

Display word length

24 bits - 12 bits for x; 12 bits for Y; 4096 positions along each axis

Display Modes

Seven modes of operation available.

Self-contained character and line generators.

Operating Speeds

333,000 points/sec

50,000 characters/sec

16,000 lines/sec

Camera Unit

Magnetically deflected 6 inch CRT slaved to 17-inch tube.

Computer operated Polaroid and 16 mm camera attachments available.

Input-Output

IBM typewriter on-line to computer.

Light pen

The pictures on the following pages are actual unretouched photographs taken by the camera unit. They are typical examples of the type of data which may be displayed.

J. Stifle

8.3.1. An Analog-Digital Computer Simulator.

During the current reporting period, a hybird (analog-digital) computer simulator called COBLOC was obtained from the University of Wisconsin and was converted for running on the new computer system. Several students in the control systems group are currently using it.

(OVERLEAF BLANK)

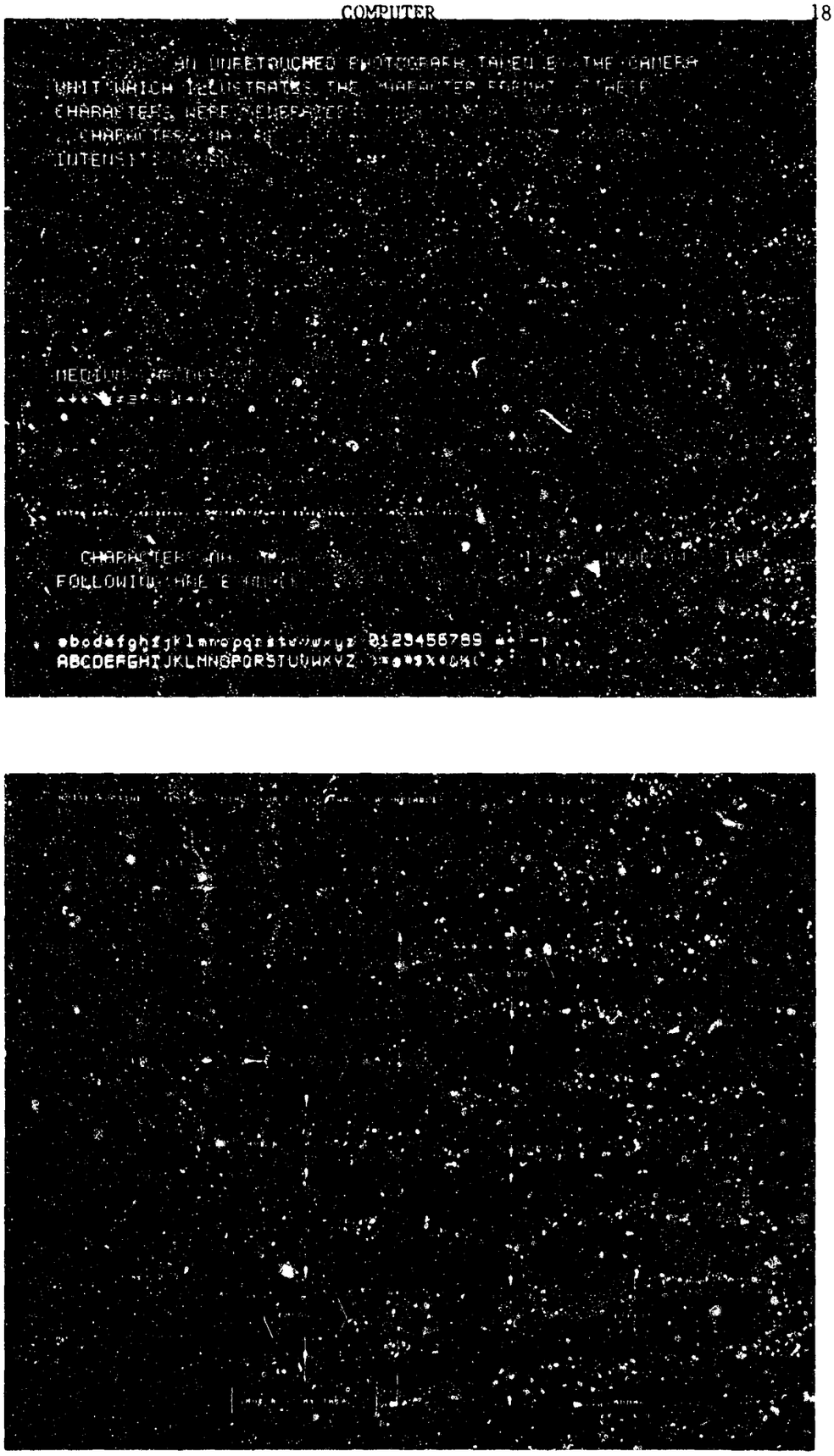

Fig. 8.2. Examples of output on CRT display.

(OVERLEAF BLANK)

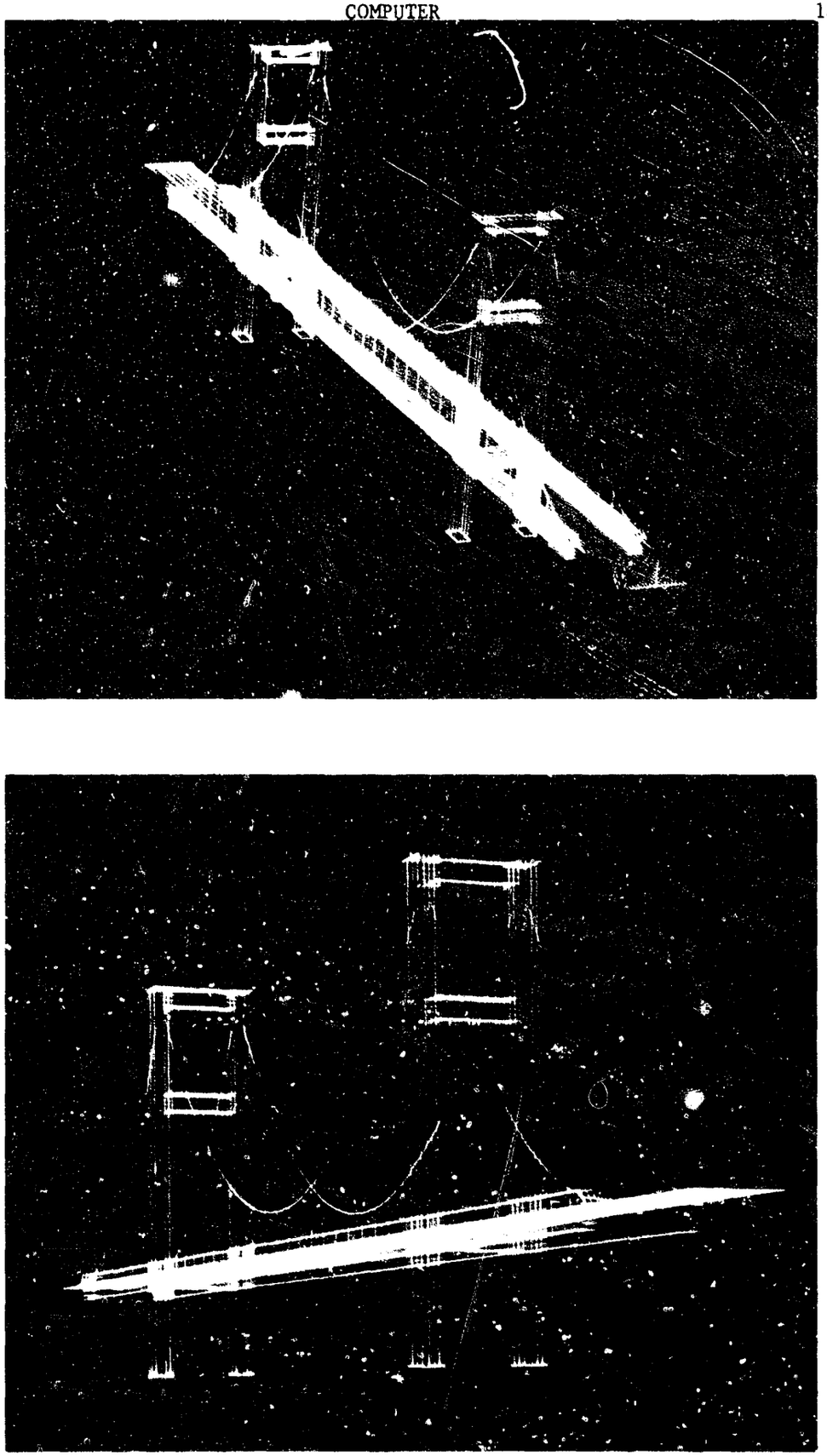

Fig. 8.3. Drawings on CRT display operating in line-generation mode.

(OVERLEAF BLANK)

During the next reporting period, an operating manual will be produced and further modifications to the system will be made.

W. J. Bouknight

8.3.2. A General-Purpose Drafting System.

Further work was done on the implementation of a flow-chart production system.

The current version is capable of complete specification, editing, and drafting of program flow charts by the computer user. No further changes in the system are contemplated at the present and only an operations manual and final debugging will be done in the next reporting period.

Fig. 8.4 shows a flow-chart prepared by this system and further processed (see Sec. 8.3.4) for output on a CALCOMP plotter.

W. J. Bouknight

8.3.3. Calcomp Incremental Plotter Operating System.

The Calcomp Plotter Operating System (CCSYSTEM) has been completed and checked out. A final report and operating manual will be issued during the early part of the next reporting period.

W. J. Bouknight

8.3.4. Programming System.

The new software system, being written at CSL, is now largely completed. Presently, the system provides a FORTRAN compiler, a flexible machine-language assembler called ILLAR, a monitor, loader, a source-language editor and a library of nearly 125 service routines. The library includes a full complement of FORTRAN-arithmetic and data-conversion

(OVERLEAF BLANK)

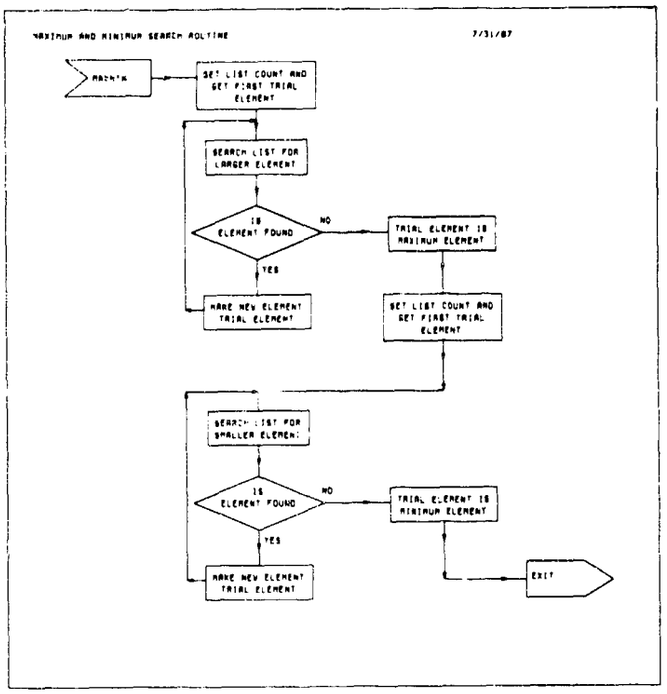

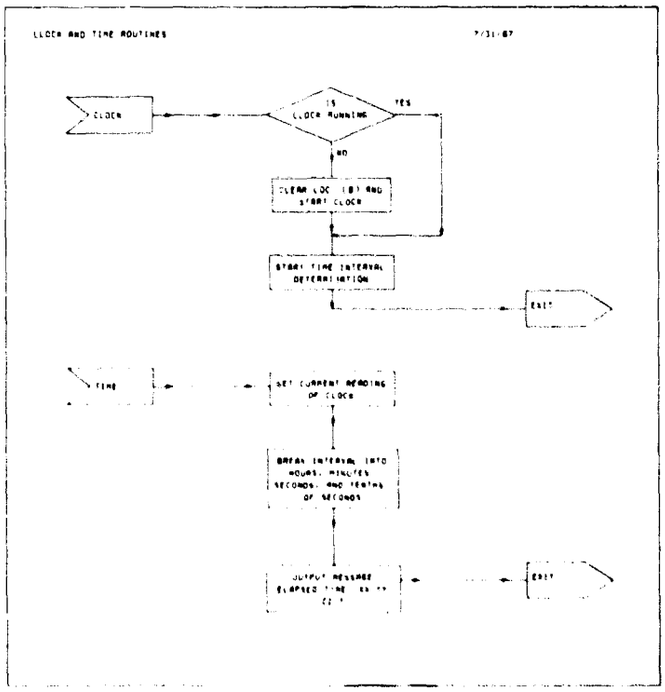

Fig. 8.4. Flow chart prepared for CALCOMP by drafting program.

(OVERLEAF BLANK)

subroutines, a set of programs to drive a CALCOMP plotter, and a set of routines to drive the CSL scope.

The FORTRAN source language is similar to Fortran 4 and provides for mixed-mode as well as complex and double-precision arithmetic. The FORTRAN compiler produces an assembly-language program compatible with the ILLAR assembler.

Additionally, the FORTRAN compiler has several unique features built into it. The following describes several of these features:

1. A special DISPLAY statement is imbedded in the compiler to provide easy use of the CSL scope facility. This statement is similar to the FORTRAN "PRINT" statement and is controlled by a special FORMAT statement. The DISPLAY statement provides for point, line, and character plotting, as well as the PRINT-statement type of alpha-numeric conversion of a list of variables.
2. The compiler allows ILLAR assembly-language statements to be mixed with FORTRAN statements. The full complement of ILLAR features may be used.
3. The compiler provides for the conditional compilation of FORTRAN statements. This feature has been implemented through the use of directive letters in column 1 of the statement. Statements with letters in column 1 will be compiled only if an appropriate letter flag is set. This feature is useful in debugging programs.
4. Additional code-checking features include options to generate program traces, both over programs and within programs over statement numbers.

The ILLAR Assembly Program converts programs written in ILLAR source language into a form suitable for loading with the system loader. Source-program input to the routine is in CARD-IMAGE format. The outputs from the assembler are an assembly listing and a binary-object program.

Source programs may be subdivided into subprograms, with each program being assembled as a separate entity. Linkages between these subprograms are accomplished through the use of global symbols and program arguments. Data communication is established through global symbols, arguments, and through the COMMON bank.

Specific features of the ILLAR Assembler include:

Recursive MACRO capability.

System MACRO capability.

FORTRAN-like CALL with arguments.

FORTRAN-like compile arithmetic operations.

Subroutine communication through arguments. The preamble for the necessary address substitution is automatically compiled.

Automatic compilation of index save-restore subroutines.

Full-word and variable-field data conversions.

Symbolic-address arithmetic.

Literal-element and literal-string capability.

Eighty pseudoinstructions to implement these and other features.

D. Lee

8.3.5. Graphics and Structures.

This work represents a joint effort between the departments of Digital Computer Science, (specifically the Illiac IV project) and the Coordinated Science Laboratory to further develop computer graphic capabilities.

Existing programs, which consist largely of routines to do three-dimensional transformation and manipulation, persepctive drawing, and an interpreter that enables a low-level language usage, have been converted to the CSL System.

A survey of techniques and programs at other installations is underway.

A program to define a variable space frame was written, and an animated film was made showing the experimental structure.

It is anticipated that the current array-type data structure will be replaced by some kind of list structure, and that experiments in color-processing techniques for computer-animated films will be pursued.

R. Resch

(OVERLEAF BLANK)

B. M. Arora
D. L. Bitzer
W. Goede
R. L. Johnson
J. Knoke
H. G. Slottow
E. Stredde
R. Trogdon

9.1. Introduction.

The Plasma Display Panel, invented at the Coordinated Science Laboratory, is a rectangular array of bistable gas-discharge cells which are insulated from exciting electrodes by thin glass panels. Combining the properties of memory, display, and high brightness in a simple structure, it is an effective, potentially-economical device for information display.

Except when information is changed on the display, every cell is excited by an alternating voltage which, by itself, is insufficient to ignite a discharge. If, however, because of an earlier discharge, there is an accumulation of charge on the insulating end walls, the corresponding wall voltage augments the exciting voltage and a new discharge is ignited. Cells in the "ZERO" state are characterized by an absence of discharge and, therefore, an absence of light. Cells in the "ONE" state are characterized by a sequence of pulse discharges which occur once each half cycle of the exciting voltage.

A recent paper[1] and preceding Progress Reports describe these processes and methods of changing cell states in detail. This report contains some recent observations of the effects of gas composition on discharge properties; it describes some observations of the use of phosphors to provide multicolor capability; and it provides a brief description

---

[1] Arora, B. M., Bitzer, D. L., Slottow, H. G., and Willson, R. H. "The Plasma Display Panel: A New Device for Information Storage and Display," Proceedings of the Society for Information Display, San Francisco, May, 1967.

of some work on the use of these cells in logical structures. It concludes with a discussion of the physical problem of providing starting particles for the state change "off" to "on."

9.2. Discharge Measurements.

Further experiments were performed to compare the discharges in rare gases, in nitrogen and in their mixtures for an 8×8 array with typical cell dimensions (hole dia, 0.015 in; thickness of each glass panel, 0.006 in). The frequency of the sinusoidal signal used in the experiment was in the range 200 to 600 kHz. The typical continuous behavior is obtained for He and Ne. The color of He is faint violet while Ne is bright orange. The gases Ar, Kr, and Xe, however, exhibit pulse behavior, and their color is a faint blue. The light and the current output for these gas and N_2 are shown in Fig. 9.1. The firing voltage and minimum sustaining voltage as a function of pressure are plotted in Fig. 9.2. The memory margin is the difference between the firing voltage and the minimum sustaining voltage. We observe that the memory margin is negligible for He and Ne but is appreciable in other cases. Since the minimum sustaining voltage becomes almost constant or rises slowly as compared to the firing potential with increase in the pressure, the memory margin increases on the right-hand side of the minimum of the Paschen curve.

The results of adding (about 4%) Ar, Kr, and N_2 to Ne, and N_2 to He, are shown in Fig. 9.3. From our observations it may be concluded that a change in the discharge behavior from the continuous type to the pulse type occurs whenever a gas of the latter group is added in small quantity (say 4%) to a gas of the former group. The change in the memory is shown in Table I.

B. M. Arora

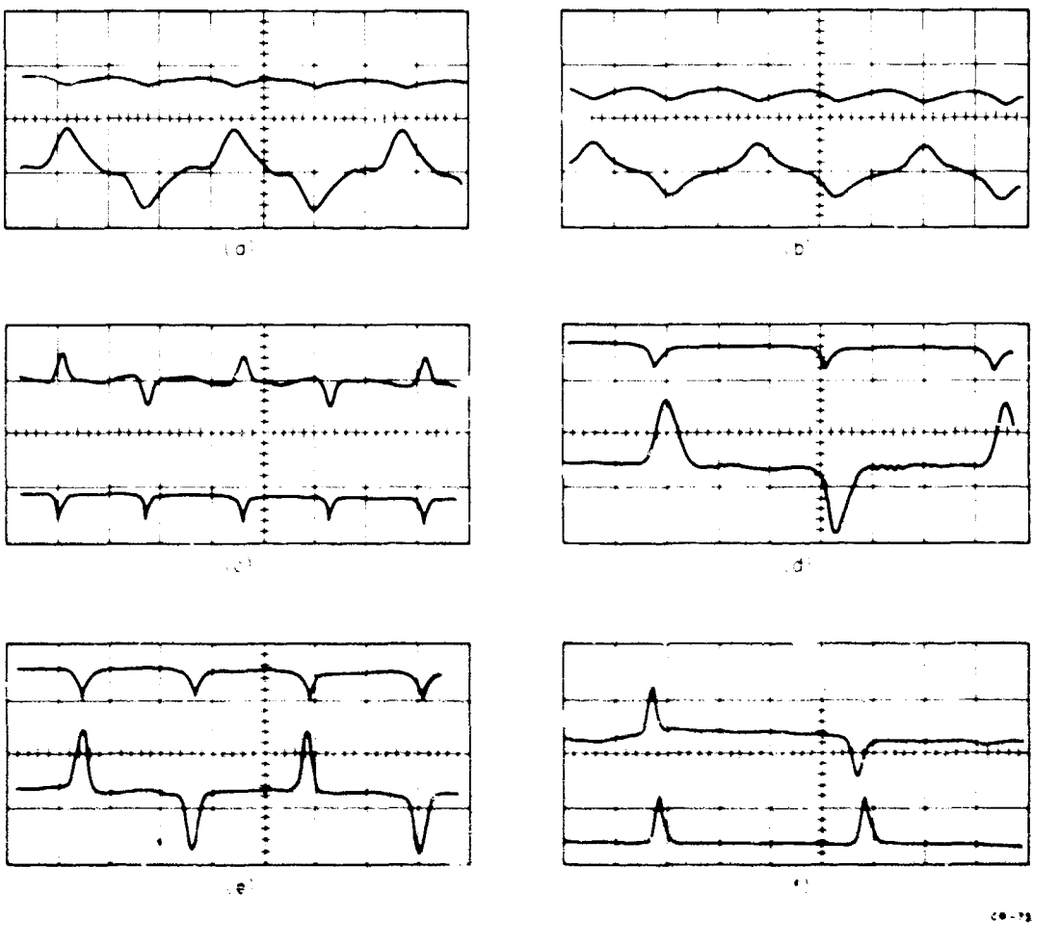

Fig. 9.1. Light and current in plasma display cell for several gases.

	Gas	Upper Trace	Lower Trace
(a)	He	Light	Current
(b)	Ne	Light	Current
(c)	A	Current	Light
(d)	Kr	Light	Current
(e)	Xe	Light	Current
(f)	N_2	Current	Light

(OVERLEAF BLANK)

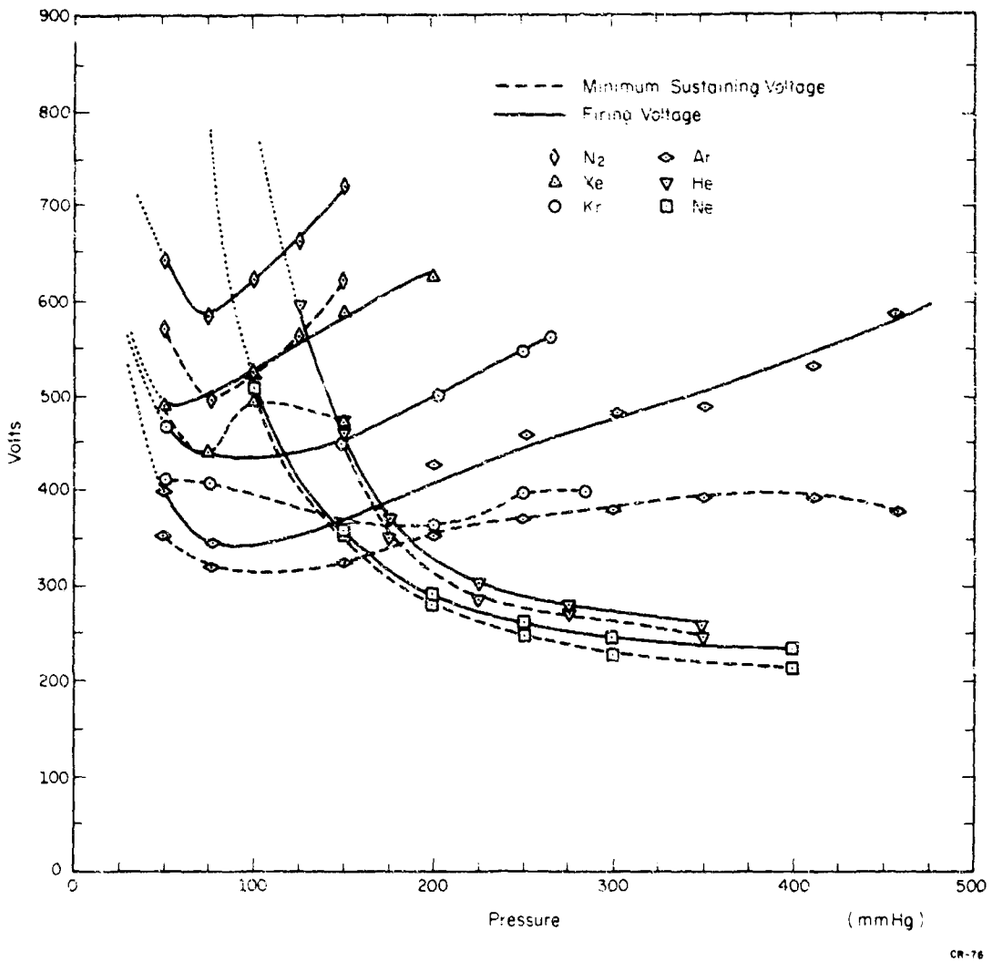

Fig. 9.2. Dependence of firing voltage and minimum sustaining voltage on Pressure for several gases.

(OVERLEAF BLANK)

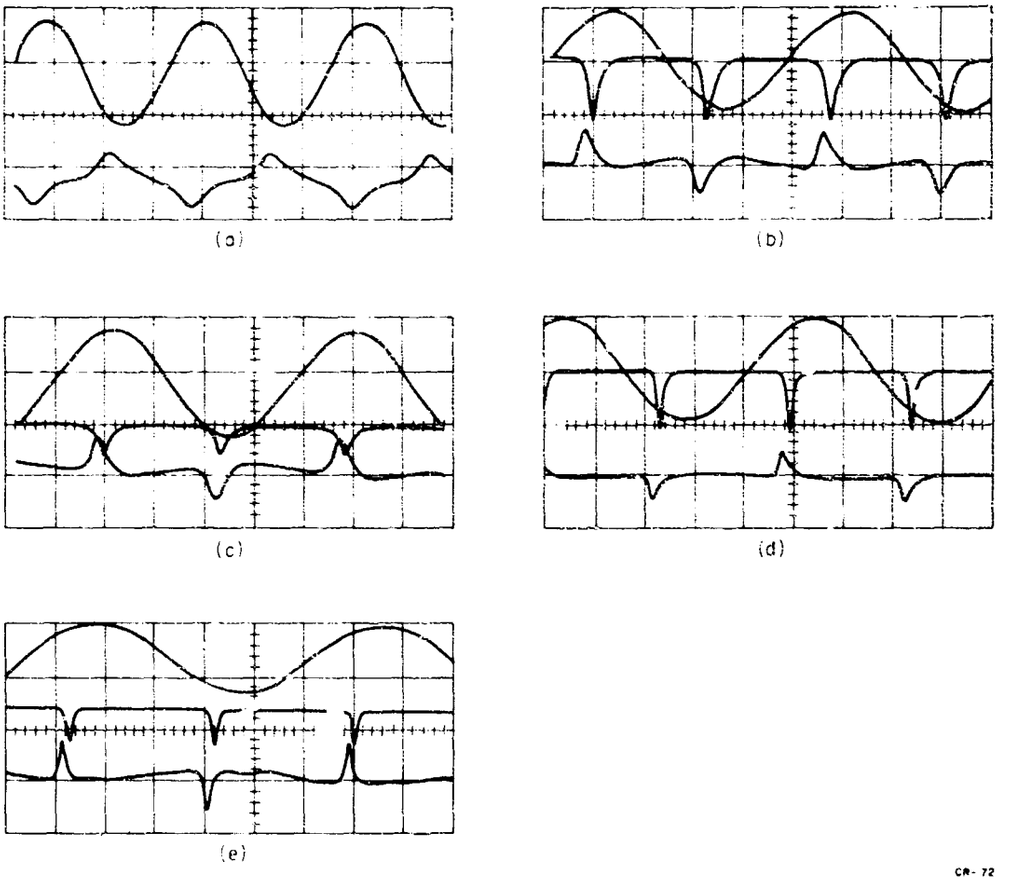

Fig. 9.3. Exciting voltage, current and light in plasma display cell for several gas mixtures.

	Gas	Upper Trace	Middle Trace	Lower Trace
(a)	Ne	Exciting Voltage		Current
(b)	Ne + A	Exciting Voltage	Light	Current
(c)	Ne + Kr	Exciting Voltage	Light	Current
(d)	Ne + N_2	Exciting Voltage	Light	Current
(e)	He + N_2	Exciting Voltage	Light	Current

(OVERLEAF BLANK)

Table 1. Memory Margin for the Tested Mixtures

Mixture	Pressure (mm Hg)	Voltage Firing	Minimum Sustaining Voltage	Memory Margin (volts)
$He + N_2$	205 + 10	625	515	110
Ne + Ar	144 + 6	460	390	70
Ne + Kr	144 + 6	550	490	70
$Ne + N_2$	144 + 6	500	375	125

9.3. Phosphors in Multicolor Displays.

A desirable extension of the plasma display technique would be the displaying of information in several colors. Beyond enhancing the versatility in information display, the development would be necessary for the Plasma Display Panel to replace the cathode ray tube in future television sets. It was decided to attempt to produce the three primary colors with phosphors since this method seemed to offer sufficient light intensity to be of practical use in a visual display. There were then two questions which had to be answered. First, is there sufficient energy in the ultraviolet light or in the electrons of the discharge to excite the phosphors? And second, what effect will these phosphors have on the memory of the cells?

A panel was constructed with three cells to test the possibility of using phosphors excited by ultraviolet light. The first cell contained a phosphor sensitive to radiation in the band centered at 2537 Å and the second contained a phosphor excited by light in this region but more strongly by radiation in the band centered at 3650 Å. A third cell did not contain a phosphor and was used as a basis of comparison to determine the effect of the phosphors on the memory. Nitrogen and each of the rare gases were tested for their ability to create a phosphor glow. Only argon, nitrogen, and mixtures containing these gases produced any appreciable glow. Both gases were capable of exciting both phosphors, with nitrogen creating glows perhaps an order of magnitude more intense than those in argon.

These phosphors, applied to one end wall of the cells, tended in all cases to reduce the memory. A substantial part of this reduction

could be attributed to the change in the geometry of the cells caused by the appreciable thickness of the phosphor and binding material. In spite of the loss, the memory margin was sufficient for application to a practical display.

A similar panel was constructed to test cathodoluminescent phosphors. In this panel, one cell contained a cathodoluminescent phosphor, and another contained a phosphor excited by ultraviolet light. The cells were filled with nitrogen and with rare gases, and relative light intensities were measured. It was found that while nitrogen had little effect upon the cathodoluminescent phosphor, the rare gases produced very strong phosphorescence, with the intensity increasing as one goes down the list of rare gases in the order of increasing atomic weights. Figure 9.4 indicates the results of these measurements.

Not only were krypton and xenon capable of producing cathodoluminescent phosphor glows greater than the strongest obtained with phosphors excited by ultraviolet light, but these gases in the cell with phosphor had memory characteristics comparable to that of an addressable display now being investigated. Figure 9.5 is an oscillograph of the current pulses in krypton in a cell containing cathodoluminescent phosphors and indicates the low recurrent voltage with respect to the applied voltage.

These preliminary investigations indicate that a multicolor plasma display is feasible. However, there remains to be investigated the long-term effect of the discharge on the phosphor and any effects which the phosphors may have on the properties of an array of cells.

E. Stredde

(OVERLEAF BLANK)

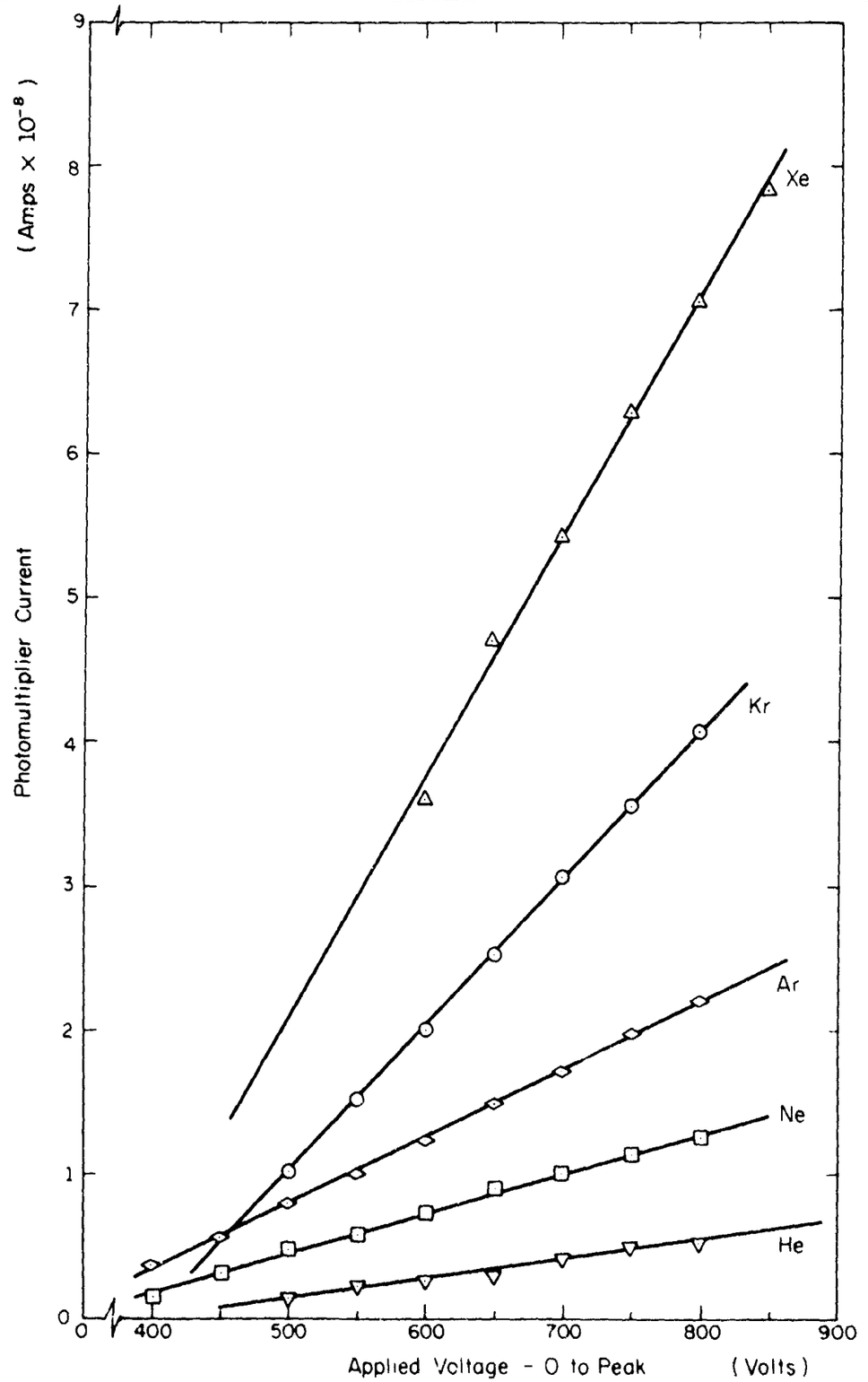

Fig. 9.4. Relative light output in plasma display cell with cathod[9P-7A] luminescence.

(OVERLEAF BLANK)

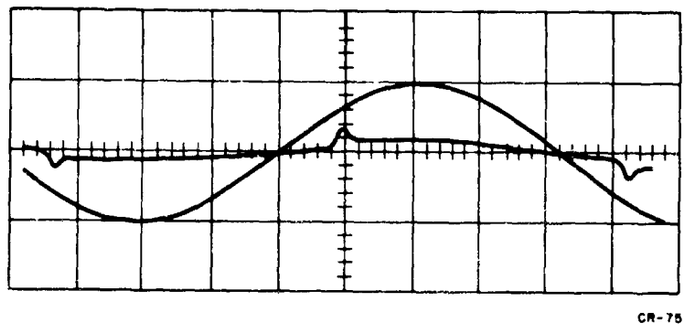

Fig. 9.5. Oscillograph of exciting voltage and current in plasma display cell coated on one surface with cathodoluminescent phosphor, and filled with krypton.

(OVERLEAF BLANK)

9.4. Use of the Plasma Cells as Logic Elements.

The memory of plasma cell resides in the wall charge. If the cells in a panel can be made to communicate with each other via a conductive link such that, if one of the interconnected cells in in "on" state, all others should have wall charge equivalent to the cell which is "on." If the operation of linking two cells is made selective, then it is possible to perform logic operations using plasma cells. In order to test whether all interconnected cells have the same wall charge if one of them is turned "on," a cell with conductive linkage between cells has been constructed (Fig. 9.6). The cell is similar in structure to the typical plasma cell, except that it has gold conductors on the inner surfaces of the cells. In order that the links be selective, the internal gold conductor covering one cell will be separated from the other by a photoconductor. At dark level, the high impedance of the photoconductor separates the two cells. On illumination, however, the impedance falls, thus establishing the conductive link. Experiments using these cells will be conducted in the next reporting period.

B. M. Arora

9.5. The Starting Proglem.

In the plasma display cell, as in other types of electrical gas-discharge configurations, the occurrence of a discharge depends upon the presence of a voltage V greater than V_f across the cell, as well as the simultaneous presence of an ionizing mechanism or source of charged particles (electrons) to initiate the discharge. Once a cell has experienced an initial discharge, the discharges of each following half cycle of the applied signal (at a frequency of 100 to 500 kHz) occur with

(OVERLEAF BLANK)

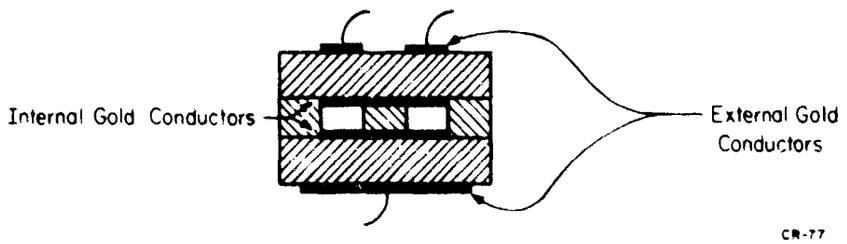

Fig. 9.6. Plasma display cell with conductive linkages.

(OVERLEAF BLANK)

such regularity that no jitter is observable even with recurrent sweeps at 50×10^{-9} sec/div on a fast oscilloscope. This regularity is thought to be supported by the presence of metastable atoms created in the volume by the preceding discharges. These metastables diffuse to the walls, where they transfer their energy, and produce secondary electrons which, in turn, are capable of starting a discharge.

Since this diffusion time is on the order of 50 to 100 microseconds, a cell that has been off for a period longer than this must depend upon some other mechanism to furnish the initial particles necessary to start a discharge sequence. In contrast to the consistent pulse-to-pulse behavior, our observations indicate considerable variability from one display to another in reliability of starting. We have observed[1] that the light from one cell on the diagonal of an 8×8 array can supply enough photoelectrons at any other cell in the display to initiate the sequence. In other arrays, however, the range of influence is as small as one intercell distance (0.025 in). The problem is further complicated by the dependence of this behavior on time. A cell which has been "off" for one second can be turned "on" more easily than a cell that has been "off" for several minutes.

Since the occurrence of a discharge in a gas cell, when the proper field conditions exist, is dependent upon the emission of electrons from the cathode surface; it is, therefore, dependent upon the electron-emission characteristics of the surface material. For ideal operation, a plasma display cell must discharge within several nanoseconds after the critical field or firing voltage occurs in the cell (i.e. under all

wall conditions and <u>every</u> time the firing voltage is reached). Consider the following idealized conditions:

1) Assume that the time allowed for a discharge to start, after the firing voltage has been exceeded, is approximately 10 nanoseconds;

2) Assume that the emission of one electron at the cathode is sufficient to start the discharge and that this electron must be emitted from a surface area of 6.25×10^{-6} cm^2;

3) Assume that the cell length is 0.015 cm.

With these assumptions, the required emission current density which must be supplied by an emission (starting) mechanism is

$$J = \frac{1 \text{ electron}/10\text{ns}}{6.25\times10^{6} cm^2} = 2.5\times10^{-6} A/cm^2 .$$

It should be noted that a current density of this order of magnitude will not cause a significant increase in the decay time of the wall charge which provides the memory in this device.

It is thought that several electron-emission mechanisms, presently being investigated at CSL, can be incorporated into the cell configuration in such a way as to provide the current density necessary for reliable (ideal) operation. The electron emission mechanisms of interest at present are photoemission, thermionic emission, and field emission. We also plan to assess the effects of a conditioning pulse that will excite discharge in every cell in the display at intervals of about a second, but which will leave the states unchanged. We expect that this will preserve the apparently higher short-term photo sensitivity. One technique that avoids the problem altogether is to decrease the time

interval between conditioning pulses until it is comparable to the diffusion time for metastables. Starting particles are then always available. The question here is psychological rather than physical. Is the contrast between cells in the two states great enough to be satisfactory?

Our understanding of these basic processes should be increased Relevant questions concern time variation of photoemissivity, charge spreading on the wall surfaces after a discharge and the possible enhancements of electric field associated with loosely-bound particles. More data should also be obtained on the photoemissive properties of a variety of insulators and on the sensitivity of these properties to surface cleanliness and the presence of certain contaminates.

R. L. Johnson

(OVERLEAF BLANK)

G. Anner
W. P. Bleha
W. D. Compton
S. Depp
R. N. Peacock
O. Reilly
A. C. Tulumello

10.1. Introduction.

The principles of operation intended for this device have been discussed in the two previous progress reports. Instead of attempting to fabricate complete thin-film display devices, the work has been concentrated on understanding some of the basic problems. Tunnel-injection samples have been made on small pieces of bulk single-crystal CdS, and light emission related to the observed current-voltage characteristics. Since it is expected that thin films of CdS and small-gap semiconductors will be needed, efforts have been made to deposit such films with properties approximating those of bulk materials. Controlling the conductivity of the films is also a serious problem.

10.2. Device Testing and Evaluation.

10.2.1. Investigation of EL Mechanism.

The immediate goal of this period was the investigation of the mechanism of electroluminescence (EL) in Jaklevic devices.[1] These comprise a single crystal of CdS contacted by metal (In) on one side. On the other side is a thin insulating layer of SiO and a second metal contact (Au or Ag).

To accomplish this goal, some 25 devices were fabricated on TO-5 or TO-18 commercial headers. Mounted in this rigid form the devices were

[1] R. C. Jaklevic, et al., Appl. Phys. Letters 2, 7 (1963).

able to withstand repeated immersion into liquid nitrogen. The I-V curves of all the devices were checked, as was their ability to give EL at liquid-nitrogen temperature.

The I-V curves of nearly all the good units, i.e., those that gave EL, were typical of rectifying barrier diodes having threshold voltages from 0.5 to 0.75 V, and having relatively soft reverse-breakdown characteristics with breakdown lying near 8-10 V. In some cases there was a relatively large leakage or tunneling component.

It is believed that the diode component is caused by small rectifying contacts between metal (Au or Ag) and the semiconductor (CdS) that are formed through pinholes in the SiO film. The reverse characteristics may in some cases be due in part to a tunneling component through the SiO film.

Unique criteria for distinguishing tunneling from other mechanisms are not available. Reasonable guides are afforded by Wilmsen and Hartwig,[2] however, who predict that in a metal-insulator-semiconductor system the tunneling I-V characteristic over a few volts range will 1) exhibit skew symmetry about zero current and the voltage needed to bring the metal Fermi level opposite the tunneling states in the semiconductor; 2) be essentially exponential; 3) be temperature dependent to some extent; 4) saturate at some negative voltage if the semiconductor is n type as with CdS.

---

[2] C. W. Wilmsen and W. H. Hartwig, "Tunneling Between a Metal and Silicon Separated by a Polymer Insulator," University of Texas, Laboratories for Electronics and Related Science Research, Technical Report No. 25, September 15, 1966.

Further analysis of the I-V curves is needed to see if a component satisfying these criteria is present.

As further evidence for the presence of a tunneling component, the light output of a typical unit was checked with a photomultiplier. The output increased exponentially with device current from roughly 40 mA (turn on value) to 70 mA. The output saturated above 80 mA of device current.

It appears that EL may take place in these devices by means of at least two different mechanisms: 1) Tunneling for which the turn-on voltage for visible EL is roughly 1.25 - 1.75 V; and 2) Impact EL with turn-on voltages in excess of 5V. It is interesting to note that some of the devices could be operated ty either mechanism, depending upon the applied voltage polarity. For forward bias (CdS negative) green EL was produced at low voltage, while reverse bias produced yellow EL at higher voltage.

Several of the devices which were fabricated did not exhibit EL, the probable causes being: too thick or too thin SiO films, or damage to the CdS crystal as the result of excess heat or other conditions encountered during fabrication.

Device capacitance versus reverse voltage was checked for several units. Typically, the capacitance varied 8 pF in 80 pF, the principal change occurring between 0 and -1 V. It appears that the tunneling barrier width is determined primarily by the SiO layer, band-bending effects being the cause of the variations.

10.2.2. Thin-Film Devices.

Even though no high quality, thin CdS films were available, a few devices were made from high-resistivity films that were deposited by chemical means onto glass slides. A planar geometry had to be used since only one side of the CdS film was accessible. It was found that relatively high voltages were required to produce EL at liquid nitrogen temperature, the light being emitted in very bright, isolated spots under the negative electrode (a in Fig. 10.1). In these devices the CdS sheet resistance is very high and it is doubtful that the tunneling mechanism is involved.

G. Anner
W. P. Bleha
R. Birtcher

10.2.3. Testing.

The major effort during this period was to construct additional equipment for the evaluation of infrared converters and their component materials. Initially, the integrating sphere was completed and made vacuum tight. A diffuse coating has not been applied to the interior of the sphere as the light output of the present samples is too small and sphere coatings are short lived.

A Jarrell-Ash spectrometer and appropriate optics were purchased and set up to measure the spectra of UV-stimulated edge luminescence and electroluminescence in the CdS samples. A dewar with glass windows and capable of being mounted on an optical bench was constructed for this purpose. It has been found that for UV-stimulated edge luminescence, the common CdS etchants (HCl and MIT Etch No. 28)[3] produce negligible changes

[3] H. C. Gatos and M. C. Lavine, MIT Lincoln Laboratory Tech. Report No. 293, AFESD-TDR-63-33.

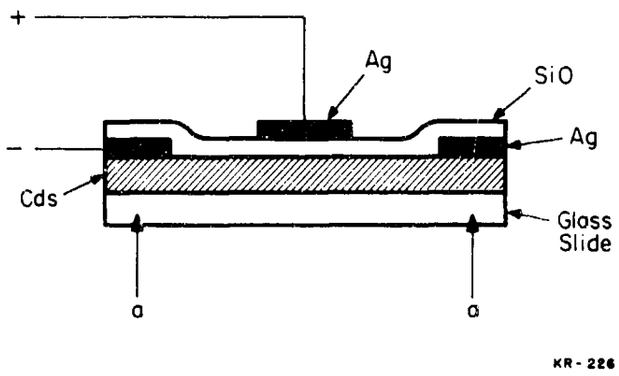

Fig. 10.1. A planar luminescent device using a CdS thin film.

(OVERLEAF BLANK)

in the spectrum. The situation with contact materials is quite different, however. Figure 10.2 shows the spectrum of HCl-etched CdS samples under various treatments. It is clear that much care must be given to contacting methods if the edge luminescence is not to be washed out.

A Van-der-Pauw measurement station was set up with a glass dewar, appropriate instruments, magnet and a switching circuit to facilitate rapid resistivity and Hall measurements of films at room and liquid nitrogen temperatures.

S. Depp

10.3. Preparation of CdS Films--Chemical Methods.

The preparation and properties of CdS by chemical methods continues to be studied. The preparation of green-luminescent cadmium sulfide can be readily accomplished by baking a sample in hydrogen and hydrogen sulfide at 450°C. The process seems to be indifferent to the source of the cadmium sulfide and works equally well on powdered as well as deposited films.

The measurement and preparation of deposits of CdS with predictable electrical properties remains a problem. On a number of occasions, deposits of cadmium sulfide have been made on germanium wafers with a qualitative resistance of less than 100Ω measured point to point. This has been accomplished by the controlled doping of the cadmium sulfide by indium. In order to make quantitative measurements of the electrical properties, it is necessary to make ohmic contacts on a Hall sample. All efforts to prepare metal Hall masks through which to deposit the CdS have resulted in the introduction of metallic impurities into the sample. A glass Hall mask is in preparation. Until the recent introduction of

(OVERLEAF BLANK)

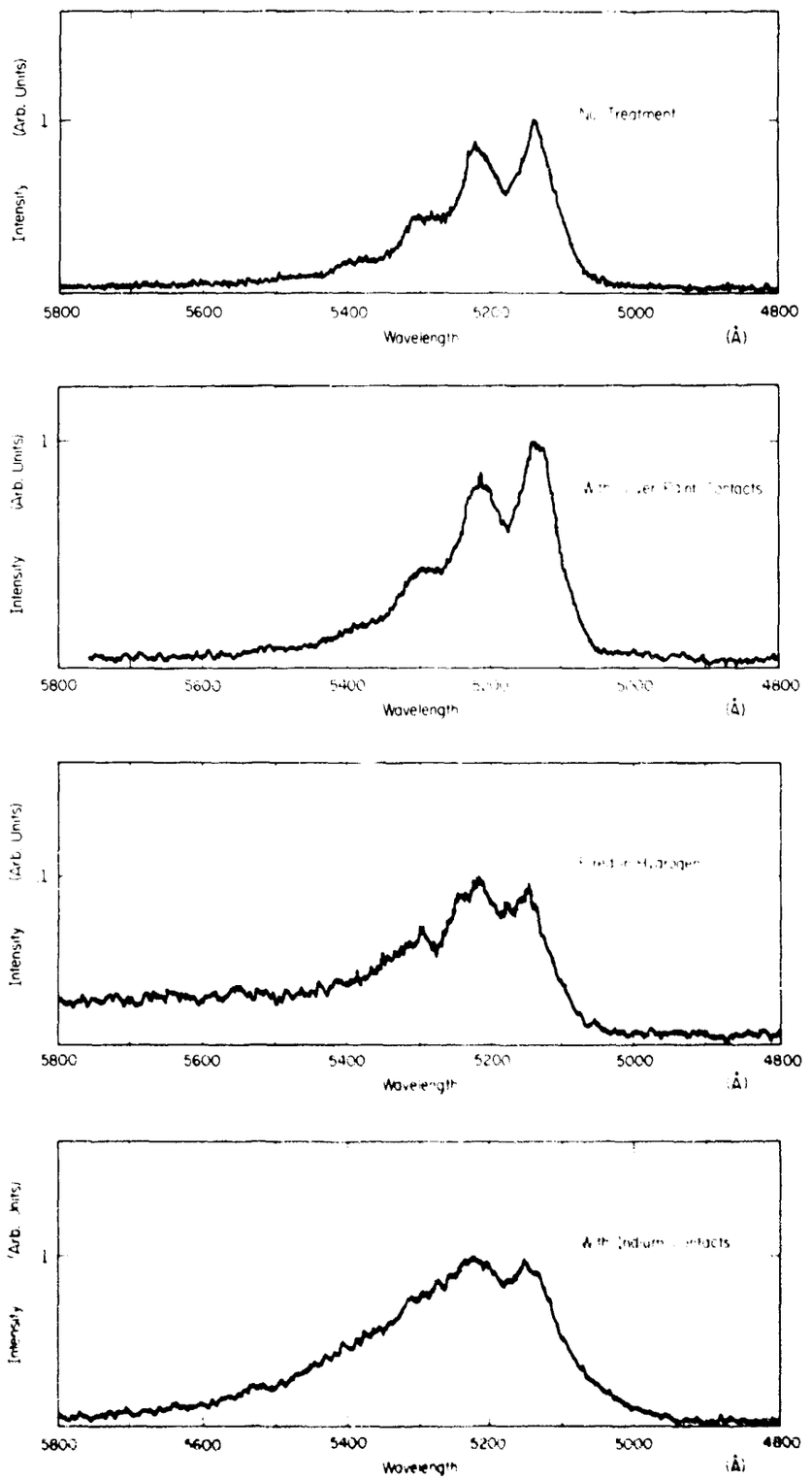

Fig. 10.2. The effect of various treatments on the UV-stimulated edge-luminescence of single-crystal CdS at 77°K.

(OVERLEAF BLANK)

ultrasonic bonding of indium, ohmic contact to the CdS has been a problem. Some efforts to prepare fluxes in which to cleanse the surface and remove oxide films, gave some success. Various acids and salts, such as acetic and tartic acids and their ammonium salts, were tested. The acetic acid was volatile before the indium melted. The tartaric gave carbon on heating. Hypophosphorous acid H_3PO_2 gave adherent indium contacts.

The controlled preparation of conducting cadmium sulfide by vapor transport has been interrupted by the need for a more uniform temperature gradient and difficulties in holding the pressure at approximately 500 mm of hydrogen. A new oven is being mad and effort is underway to obtain semiconductor-grade materials as reagents. The presence of small amounts of oxygen (21 ppm) in the hydrogen seems to be necessary to give higher conductivity. This is in agreement with Woodbury's observation.[4] Too much oxygen is reported to remove indium. This would decrease the conductivity. Further study and isolation of these variables is projected when movement to the new building is completed.

Spray deposition of CdS on a substrate of glass quartz and germanium has given edge-luminescent CdS on a soft-glass slide maintained at 450°C. If two slides are placed on the hot plate, one of them quartz and the other lime glass, and the hot plate raised to a temperature sufficient to maintain a temperature of 450°C at the surface of deposition; the glass slide begins to soften and the quartz slide does not. When the surface is sprayed with an 0.1-M $CdCl_2$ solution containing 0.4-M NH_4CNS a green-luminescent coating is seen on the formerly-softened glass slide. This does

[4] H. H. Woodbury, Phys. Chem. Solids 27, 1257-1261 (1966).

not occur on the quartz slide. This technique has thus far only resulted in high-resistance CdS.

A. Tulumello

10.4. CdS Vacuum Evaporation.

Work has continued on the vacuum evaporation of CdS with the emphasis on making green-photoluminescent (77°K), low-resistance films that could be formed on Ge substrates. As was previously reported, vacuum-evaporated CdS films that were post baked in H_2S atmosphere showed bright-green photoluminescence and the characteristic excition structure of CdS single crystals. These films were of high resistance which is not usable in the device. Thus, other methods for forming low-resistance films must be developed.

Indium doping of CdS provides room-temperature green photoluminescence with low resistance. An attempt was made to mix the CdS evaporation powder with 0.1-Mole-% indium nitrate and to evaporate this mixture onto heated substrates. The indium metal evaporated from the source before the CdS started to evaporate and poor-quality films resulted. Other researchers have abandoned co-evaporation techniques for dopants into II-VI compounds because of nonreproducibility and thus it was decided to abandon this approach and concentrate on pure CdS films.

Films that show a yellow-green luminescence (77°K) and resistance of 10^2 to 10^3 Ω-cm can be made by evaporation of CdS onto a 300°C glass substrate. It has been found in preliminary experiments that more nearly green photoluminescence that is visible only below 77°K can be obtained from CdS which has been evaporated on a Cd film held at 200°C. Since Cd has an appreciable vapor pressure at this temperature compared to the

vacuum chamber of 10^{-5} Torr, it might be expected that there was Cd doping of the CdS film. The quality of the films will have to be improved before accurate resistivity measurements can be made.

While continuing work on Cd-doping films during the evaporation process, experimentation will also include post-evaporation treatments to lower the resistivity of the CdS films. Processes must be found that do not effect Ge so that Ge substrates can be used for the CdS films.

W. P. Bleha

10.5. Small-Gap Semiconducting Films.

In the previous Progress Report it was stated that attempts to make high-mobility-InSb thin films using conventional evaporation methods were totally unsuccessful. The results of the Hall mobility measurements showed that the films were more metallic than semiconducting.

It was then decided to use flash-deposition techniques utilizing the "Ultrasonic Particle Feeder" developed by J. R. Eckardt and R. N. Peacock.[5] Some time was spent on further development of the feeder and in adapting it to our vacuum system.

Single-crystal intrinsic InSb was mechanically polished, chemically etched, and crushed into a coarse powder, and then loaded into the feeder. The feeder would then drop a few grains of InSb at a time onto a hot molybdenum boat. These evaporations were carried out at a pressure of 1×10^{-6} Torr.

In the first attempt at flash deposition three samples were made on a glass substrate heated to a temperature of 322°C. Resistivity and

[5] J. R. Eckardt and R. N. Peacock, J. Vac. Sci. Technol 3, Nov.-Dec., 1966.

and Hall mobility measurements of these and subsequent films were made by the van der Pauw technique.[6] The highest Hall mobility measured in this first batch of films was 112 cm^2/Vsec.

In the next evaporation, four samples were made on a glass substrate held at 315°C, annealed for two hours and thirty minutes at this temperature, and then slowly cooled to room temperature. The highest mobility in this group of films was found to be 1760 cm^2/Vsec. The resistivity of the above film was 4.6×10^{-2} ohm cm as compared to a resistivity of 5.75×10^{-3} ohm cm for the bulk intrinsic material. This data agrees well with the values given by Carroll and Spivak[7] for their films prior to recrystallization in an argon atmosphere. Carroll and Spivak report that this recrystallization process changed the mobility of their films by a factor of about 100.

The post-treatment recrystallization process was tried on the third group of films. The best film in this group had a mobility of 3060 cm^2/Vsec. This is far short of the 30,000 cm^2/Vsec obtained by Carroll and Spivak and yet much better than our very first films which had mobilities comparable to those of a metal, i.e., $\mu_H \ll 1$ cm^2/Vsec.

A study of the literature concerning small-gap semiconductors such as lead salts, tellurides, etc., is underway. Some materials will be selected and films tried.

J. Robinson

---

[6] L. J. van der Pauw, Philips Research Reports, 13, 1-9, 1958.

[7] J. F. Spivak and J. A. Carroll, Solid State Elec. 9, 383 (1966).

10.6. The Insulating Film Separating Germanium from Cadmium Sulfide.

Thin-film literature referring to insulators of tunneling thicknesses is being surveyed. The need is for a stable and continuous insulating film less than 200 Å thick formed by direct deposition with controlled uniform thickness. Methods have been reported meeting some of these criteria but not all of them. Tunneling-thickness insulators have usually been prepared by oxidizing the surface of a metal. Most reports and studies on insulators have been done at thicknesses of 1000 Å or more with interest in high insulation and quality control rather than tunneling. Some effort will be required to meet our criteria since more research is required on insulators less than 500 Å thick.

Perhaps the approach of Wilmsen and Hartwig[8] is worth consideration. These authors did a tunneling experiment using an insulating film formed by polymerizing a silicone oil by electron bombardment. A diffuse, uniform, electron beam is required for this method. Toward this end, an electron gun of the type used in cathode ray tubes has been modified for use in a bell-jar vacuum system.

O. G. Reilly
S. W. Depp

---

[8] C. W. Wilmsen and W. H. Hartwig, "Tunneling Between a Metal and Silicon Separation by a Polymer Insulator" University of Texas, Laboratories for Electronics and Related Science Research, Tech. Rep. No. 25, Sept. 15, 1966.

(OVERLEAF BLANK)

11. INFROMATION SCIENCE†

R. T. Chien
R. B. Ash
L. Bahl
K. Biss
D. Butler
D. Carroll
D. Chow
A. Haddad
C. Hartmann
S. J. Hong
K. Kelley
S. Li
G. Lipovski
T. Mandel
F. Preparata
S. Ray
P. Reynolds
F. Stahl
R. Tracey
J. Tummelson
K. Tzeng
P. Weston

11.1. Computer-Based Information Retrieval.

Along with the continuing theoretical investigation of problems and aspects of computer-based retrieval systems (such as clustering theory and file organization), as well as with the activity of construction of an articulate data base, the main effort has been devoted to setting up an interactive system on the CDC 1604. In order to take advantage of the recent addition to the 1604 of a cathode-ray display unit, equipped with light-pen and typewriter facilities, the necessary software has been developed to incorporate such powerful interactive capability in the Information Search Language (ISL). Furthermore, ISL has been embedded into ILLAR, a very flexible, locally-developed, assembly language. The resulting language possesses the search capabilities of ISL as well as the general housekeeping power of ILLAR.

Details on each of the mentioned research areas are given in the following sections of this report.

11.1.1. File Organization and Search Strategy for Mass-Storage Systems.

As information-retrieval systems transit from the research environment into an operational environment, the question of efficiency becomes increasingly more important. In automatized systems, efficiency is directly expressed by the complexity of a retrieval task, and, for a

†This work was supported in part by the National Science Foundation under Grant GK-690.

given system, the total required retrieval time is an adequate evaluation parameter. Since a retrieval task is the application of a search algorithm over a file organization, the investigation of these two elements is of primary importance. Most of the work done so far has concentrated on systems equipped with a unidimensional tape file, but the recent advent of large-scale, mass-storage systems, with their operating flexibility, has disclosed new possibilities for a more efficient implementation of retrieval systems. Therefore, a study has been undertaken of the problems posed by these new hardward devices (mass storage memories with some random access capability) with reference to documents-retrieval systems employing coordinate indexing.

Two important types of queries have been analyzed, i.e. the "Boolean Query" and the "Linear Query." The mass storage is assumed to be subdivided into "buckets," each of which can be individually accessed in a random fashion. The main result of the study is that the two different queries can be handled with very similar philosophies, having these basic traits:

a) An inverted file structure for the random-access memory as a whole.

b) A serial file structure for each bucket of the random-access memory.

c) The search consists of two steps: determination of a convenient (possibly minimal) set of buckets to access, and the screening of the data contained therein.

The fundamental difference between the two cases resides in the allocation of descriptors to buckets, namely in the nature of the descriptor

clusters. The clusters are "thesaurus groups" for the Boolean query, while they are "contiguous sets" for the linear query (in other words, they are generated by second-order or first-order correlations in the two cases, respectively).

The analysis also suggests that the original descriptor dictionary should be replaced by a reduced dictionary, not containing those descriptors which index a number of documents exceeding a certain threshold (i.e. the less specific descriptors).

The most important problem that this study opens seems to be the theoretical-experimental investigation of the relation existing between the sizes of the buckets, the collection, the original dictionary, and the reduced dictionary. These questions are the subject of continuing investigation.

R. T. Chien
F. P. Preparata

11.1.2. Clustering Theory.

The "clustering problem," namely the identification of sets in such a fashion that objects within a set are similar to each other but are dissimilar from objects outside the set, is central in information retrieval. Particularly so in document retrieval, with reference to document classification, indexing, and efficient file organization (see section 1.2). Several clustering techniques have been developed by other authors, all based on the criterion of assigning a document to the cluster with which it has the highest "global" association. Our approach drew its motivation from computer-based systems whose data base is a linked structure, specifically a citation graph. If a search progresses through

the links of the graph, its complexity is obviously reduced if items which are likely to be wanted together are located physically close in the memory structure. This objective is accomplished by mapping the given graph onto a unidimensional array and by successively rearranging the locations assigned to documents. The criterion governing the location assignment is the reduction of the "stretching" of graph links as produced by the mapping. This is equivalent to the reduction of the total stretching (objective function) and, on the average, brings to close-by locations in the array documents which are close in the graph. The proposed iterative algorithm is effective in the sense that only reductions of the total stretching are produced; in a slightly modified version, it is efficient since its complexity from a computational standpoint grows only as $N^{3/2}$, where N is the size of the collection

Very interesting experiments have been recently performed after the algorithm had been translated into a computer program for the CDC 1604. Operating with a graph of 100 nodes, convergence of the method has been attained after very few iterations (usually less than 5). For N=100 each iteration of the modified algorithm requires an average of approximately 2 minutes on the 1604.

F. P. Preparata
R. T. Chien

11.1.3. A Survey of Clustering Techniques.

In the general area of library automatizaton a primary necessity is a memory facility (namely, a computer memory) to store information concerning the books, papers, documents, etc., available in the library. The allocation of data has to be guided by the objectives of speed and

efficiency of the retrieval task. One way of storing the documents is by grouping together "similar" documents in clusters.

It is our feeling that this area has great potentialities, and we are presently interested in a survey about "Clustering Techniques," with application to Information Retrieval. More than 20 papers have been selected and a survey report is forthcoming.

Carlos Hartmann
Kenneth Biss

11.1.4. Data Base.

During the present report period, work has continued on the development of a data base of computer-processable bibliographic information reflecting a corpus of documents in the field of computer science and technology as initially defined by contributions in two of the leading journals in the area, the Journal of Association for Computing Machinery and the IEEE Transactions on Electronic Computers. In the previous report period, contributions in these source journals were processed (coded, keypunched, and stored on magnetic-tape) for the year 1965; in the present report period, processing has been substantially completed for the year 1962 (which was chosen as the second target year on the basis of samplings suggesting the desirability of a 3-year interval to reveal most quickly at least the general features of the underlying relation network of interacting documents), and approximately half of the contributions for the third target year 1966 were also processed.

As the general structural features of the data base began to emerge more clearly, the decision was made to begin processing also contributions for the year 1965 in a third source journal, American Documentation, in order to add materials in a different but still related

subject area, to facilitate comparative analyses and provide a desired experimental control. As in the case of contributions in the other two source journals, the same kinds and relatively extensive amounts of data were selected for recording for each article and cited reference in the third source journal (i.e., authorship data, title words, text language, literary form, citation-contexts, etc.). The same pattern or sequence of target years is also anticipated for each source journal, notably (1) 1965, (2) 1962, (3) 1966, (4) 1963, (5) 1967, (6) 1964, (7) 1968, (8) 1969, etc.

At the end of the previous report period, some 200 source articles containing on an average approximately 10 citations had been processed, yielding a total population of some 2,200 titles available for analysis. As anticipated, during the present report period these levels were increased to slightly less than some 600 and 6,600 titles respectively. This improved rate is reflective of a more complete regularizing of the processing routines as summarized in an instructional manual which is now enjoying a further revision in light of the first actual test programs run on the data base at the beginning of the summer.

D. E. Carroll

11.1.5. Information Search Language and the Interactive System.

During the early month of this reporting period, the Information Search Language (ISL) was developed into a working system. The final version has a repertoire of 21 instructions as opposed to the 14 originally envisioned. The additional instructions add to the flexibility of

the system. The STRING instruction provides a method of inserting strings of characters into the program area to facilitate comparing of the raw data. With the V-SEARCH instruction one can make a search for other occurrences of a string of characters read from magnetic tape. The CONVERT instruction allows printing in decimal form any positive integer such as counters used in a program. The T-STRING instruction enables the user to input a string from the typewriter at run time. A natural extension of this is the T-JUMP instruction which allows user control of jumps to various parts of a program.

This information search language was used to write several "service" routines to be used in getting the data base into a workable form. Among these are such functions as listing data tapes, copying data tapes, and packing the data into a condensed form. Each of these programs was kept on paper tape because the language had no facility for saving programs in machine language or assembling from magnetic tapes. Also a standard Codap program was written to translate card-image records on magnetic tapes from the IBM 1401 to tape images readable by the variable-length read instruction of ISL.

Once the data has been extracted from journal articles and punched on cards, the following steps are followed:

1. The cards are transferred to magnetic tape on an IBM 1401 or similar machine.

2. This tape from the 1401 is then translated into records readable by ISL's read instruction. Since the data records normally read by ISL are of variable length, the first word (8 characters) of the ISL

record must be a number indicating the length of the record. After this step, the next two are both done on these card-image tapes.

3. The data is then packed into long records. On one record is placed all of the information concerning one source article. All blanks are suppressed from the "cards," and dashes are inserted to separate the cards. This procedure reduces greatly the length of tape taken up by record gaps and spaces; thus, reducing the amount of core and time needed to handle the record. All searches and experiments are then carried out on these packed records.

4. The data is checked. The ISL syntax checking routine is a prime example of the usefulness of ISL. Errors such as missing titles and authors, descrepancies between the acronym codes and the number of citations and/or citation-context strings, and improper or misplaced cards are flagged on a listing so that the data can then be corrected.

5. Errors in the raw data are corrected at the card level and then steps one through four are repeated.

Thus, the Information Search Language was a functioning system by June of this year and had been used to facilitate preparation of the actual data it was designed to handle. At this point, it seemed pertinent to attempt to develop an interactive system that would allow a user to sit at the scope and interact with the machine to do searches for requests entered at the typewriter. Work was begun immediately to implement such a system.

However, the ISL system as it then existed did not lend itself well to such a large programming problem. The system had no capability for convenient subroutine structure or saving of program parts for later

use by another program. Thus, each program in ISL had to be inserted completely by paper tape and assembled every time. The solution to this restriction presented itself almost immediately. The computer programming group of the Coordinated Science Laboratory was in the final stages of developing a programming system (ILLAR) which makes very convenient all of the features that we required to overcome the shortcomings of ISL as it existed at this point. During the summer months, with the help of Mr. Don Lee of the Laboratory, the Information Search Language has been transformed into an ILLAR programming system. What now exists is a much more powerful programming tool. In this system, the user may write a program with only the 21 ISL instructions--but in addition he may use any of the ILLAR-system routines, any machine-language instructions, and also may make use of recursive macros, subroutines called by arguments, and may develop his own library of subroutines. In order to implement this system, we have had to forfeit some of the free format that was perculiar to the original ISL, but the gains in potential far out weigh the losses.

Concurrently with the implementation of this system, programs were developed to display the data on the cathode-ray tube display that recently has been added to the 1604 at the Coordinated Science Laboratory. These programs are in the form of subroutine tools to be used by the interaction program. By the end of August, this display capability was written into the system and work was begun on the actual interaction program. Certain portions of this program were already working at the end of August. Also by the end of August, the "service" routines were rewritten in the new system. The intention is to develop an ISL monitor to facilitate copying, listing, translating from IBM 1401, packing the data, and check[illegible] the

syntax of the data. All of these programs are working, and the entire data-development sequence can be done in considerably less time. These routines now can be driven from the typewriter and because of the ability to enter arguments from the typewriter, the functions can be performed between or from any of the eight tape units available. Previously, these were restricted to only a given tape or tapes for each program. Currently, the entire data-development process can be accomplished without unmounting and replacing any tape reel. The time for translating from IBM 1401 has been cut from about 30 minutes for a reel of tape to about 3 minutes by use of a fast read on interrupt and a fast write on the ISL tape.

In the months following August of this year, primary emphasis will be directed to the full development of the interactive system and the concurrent development of a working ISL monitor. In the immediate future we expect to receive from Control Data Corporation a 1604 SORT routine, which is needed to facilitate completion of key word in context programs, word-frequency counts, and the construction of a key-word dictionary. These programs are written to the point where the SORT routine is essential, and will be completed within a short time after the SORT becomes operative.

S. Ray
K. Kelley
P. Reynolds
F. Stahl

11.2. Coding Theory.

The main effort in coding is the area of cyclic codes. Several new classes of codes were derived through geometrical considerations. Other classes were derived by combining known codes of smaller lengths.

A new way of deriving the Barrows-Mandelbaum code has been discovered. The new approach shows considerable promise in the construction of general residue codes for multiple error correction.

Details on the individual researches are given in the following sections.

11.2.1. Coding Methods for Information Retrieval.

As mentioned in the previous Progress Report, threshold decoding is applicable to information retrieval because of its easy implementation. A new threshold decodable code which has been shown to be decoded by one-step threshold decoding (not necessary orthogonal parity checks) is found to be decodable by an u-step orthogonalization procedure.

Let α be a primitive root of $GF(q^m)$. Let C be a code whose generator polynomial contains α^h as roots for h satisfying the condition

$$0 \leq w_q(hp^j) \leq (m-u)(q-1)\,;\ 0 \leq j \leq s-1$$

where $q=q^s$ and $w_q(x)$ is the digit sum of the q-ary representation of the integer x. The code C has minimum distance at least $2+q+\ldots+q^{m-u}$. This code contains all the u-dimensional flats of EG(m,q), i.e. the Euclidean geometry of m-dimension over GF(q), and can be decoded by an u-step orthogonalization procedure. The guaranteed decodable distance by this method is

$$d_u = 2+q+\ldots+q^{m-u} = 1 + (q^m-q^{u-1})/(q^u-q^{u-1}).$$

The guaranteed decodable distance by the one-step decoding method is

$$d_1 = 1 + [(q^m-1)/(q^u-1)].$$

The distance d_u is greater than d_1 in general. We call the code C an Euclidean geometry code.

Let $g(x)$ be the general polynomial of an Euclidean geometry code. The code generated by $g(x)/(x-1)$ has minimum distance at least $1+q+\ldots+q^{m-u}$ and can be decoded by u-step orthogonalization procedure up to the distance $1+q+\ldots+q^{m-u}$.

D. Chow

11.2.2. BCH Decoding and Implementation.

Previous algebraic decoding algorithms for Bose-Chaudhuri-Hocquenghem codes have inevitably involved a certain amount of matrix inversion or the evaluation of determinants and thus do not lend themselves to simple implementation. Therefore, the recent introduction of an iterative algorithm by E. Berlekamp as well as J. Massey's followup with a "Feedback Shift-Register Synthesis" algorithm, which are free from matrix work, represent a significant development in the art of decoding BCH codes. However, an investigation of their work has revealed that their approaches have a lot in common and a combined treatment has led to the following algorithm and some other results more general in formulation.

Algorithm:

(1) Examine $S_1, S_2, \ldots, S_{d-1}$

If $S_j \neq 0$ for $j \geq 1$ and $S_i = 0$ for $1 \leq i \leq j-1$ (when $j > 1$)

Then let $\sigma^{(j-1)} = 1$ and $\sigma^{(j)} = 1 - S_j z^j$

$\omega^{(j-1)} = 1$ $\omega^{(j)} = 1$

$D^{(j-1)} = 0$ $D^{(j)} = j$

$\Delta^{(j-1)} = 0$

$$\Delta(n) = \sum_{i=o}^{\deg \sigma^{(n)}} \sigma_i^{(n)} S_{n+1-i}, \quad (\sigma_o^{(n)} = 1), \quad \sigma^{(n+1)} = \sigma^{(n)}.$$

If $\Delta(n) = 0$ Set $\omega^{(n+1)} = \omega^{(n)}$

$$D(n+1) = D(n).$$

If $\Delta(n) \neq 0$, choose smallest $n'(j-1 \leq n' < n-1)$ such that $D(n') \neq 0$ and $n'-D(n')$ has the largest value.

Set
$$\sigma^{(n+1)} = \sigma^{(n)} - \Delta(n)\Delta(n')^{-1} Z^{n-n'} \sigma^{(n')}$$
$$\omega^{(n+1)} = \omega^{(n)} - \Delta(n)\Delta(n')^{-1} Z^{n-n'} \omega^{(n')}$$
$$D(n+1) = \max [\deg \sigma^{(n+1)}, \deg \omega^{(n+1)}]$$

where S_i are the syndrome terms

σ is the error locator polynomial

ω is the error evaluator polynomial

$D = \max [\deg \sigma, \deg \omega]$

Δ is a quantity called discrepancy

(readers are referred to the original papers for more detailed definitions).

This algorithm is the result of a reduction of Berlekamp's work to the kind of simplicity achieved by Massey without using the concept and language of "Feedback Shift-Register Synthesis." But compared to Massey's algorithm, there are a few points which give the above algorithm some advantage.

(1) The initial condition is flexible. It starts at $n = j-1$, $j \geq 1$ rather than at $n = -1$. When, as it frequently happens, several initial steps may be omitted, a saving in decoding time results.

(2) The error magnitude evaluator, $\omega(z)$, is included in the iteration.

(3) The iteration guiding parameter D is exactly Massey's register length. But as the upper degree bound of σ and ω, D is more easily obtained.

The other detailed results are included in a thesis proposal and will appear in a technical report .

In spite of its simplicity, the iterative algorithm, like the previous ones, showed a basic drawback in that it is unable to correct more than $\lfloor\frac{1}{2}(d-1)\rfloor$ errors where d is the BCH bound on minimum distance and $\lfloor\frac{1}{2}(d-1)\rfloor$ denotes the largest integer smaller than $\frac{1}{2}(d-1)$. It is known that many BCH codes have minimum distance d_o greater than d and are able to correct up to $\lfloor\frac{1}{2}(d_o-1)\rfloor$ errors. Therefore, these decoding algorithms have not fully utilized the error-correcting ability of the codes. However, the iterative algorithm has demonstrated some ability in tackling the problem of decoding BCH codes up to a minimum distance and will be further extended for development in this direction.

K. Tzeng

11.2.3. Linear Residue Codes.

The family of arithmetic codes of the form AN, where A is derived from a generator called B through the relation $A = (2^e-1)/B$ (e is the exponent of 2 modulo B), has been the subject of considerable continuing investigation. The initial results as to its error correcting capability and the number or code words it can handle have been reported by Barrows, Mandelbaum and the author in separate papers.

As was suggested in the author's previous report (CSL Report R-336), the procedure of finding the minimum distance for non-prime generators B and for prime generators that do not have 2 as primitive root, has been completed. These are the most important cases because of the higher efficiency, although a closed-form relation instead of a procedure is yet to be found. Using the CSL computer (1604), all the odd composite generators (B) up to 10,000 have been examined. Thus, in a practical sense, the answer is at hand now, for one only has to look up the table of all the B's and their minimum distance and code lengths thus found.

At present, the research focusses on the theoretical solution with the help of number theory and the data obtained from the computer. Some interesting results have been noted from the data as to the formation of orbits of permutation function $\mu(\alpha) = 2\alpha \bmod B$, particular prime components that contribute more useful codes, and a relationship between participant primes of the generator and minimum distance and length of the code. The final results will soon appear in a CSL report.

S. J. Hong

11.3. Digital Systems.

11.3.1. Row-Column Minimization of Sequential Machines and Related Problems.

The study of two algorithms for simultaneous row-column reduction was completed and reported in the Coordinated Science Laboratory Report R-355. Aside from the self-consistent and complete presentation of the reduction theory--the definition of compatibility is based on

total states; the propositional calculus used in implementating the algorithm is explored as a Boolean algebra; and the minimization criterion is identified as a lattice inequality--this report contains three significant developments.

Firstly, the cc table of Grasselli and Luccio's algorithm may become cyclic, in which case the algorithm becomes tedious and inefficient. Two rules can be extracted from our presentation which significantly improves the manipulation of cyclic tables.

Secondly, the cc table is a very general graphical device for solving large collections of propositions, and many related problems can be expressed as a collection of propositions. Unfortunately, two very powerful rules in Grasselli and Luccio's algorithm depend upon eliminating certain solutions because of a lattice inequality, and the related problems may not have this property. Nevertheless, we have found a recovery technique by which the solutions eliminated by lattice inequalities may be recovered. Consequently, the two powerful rules may be used in many problems related to this. This extends the applicability of what was once just a covering table to general propositional algorithms--a large class of problems.

Lastly, the tree method which was applied by Meisel to row minimization was extended to simultaneous row-column minimization. This eliminates the cc table altogether, and thus sidesteps the problem of cyclic tables. Moreover, both Meisel's tree and this tree are made more efficient by the application of a new corollary, which allows one to discard redundant g covers. The resulting algorithm is well structured, easy to use and easy to check.

A study of largest-combinable-class solutions was begun. One is given a set of pairs of elements which are combinable, and from this one finds the largest classes such that every pair of elements is combinable, in this type of problem. The problem is general; it appears, for example, in row-column minimization assignment of asynchronous machines, and in other algorithms.

The solution which was developed was reported in Coordinated Science Laboratory Report R-362. It is a surprisingly simple manipulation of columns in a staircase table to write a tree, yet it proves to be a solution of a propositional function written as a tree by using the distributive and absorption of rules of Boolean algebra. However, the method already in use is in many ways, as simple as the method developed in this report, particularly for staircase tables with few blanks. Nevertheless, the new method is simpler to check in manual use, and uses substantially less memory space in its programmed form than the older method.

G. J. Lipovski

11.4. Communication Theory.

11.4.1. Optimum Filtering With a Class of Nonlinear Systems.

The purpose of this work is to propose a simple class of nonlinear filters composed of a linear system in parallel with a zero-memory nonlinearity (ZNL) preceded by a variable delay. This class of filters is shown to be very convenient for the filtering, prediction, and reconstruction of random signals. The problem considered is the minimum-mean-squared error (MMSE) filtering of a signal s(t) corrputed by additive noise n(t) from a finite number of input samples: $x(kT-iT) = s(kT-iT)$

+n(kT-iT), i=0,1,...,N. To simplify the optimization problem the signal and noise are assumed to be of the separable class.[1] The filter output may be represented by the following expression

$$y(t) = \sum_{i=1}^{N} a_i x(kT-iT) + g[x(kT-\ell T)]$$

where the a_i represent the linear part of the system and the g(x) is the ZNL.

The optimization may be performed in two steps. First the linear filter is fixed and the MSE is minimized with respect to the ZNL g(x). Then the resulting error is further minimized to derive the linear filter $a_0, a_1, \ldots a_N$. The results of the optimization may be summarized as follows: The linear part of the optimum system is given as a linear combination of the optimum linear filters for estimating s(t), s(kT-ℓT), and n(kT-ℓT) from the input samples. Therefore, there is no need to invert a new matrix (or to solve a new integral equation for the continuous-time case), and the results obtained in the case of optimum linear filtering may be used. The nonlinearity g(x) for the optimum system is proportional to the MMSE zero-memory estimate of s(t) from x(t), i.e. $g(x) = CE\{s|x\}$ which depends only on the first-order probability densities of the inputs. These properties makes it possible to use the results of the optimum zero-memory nonlinear filtering and the optimum linear filtering problems to construct the optimum scheme of the class defined here.

Furthermore, as a byproduct of the optimization procedure, a new suboptimal filtering scheme is obtained. This scheme is constructed

---

[1] A. H. Nuttall, "Theory and Application of the Separable Class of Random Processes," TR 343, Research Lab. of Electronics, M.I.T., May 1958.

by adding a modified ZNL to the optimum linear filtering system. The resulting scheme exhibits a smaller MMSE than the linear system alone. However, it is not too much inferior to the optimum nonlinear scheme discussed earlier. Therefore, it may be more convenient to use the suboptimal scheme, since it is much simpler to construct.

The improvement in the MMSE of the optimal and suboptimal schemes over the linear system depends on the delay of ℓ sample. This delay should be chosen so as to obtain maximum improvement. However, it is not easy to derive the best delay in general. It might seem intuitively true that the delay should be chosen such that the correlation between s(t) and s(kT-ℓT) is the largest. The result could be verified only for two cases:

(1) The power spectral densities of s(t) and n(t) have the same shape.

(2) The linear filter is unrealizable with large memory.

For other cases the assertion is no longer true, and computational methods may be used to derive the best delay. An example is considered to illustrate the error improvement and its dependence on the delay.

A. H. Haddad

II.5. Networks With Specified Survivability.

Network models of communication nets were investigated with regard to their survivability, defined in terms of the number of nodes or links which can be removed without disconnecting other parts of the system.

Classes of networks with specified survivability are constructed. The results are summarized in a forthcoming technical report.

D. Butler
R. T. Chien

11.6. Coding for the Continuous Channel.

A class of explicit codes for time-discrete amplitude-continuous channels is presented. These codes, called lattice codes, can maintain positive transmission rates while simultaneously reducing the probability of error to zero. A lattice in n-dimensional Euclidean space is the set of all integer linear combinations of some n independent basis vectors. A lattice code for a given time-discrete continuous channel is formed from a lattice by taking for code words all those vectors of the lattice which satisfy the channel constraints. Communication over memoryless time-discrete continuous channels with either amplitude or average power constraints is considered. An analysis is given for such channels when lattice codes are used together with bounded distance decoding. Bounds on the channel capacity are found, and, for fixed transmission rates less than capacity, bounds are found for the best attainable probability of error as a function of the code length n. Finally, the construction of lattice codes is considered, and a sequential decoding algorithm is given.

A paper is being prepared for publication.

R. B. Ash
R. J. Tracey

12. NETWORKS[†]

J. J. Bourquin
W. Mayeda
A. Ong
A. C. Sabino
S. Toida
T. N. Trick
N. Wax

12.1. Mapping of Linear Graphs onto a Doughnut.

Psuedocuts of a planar graph which have 1-1 correspondence with paths in a dual graph are investigated further. By defining a dual graph G' of a given graph G drawn on a doughnut properly, we can investigate the properties of G' by studying psuedocuts. By extending the definition of pseudocuts, we hope that we can obtain necessary and sufficient conditions such that a linear graph can be mapped onto a doughnut with some proper restrictions. Furthermore we wish to relate these conditions to the circuit and the cut-set matrices of a given graph so that by testing them, we can find whether a graph can be mapped on a doughnut under the given restrictions. At present, we are searching for proper restrictions for mapping a graph on a doughnut so that the dual graph can be defined uniquely.

W. Mayeda

12.2. New Topological Formulas for Networks Containing Ideal Transformers.

New topological formulas for the analysis of electrical networks with ideal transformers are derived. They are more general than conventional ones.

Let, A be the incidence matrix of a given network, Y be the admittance matrix of the network, V be the branch voltage matrix of the

[†]This work was supported in part by the Air Force Office of Scientific Research under Grant No. AFOSR 931-66.

network, and J be an independent current source matrix. Then Kirchhoff's law gives AYV=J. This equation contains unknown admittances such as I_1/V_1 shown in Fig. 12.1.

Let us label the terminals of an ideal transformer as shown in Fig. 12.1, and let

$$P_i = \left[\begin{array}{c|ccc|c} U_1 & \multicolumn{3}{c|}{0} & 0 \\ \hline & 1 & 0 & 0 & \\ 0 & n_i & 0 & 1 & 0 \\ & -n_i & 0 & 0 & \\ \hline 0 & \multicolumn{3}{c|}{0} & U_2 \end{array}\right]$$

where U_1 and U_2 are identity matrices, n_i is the turns ratio of the i^{th} ideal transformer, and the first row (the first column) of a submatrix

$$\begin{bmatrix} 1 & 1 & 0 & 0 \\ n_i & 0 & 1 & 0 \\ -n_i & 0 & 0 & 1 \end{bmatrix}$$

corresponds to the first terminal of the i^{th} transformer.

Then we can eliminate the unknown admittances by multiplying P_i's and $P_i{}^t$'s as

$$P_K P_{K-1} \cdots P_2 P_1 A Y A^t P_1{}^t P_2{}^t \cdots P_{K-1}{}^t P_K{}^t V_n = J_t, \qquad (1)$$

where J_t is the independent current-source matrix, changed appropriately, and K is the number of ideal transformers in the network. Now we can solve Eq. (1) for the node voltage V_n.

Let $$A_T = P_K P_{K-1} \cdots P_2 P_1 A,$$

and $$A_T{}^t = A^t P_1{}^t P_2{}^t \cdots P_{K-1}{}^t P_K{}^t.$$

The network represented by A_T can be obtained from the original network by doing the following operations repeatedly until all ideal transformers are removed from the network:

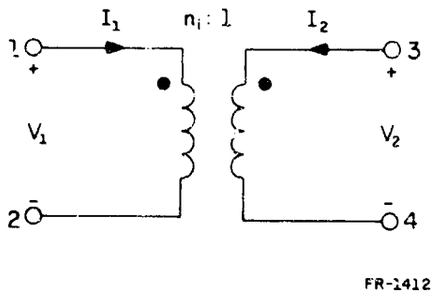

Fig. 12.1. Ideal transformer.

(OVERLEAF BLANK)

1. Put n_i times all admittances incident at the first node between the third and the fourth nodes.
2. Short the first and second nodes and remove the i^{th} transformer.

We wish to compute the determinants

$$\Delta = \det(A_T Y A_T^t),$$

and

$$\Delta_{ij} = \det(A_{T-i} Y A_{T-j}^t).$$

The determinants Δ and Δ_{ij} can be obtained by applying a topological formula slightly different from the conventional ones to the new network.

Theorem 1. We can break up each major of A_T into an appropriate number of matrices $M_1, M_2, \ldots, M_k$ so that the determinant of a major is equal to

$$\sum_{j=1}^{k} \det(M_j)$$

and each column of M_j has only one pair of non-zero entries $[1,-1]^2$ or $[n_i,-n_i]$.

Theorem 2. $\mathrm{Det}(M_i)$ is the admittance product of one of the trees of the network represented by $A_T Y$ in which each admittance appears at most once.

Theorem 3. The determinant Δ is the product between $\Sigma[\Sigma_j \det(M_j)]$ and the corresponding tree product, where the first summation is over all tree products of the network represented by $A_T Y$ in which each admittance of the original network appears at most once.

Theorem 4. The sign of $\det(M_i)$ is determined by the following procedure: In the tree represented by M_i we can give a direction to each path from the reference to each node. Let the positive direction be away from the reference. Associate each edge of the tree with the node which is at

the positive end (with respect to the given direction) of the edge. Since the graph which represents a given network is directed, each edge is either incoming or outgoing at the node associated with it. The association also gives a permutation, if we look at the orderings of edges and nodes.

If the permutation is odd, the number of incoming edges is even, or if the permutation is even, and the number of incoming edges is odd, then the sign of $\det(M_i)$ is minus, otherwise it is plus.

We will not calculate Δ_{ij}.

Definition. The coefficient of a 2-tree product is a 2-tree product divided by the product of the admittances of the branches of a 2-tree.

Theorem 5. The determinant Δ_{ij} is given by

$$\Delta_{ij} = (-1)^{i+j}\Sigma\pi\{T_2(i,1')\}\Gamma\{T_2(j,1')\}$$

in which $\pi\{\ \}$ denotes the 2-tree product and $\Gamma\{\ \}$ denotes the coefficient of such a product.

S. Toida

12.3. Stability of Nonlinear Time-varying Networks.

It has been shown that if a nonlinear time-varying capacitor, whose incremental capacitance is finite and greater than zero for all time, is embedded in a lumped, linear, passive, time-invariant, RC network, then the network is always bounded-input, bounded-output stable. In fact, if the input is periodic with period T, then the transient response asymptotically approaches a unique bounded periodic response with period T. This implies that such a circuit can never to into subharmonic oscillation.

The circuit considered is shown in Fig. 12.2. It is assumed that the nonlinear element satisfies the constraint

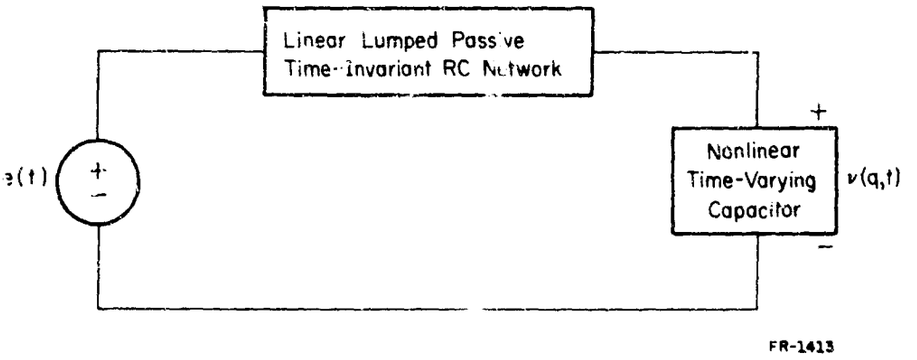

Fig. 12.2. Thevenin equivalent of a network containing a nonlinear time-varying capacitor.

(OVERLEAF BLANK)

$$\alpha \leq [v(q_1,t)-v(q_2,t)]/(q_1-q_2) \leq \beta,$$

for all q and t, and where α and β are positive constants. The integral equation for this network can be put into the form

$$q(t) = \int_a^t h(t-\tau)[e(\tau)-v(q(\tau),\tau)+\tfrac{1}{2}(\alpha+\beta)q(\tau)]d\tau,$$

where $$H(s) = [sZ(s)+\tfrac{1}{2}(\alpha+\beta)]^{-1}.$$

It can be shown that a sufficient condition for the networks to be bounded-input, bounded-output stable is that

$$r = \tfrac{1}{2}(\beta-\alpha)\int_0^\infty |h(t)|dt < 1.$$

Since the linear time-invariant network is RC, it follows that the problem can be formulated such that

$$\int_0^\infty |h(t)|dt < \infty,$$

and $$h(t) > 0, \text{ for all } t.$$

Hence,

$$\int_0^\infty |h(t)|dt = \int_0^\infty h(t)dt = H(s)\Big|_{s=0},$$

and therefore,

$$r = (\beta-\alpha)/[2sZ(s)+\alpha+\beta]\Big|_{s=0}.$$

It follows that $r < 1$, provided that $\alpha > 0$.

The above results are being extended to the case in which N nonlinear, time-varying capacitors are imbedded in a lumped, linear, time-invariant RC network.

T. N. Trick

12.4. Nonlinear Oscillations.

Work during this period centered about one main topic, the behavior of a system of coupled oscillators. Two special limiting cases are being investigated, one in which the oscillators are coupled weakly to each other, and the other in which the coupling is very strong.

Some results have been obtained in the weak-coupling case. The phenomenon of frequency entrainment, or locking, of a system of almost identical oscillators excited by a small external signal was studied. This work was accepted for publication, and is to appear shortly. A generalization, a system of arbitrary oscillators excited by an external signal, is being studied.

An analytical study of the Abraham-Bloch multivibrator circuit with stray capacitances, grid currents, and general nonlinear tube (or transistor) characteristics, is being pursued by Peter J. Ponzo and N. Wax.

N. Wax

12.5. Stability of Uniformly Distributed Networks.

In the previous Progress Report a result[1] was described concerning the stability of linear, time-invariant systems for which transfer functions are rational in $w = e^{\sqrt{(Ts)}}$, in which s is the complex frequency variable, and T is a constant; specific examples of this class include the uniformly distributed RC network (UDRC) with either open-circuit, short-circuit, or matched termination. An effort has been made to extend this investigation of stability to functions rational in w, $\theta = \sqrt{s}$, and s, an important physical example of which the UDRC terminated in any

[1] J. J. Bourquin and T. N. Trick, "Stability of Distributed RC Networks," Tenth Midwest Symposium on Circuit Theory, Purdue University, May 1967.

linear, time-invariant, lumped impedance.[2] Toward this objective two results have been obtained:

(1) If two transfer functions, H(s), an irrational function of s, and B(s), a rational function of s, for which the impulse responses are respectively h(t) and b(t), satisfy the condition that $H(s) = B(\sqrt{s})$, then

$$\int_0^\infty |h(t)|\,dt \leq \int_0^\infty |b(t)|\,dt.$$

The importance of this result is that a system with a transfer function H(s) exhibits bounded-input, bounded-output stability if the system corresponding to B(s) is bounded-input, bounded-output stable. As applied in this investigation, if H(s) is a rational function of w, θ, and s, then B(s) is a rational function of e^{ks} and s. The stability of the latter class of functions has been well discussed in the literature under the general headings of time-delay systems, sampled-data systems, differential-difference equations, etc.

(2) A necessary and sufficient condition for bounded-input, bounded-output stability of a system for which the transfer function is rational in $\theta = \sqrt{s}$, and the degree of the numerator is not greater than the degree of the denominator, is that no pole of the transfer function occur on, or within the quandrant bounded by, the $\pm 45^\circ$ radial lines in the θ plane.

---

[2] J. J. Kelly, M. S. Ghausi, J. H. Mulligan, Jr., "On the Analysis of Composite Lumped-Distributed Systems," IEEE International Convention Record, Part 7, 1966, pp. 308-318.

Although this region of the θ plane is the same as that described in Brin's results,[3] this statement of stability is stronger than Brin's. By stability he essentially meant bounded step response.

J. J. Bourquin

---

[3] A. Brin "On the Stability of Certain Systems with Distributed and Lumped Parameters," Automation and Remote Control, Vol. 23, No. 7, July 1962; pp. 798-807.

13. CONTROL SYSTEMS†

J. B. Cruz, Jr.
S. D. Agashe
C. I. Chen
J. E. Heller
J. P. Herner
P. Kokotovic'
J. Medanic'
W. R. Perkins
D. M. Salmon
P. Sannuti
H. Schmeichel
R. Stefanek
D. F. Wilkie

13.1. Introduction.

This group is concerned with the analytical, computational, and simulation aspects of control-system analysis and design. During this reporting period, major emphasis has been given to a detailed investigation of parameter-variation effects (sensitivity). Design of minimum-sensitivity systems (minimum trajectory sensitivity) has been studied from several points of view. Techniques involving the comparison sensitivity matrix, sensitivity functions, and differential games have been utilized. Sensitivity models have received additional study, with emphasis on adjoint models. The connections between optimality and sensitivity has been studied, including a study of adaptive control. Computer simulations have been made of systems with discontinuities and of systems utilizing Davidon's method as an algorithm for automatic parameter adjustment. A technique for minimax controller design, using a new algorithm for solving algebraic minimax problems, has been developed.

W. R. Perkins

13.2. Design of Minimum Sensitivity Systems.

A design method yielding a low-sensitivity system is developed. The method is an extension of an approach suggested by

† This work was supported in part by the Air Force Office Scientific Research under Grant No. AFOSR 931-67.

Mazer, and further developed by Gonzales. The method utilizes the comparison sensitivity matrix and corresponding scalar sensitivity performance index introduced by Cruz and Perkins. The scalar index is optimized, subject to realization constraints on the controller structure, and on the desired nominal transfer-function matrix. A non-trivial multi-variable example, using a minimax parameter optimization procedure on the CDC 1604 computer, illustrates the procedure.

The method provides a suitable solution for the widely-discussed problem of minimization of trajectory sensitivity (see Sec. 13.4).

An article reporting the method in detail is in preparation.

W. R. Perkins
J. B. Cruz, Jr.

13.3. Sensitivity Models and Parameter Optimization.

Continuing the research surveyed in the last report, an analytical form of the adjoint sensitivity model is obtained and the resulting formula for gradient of a performance index is compared with the direct formula based on direct sensitivity model. The advantage of the adjoint form is that the adjoint sensitivity vector does not depend on the dimensionality of the parameter space and, hence, can be used even if the number of parameters tends to infinity. It serves as a basis for a unified approach to optimization in parameter and function spaces. An account of this result, with examples, is in preparation.

P. Kokotovic'

13.4. Minimization of Trajectory Sensitivity.

A critical evaluation of methods for trajectory minimization has shown that the existing approach is neither well motivated nor analytically correct. The essential drawback results from the influence which the minimization of the sensitivity has on the minimization of the basic index. A method by which the trajectory sensitivity is minimized while preserving the nominal optimal behavior unchanged is being developed. The method consists in minimizing the sensitivity index only, but under the condition that the nominal trajectory is already optimal with respect to the original system. An additional "sensitivity controller" acts only if a parameter variation occurs. A block diagram of the whole system is given in Fig. 13.1, where ξ and ν denote $\partial x/\partial q$ and $\partial u/\partial q$, and u^* and x^* are nominal optimal control and trajectory.

P. Kokotovic'

13.5. Design of Optimally Sensitive Systems.

The "trajectory insensitivity" approach of Sec. 13.4, although applicable to a number of practical problems, suffers from the fact that the resulting system is insensitive not only to unfavorable parameter variations, but also to those which could have improved its performance. Another approach is to synthesize an "optimally sensitive" rather than "insensitive" system. An "optimally sensitive" system is defined as a first order approximation of an optimally-adaptive system. A straightforward analytical method for the design of optimally sensitive systems is developed which refines and generalizes the Werner-Cruz results and extends the notion of the neighboring optimal control.

(OVERLEAF BLANK)

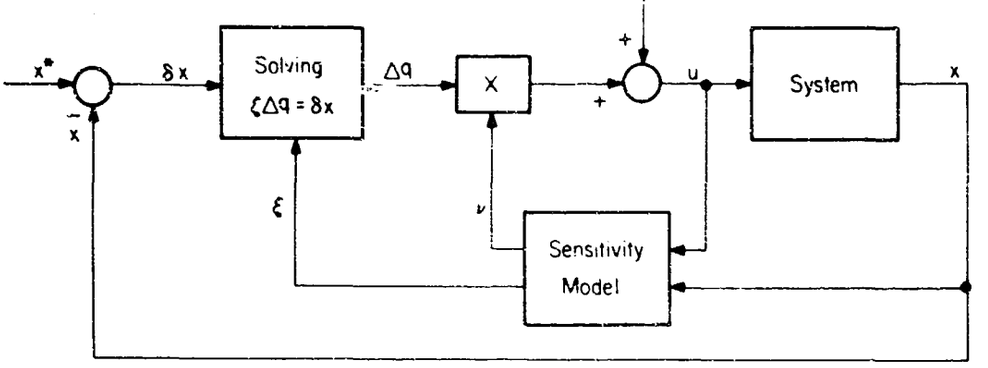

Fig. 13.1. Block diagram of trajectory minimization scheme.

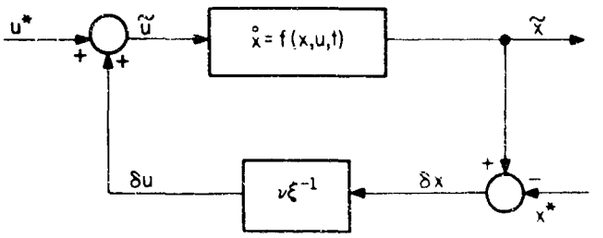

Fig. 13.2. General form of optimally insensitive system.

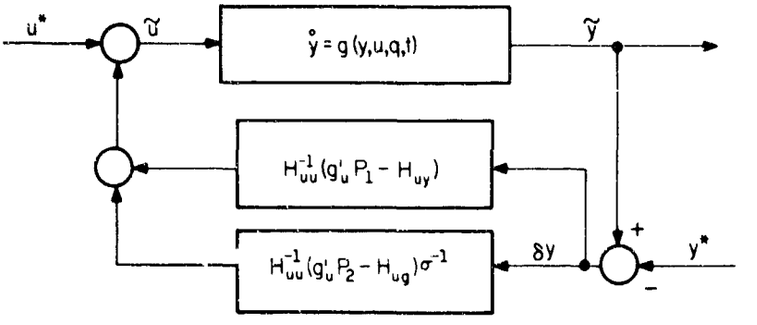

FR-1411

Fig. 13.3. A system optimally insensitive with respect to a plant parameter q.

(OVERLEAF BLANK)

A general form of a system optimally sensitive with respect to initial condition is given in Fig. 13.2 where γ and ξ are the "optimal sensitivity functions," obtained as a solution of two-point boundary value problem for canonic sensitivity equations. A system optimally insensitive with respect to plant parameter ζ is shown in Fig. 13.3 where H_{uu}, H_{uy}, H_{ug} are matrices of second derivatives of Hamiltonian, σ is the optimal sensitivity with respect to parameter ζ, P_1 is a symmetric matrix obtainable as a solution of the Riccati sensitivity equation and P_2 is the solution of linear differential matrix equation. A complete derivation of the method is given in a paper to be presented at the Fifth Annual Allerton Conference on Circuit and System Theory.

P. Kokotovic'

13.6. Multipoint Approximation of Optimally Adaptive Controllers.

A method is developed by which optimally adaptive behavior can be achieved at n+1 "representative" points of the plant-parameter space or initial-condition space. At these representative points both performance sensitivity and its first derivative are zero. A higher order approximation for the neighborhood of a lower number of representative points is possible if the optimal sensitivity functions from Sec. 13.5 are used. The description of the method and the results obtained on nontrivial examples are to be presented at the Fifth Annual Allerton Conference on Circuit and System Theory.

P. Kokotovic'

13.7. Three-Segment Sensitivity Design.

Research on sensitivity problems in optimal control has been directed mainly at designs that assure satisfactory performance of the

control system under plant variations, disturbances or variations of initial conditions. This amounts to considering a set of admissible plants (or disturbances or initial conditions) with respect to which the controller should be designed. It is therefore appropriate to select the best control with respect to the whole set of admissible plants, as opposed to the design of an optimal control which is optimal for a specific plant.

To analyze the problem, the segment of efficiency $E(u) = [J_l, J_h]$ corresponding to the control $u \in U$ has been introduced and appropriately defined by its lower and upper bounds:

$$J_l = \min_{A \in S_A} J(u,A), \tag{1}$$

$$J_h = \max_{A \in S_A} J(u,A), \tag{2}$$

where S_A denotes the admissible set of plant, A is an element of S_A and J is the performance criterion. It is the aim of the proposed design procedure to obtain the best segment, denoted as the realistic segment, and to control the system with the corresponding realistic control.

With the help of the basic notion of the segment it has been possible to analyze the problem and ascertain the following for a general class of control systems:

Particularly important are two segments; the pessimistic segment defined by

$$P_h = J(u^s, A^s) = \min_{u \in U} \max_{A \in S_A} J(u,A), \tag{3}$$

$$P_l = \min_{A \in S_A} J(u^s, A), \tag{4}$$

and the optimistic segment, defined by

$$O_l = J(u^b, A^b) = \min_{u \in U} \min_{A \in S_A} J(u, A), \tag{5}$$

$$O_h = \max_{A \in S_A} J(u^b, A). \tag{6}$$

The pessimistic segment is always contained in the optimistic segment, or

$$E(u^s) \subset E(u^b). \tag{7}$$

A segment corresponding to any admissible control cannot have a lower bound less than O_l.

A segment corresponding to any admissible control cannot have an upper bound less than P_h.

Controls that have an upper bound (of the corresponding segment) greater than O_h can be dismissed from further consideration since they are worse than the optimisitc control u^b.

Controls that have a lower bound greater than P_l can be dismissed from further consideration since they are worse than the pessimistic control u^s.

All admissible controls can be divided into four types of which only one type can give better overall performance than u^s or u^b. This set of controls is termed the set of satisfactory controls, denoted by U^o and each element $u \in U$ possesses the property

$$E(u^s) \subset E(u) \subset E(u^b). \tag{8}$$

There are systems in which the pessimistic or the optimistic controls are satisfactory. In general, when this is not so, it is the aim of the three segment sensitivity design procedure to extract the

best realistic segment satisfying (8) and control the system with the corresponding realistic control. It is possible to obtain the realistic control by fixing the position of the realistic segment with respect to the position of the pessimistic and the optimistic segments. Since the realistic segment cannot be fixed absolutely, because its upper and lower bounds are not entirely independent, it is proposed that the designer fix the upper bound of the realistic segment at some value J_h that he does not want to be exceeded in system operation. There will be in general a set of segments having the same upper bound J_h and the realistic segment will be the one with the minimal lower bound. The control corresponding to this segment is the realistic control.

Variational methods as in optimal control design can be applied to obtain the realistic control, and results have already been obtained for linear systems and quadratic performance criteria.

J. Medanic'

13.8. First-Order Variation of the Cost Due to Changes in Parameters of the Plant.

Consider the plant

$$\dot{x} = f(x,u,q,t),$$

where x = n dimensional state vector,

u = m dimensional control vector,

and the performance index

$$J = \int_{t_o}^{t_f} V(x,u,q,t)\,dt,$$

with M_o and M_f as initial and final manifolds. Then the following general statement is proved.

Statement. In all control schemes which produce an optimal control for a given q^* of the parameter vector q, and which lead to satisfy the terminal constraints, the first order change in the performance index due to first order changes in the parameter is the same.

From this statement, the result of Pagurek, generalized by Witsenhausen with regard to open-loop and closed-loop implementations of the control scheme, is obvious for M_o to be a fixed point and M_f to be free.

P. Sannuti

13.9. The Solution of a Two-point Boundary Value Problem for Inhomogeneous Ordinary Linear Differential Equations.

In the synthesis of optimal controllers for linear plants and in the design of neighboring optimal controllers for nonlinear plants one has to find the solution of the linear differential equations

$$\begin{aligned} \dot{x} &= Ax+By+Z, \\ \dot{y} &= Cx-A'y+V, \end{aligned} \tag{1}$$

where x, y, Z, V are n vectors; A, B, and C are $n \times n$ matrices; and A' is the transpose of A. The boundary conditions are

$$x(t_o) = x(0), \; y(T) = Fx(T), \tag{2}$$

where F is symmetric.

In the homogeneous case Z=V=0, the above two-point boundary value problem is reduced to the solution of a Riccati matrix

differential equation. A similar procedure is developed for the inhomogeneous case. Besides a matrix Riccati equation, (3), one has to solve a linear matrix equation, (4).

$$\dot{k}+kA+A'k+kBk-C = 0, \tag{3}$$

$$\dot{R}+(kB+A')R+kZ-V = 0, \tag{4}$$

with boundary conditions

$$K(T) = F \text{ and } R(T) = 0.$$

P. Sannuti

13.10. Estimation of Parameter Variations.

In trying to design a neighboring optimal controller around the optimal trajectory for a nominal parameter vector q*, one is faced with the difficulty of estimating the changes in parameters from q*. It is found that if one could invert the sensitivity matrix $\partial x/\partial q$, then the change in q from q*, namely δq, can be written as

$$[\partial x/\partial q]^{-1}(x-x^*),$$

where $(x-x^*)$ is the change of the system state vector from its nominal value. But unfortunately in general $\partial x/\partial q$ is a $n \times \ell$ matrix, i.e. non-square, and hence the inverse of it in the true sense does not exist. The possibilities of using a pseudo inverse has been studied.

P. Sannuti

13.11. Optimal Control of Systems with Varying Parameters.

The problem of designing a controller for a dynamic system $\dot{x} = f(x,u,t,v)$, where x is the state vector, u is the control vector,

is being considered when v is unknown and the performance of a control vector u(t) for a given v(t) is evaluated by a scalar functional S(u,v). The approach undertaken is based on a fixed-form controller and consists of determining the particular control u* of the prescribed form which attains

$$\min_{u \in U} \max_{v \in V} S(u,v).$$

Problems of this type, which differ from the differential game problem since

$$\min_u \max_v S \stackrel{?}{=} \max_v \min_u S,$$

have been previously investigated when v(t) is a constant[1] or in which u(t) is a constant and the system is of the form[2]

$$\dot{x} = f(x,u,t) + d(t)v(t).$$

The development of a computational algorithm to obtain u* for a larger class of systems than previously considered is proceeding at this time with promising results.

J. E. Heller

13.12. Sensitivity of Discontinuous Systems.

Preliminary studies have been undertaken involving the sensitivity of systems having certain types of discontinuities. In

---

[1] D. M. Salmon, "Minimax Controller Design," Report R-358 Coordinated Science Laboratory, University of Illinois, Urbana, Illinois, July, 1967.

[2] A. J. Koivuniemi, "Parameter Optimization in Systems Subject Worst Disturbance," IEEE Transactions on Automatic Control, AC-11, 3, July, 1966, pp. 427-433.

particular, consider the nonlinear, time-varying system of equations.

$$\dot{\underset{\sim}{x}}(t) = \underset{\sim}{f}(x_1,\ldots,x_n,u,\alpha,t)$$

where $\underset{\sim}{x}$ and $\underset{\sim}{f}$ are n vectors, α is a parameter, and u is a scalar control. The sensitivity equations with respect to α cannot be obtained in the usual way for this system when the control is discontinuous. However, a means of obtaining the sensitivity equations for this problem is being studied, and results so far are encouraging.

Computer simulation has been used extensively in this project, and numerical results have been obtained which indicate the accuracy of the proposed analytical method. A paper describing the derivation and computer implementation of the sensitivity model, and giving the results of the simulation, is now being prepared.

Attempts have also been made to use the sensitivities thus obtained in the determination of the optimal control for the system. Various performance indices have been minimized using the method. Techniques for improving the speed of convergence while using a digital computer in the optimization process have been tested. Many of these techniques have been incorporated in several computer programs. Since results to date are promising, research will continue towards further improvement of existing programs, and consideration will be given to related types of optimization problems.

R. Stefanek

13.3. Investigation of Numerical Methods in Adaptive Systems.

Consider the problem of automatic adjustment of the parameters of a system described by

$$\dot{\underset{\sim}{x}} = f(x,\underset{\sim}{q},t),$$

where $\underset{\sim}{x}$ is the state vector, and $\underset{\sim}{q}$ is a time-invariant parameter vector, with the goal of minimizing a system performance index given by

$$J(\underset{\sim}{q}) = \int_0^\infty V(\underset{\sim}{x},\underset{\sim}{q},t)\,dt.$$

Some numerical technique must be employed to minimize the functional $J(\underset{\sim}{q})$ by finding the appropriate value of $\underset{\sim}{q}$, having begun with some initial guess, say $\underset{\sim}{q}_0$. Typically some form of the gradient technique or Newton-Raphson technique has been used. In this work, a numerical technique known as Davidon's method is being investigated, and preliminary results indicate it converges more rapidly and more reliably than the gradient method in most cases. The advantage of Davidon's method over gradient and Newton-Raphson type techniques is that it converges faster than the gradient but avoids inverting the matrix of second partial derivatives that is necessary for the Newton-Raphson method.

All of these techniques require the components of the gradient vector of J with respect to $\underset{\sim}{q}$ for their implementation. These have been obtained through the use of sensitivity models of the system being optimized. This means the gradient components of $J(\underset{\sim}{q})$ can be fairly easily obtained simultaneous with the system operation, and hence it is hoped that a fast, on-line adaptive scheme for optimizing systems can be developed.

D. F. Wilkie

13.14. Some Generalizations in System Theory and Their Applications to Control Systems.

This project was completed by S. D. Agashe in June, 1967. A report, R-356, was written and issued in May. The report is identical to the Ph.D. thesis submitted in partial fulfillment of the requirements for the Ph.D. degree of S. D. Agashe. A brief abstract of the report follows:

A fundamental definition of a system is given. Two new concepts, namely functional dependence and quasifunctional dependence are introduced, by means of which the concepts of output, input, and state sets are defined. Index sets are defined. Index sets, attribute sets, and versatility of a system are used for comparing systems. Two theorems regarding the versatility of linear systems are proved.

A new perturbation process is described in detail. It is more general than the perturbation process described in the book, "Mathematical Theory of Optimal Processes," by Pontryagin, et al. A formula for an effect vector of the process is derived. The formula is used to derive very simply the Maximum Principle and a few other results. A new interpretation of the unit impulse response of a linear system as well as a nonlinear system is provided using the new perturbation process.

J. B. Cruz, Jr.

13.15. Controller Design.

This project was completed in July, 1967, and a report R-358, "Minimax Controller Design" by D. M. Salmon was issued in July. This

report is identical to the Ph.D. thesis of D. M. Salmon. Two papers based on the report have been submitted for publication. A brief abstract of the report is given below:

The control of an uncertain dynamic system requires a compromise between controller complexity and system performance. At one extreme is the optimal adaptive controller which is generally difficult to realize but yields ideal performance, and at the other extreme is an overly simplified controller which yields unacceptable performance. A reasonable controller structure with a number of free parameters can often be determined by the designer. The report describes minimax methods for determining the free parameters.

The concept of performance sensitivity is introduced to meet the usual criticism of worst-case design, that it is too pessimistic in concentrating attention on the worst parameters. Properties of minimax control with a performance sensitivity as the index are developed. It is shown that the usually desired range of system properties can be achieved by minimaximizing either the system performance index or a performance sensitivity.

A new algorithm for solving algebraic minimax problems, regardless of the presence of a saddle point, is presented and proved to converge. The rate of convergence, and simplifications which occur when the system is linear or when the index has convex properties, are discussed. The algorithm is extended to the case of time-varying minimizing parameters, and methods and problems of computation are discussed.

A method of obtaining multipoint optimality with time-varying controllers is presented. This method is of particular value when the

computational difficulties of finding minimax time-varying parameters are prohibitive. Several examples illustrate the utility and practicality of the methods developed above, including the position control of a string of moving vehicles, and the speed control of a rotary shear.

J. B. Cruz, Jr.

13.16. Sensitivity Reduction Using Optimally Derived Controllers.

This project was completed in May, 1967, and is reported in R-353. This report is identical to the Ph.D. thesis of James P. Herner. A brief summary of the report follows.

Feedback structures which reduce the parameter sensitivity of a linear system are derived from the solution of the classical linear regulator problem. Linear time-varying systems with several inputs and outputs are treated, and simplifications in the design are noted for the time-invariant case. Throughout the discussion, problems of implementation are considered as constraints on the design of the system. Sepcifically, unbounded elements in the controller are not allowable. It is shown that for a special structure, called the Nth order feedback, the sensitivity of the system may be reduced to an arbitrarily small value.

W. R. Perkins

13.17. Suboptimal Design of Higher-Order Systems.

A possibility for the design of suboptimal controllers for higher order plants having two dominant poles has been investigated.

The first stage of the design is the synthesis of an optimal controller for the "degenerate" second-order plant. In the second stage, small parameters are included which make the system order higher than two. Sensitivity functions with respect to these parameters are used for the correction of the previously synthesized switching line. Several examples have demonstrated the applicability of the procedure for one class of practical problems. Further improvements are needed to make the method applicable for a wider class of problems. The results are reported in the CSL Report R-365, August, 1967, "Simplified Switching Functions for Time-Optimal Control Systems," by Harry Schmeichel.

P. Kokotovic'

(OVERLEAF BLANK)

14. SWITCHING SYSTEMS†

G. Metze
E. S. Davidson
T. Gaddess
R. Isenhart
T. Powell
S. Seth

14.1. Modular Decomposition of Combinatorial Logic.

Attention was focused on finding NAND networks for sets of combinatorial functions. A branch-and-bound algorithm was developed to find such networks while minimizing the cost, taken as a linear combination of the inputs and outputs of all NANDs in the network. This algorithm is being programmed for the CDC 1604. In order to keep the entire program in core memory, problems will be restricted to less than 12 variable functions and 96 gate networks. A contemplated program modification will allow maximum fan in, fan out, and level constraints to be imposed on the network.

E. S. Davidson

14.2. A Relation Between Flow Graphs and the Traveling-Salesman Problem.

Investigations into this relation were carried further to provide:

(1) A tighter lower bound on the value of the minimum solution of a traveling-salesman problem containing a given partial solution,

(2) An upper bound on the number of solutions of a traveling-salesman problem containing a given partial solution,

(3) An economic expansion for representing connections or selected one connections of a flow graph as a single tree,

---

†This work was supported in part by the National Science Foundation under Grants NSF-GK 36 and NSF-GK 1663.

(4) An iterative method for developing such a tree so that large-gain connections may be found first, allowing approximate solutions with error bounds by constructing partial trees.

G. Metze
E. S. Davidson

14.3. Error-Detecting Binary Adders.

Further work was done on the material described in Report R-337. The type of adder considered for error-detecting possibilities was generalized beyond the particular design described in the report. Two basic block diagrams--for adders with either serial- or parallel-carry prop propagation--were used to provide an overall description of the circuit. Results for both types of systems show that a single permanent fault can at most produce a sum error only slightly more complicated than the error for the special case considered previously. In the new general case, it is still possible to use residue codes of the form $(2^x-1)n$ for error detection. Such codes allow an especially economic and reliable hardware-shared implementation for the adder-checker system.

The results and conclusions were rewritten in the form of a technical paper entitled "An Error Detecting Binary Adder: A Hardware--Shared Implementation," to be presented at the First Annual IEEE Computer Conference, Chicago, Illinois, on September 6, 1967. The paper is also being considered for publication in the IEEE Transactions on Electronic Computers.

T. Gaddess

14.4. Selection of a Minimal Set of Diagnostic Tests.

The study of fault tables for multiple-output combinatorial nets has led to the development of a new matrix procedure to determine the minimum set of tests which will completely diagnose the net. The extension of this procedure to sequential circuits is being investigated.

R. Isenhart

14.5. Fault Diagnosis to the Package Level.

A procedure has been developed for selecting a near-optimal set of tests from a given set of tests for the diagnosis of combinational logic to the package level. Since less information is required to identify the package which contains the fault, rather than the specific fault, fewer tests will usually suffice to diagnose the network.

For the procedure, weights are given to all tests according to the degree with which their outputs partition the faulty packages. The test with the highest weight is selected, and new weights are given to the unchosen tests according to the degree with which these tests partition the faulty packages further. Again, the test with the highest weight is chosen and added to the list of diagnostic tests. This process is continued until each package has been distinguished from all other packages or until no further destinctions can be made. This procedure is described in more detail in report R-354.

T. Powell

14.6. Computer Compiler.

A target language for the system has been selected and the coding of a computer compiler for a simple hypothetical machine like CSLIAC is now in progress. This experience with a simpler machine will hopefully

suggest improvements in the coding procedure for a more elaborate machine which will next be studied.

S. C. Seth

(OVERLEAF BLANK)

Abstract continued

The high-frequency instability resulting from the interaction of a cold electron beam with a cold plasma is investigated in the collisionless as well as the collision-dominated regime. Measurements of the beam distribution function show that the instability is heavily damped at high plasma densities and exhibits a maximum at intermediate densities. The results are in good agreement with theoretical calculations invoking Coulomb collision as the main damping mechanism.

Solutions of the nonlinear Boltzmann equation have been obtained for two problems: a strong shock wave (Mach number 4.0); and heat transfer in a rarefied gas for several values of the Knudsen number and of the ratio of the plate temperatures. These solutions can be compared in detail with results of Navier-Stokes and Krook theory by using a new program that calculates mean values and probable errors for each of some 80 functions of interest at each station in the gas.

An improvement by a factor of three in the voltage-holding capabilities of copper electrodes at ultrahigh vacuum may be realized by gas conditioning of the electrodes. Under certain conditions, whiskers are found to grow or appear on tungsten tips in the field-emission microscope. No whisker growth has been observed on clean tungsten tips.

The accuracy requirement of the general-relativity-effect measurement has been reappraised. Realistic data were used to estimate the center of noisy photographic images by computer simulation. From these data the overall readout accuracy was estimated. Possible flash-angle distributions for the satellite for various orbital inclinations are presented. A computer program for calculating the solar-radiation-pressure-induced precession has been extended to include the effects of orbital regression and advance of perigee for orbital inclination values. An experiment for estimating the sensitivity to NO of a proposed balloon-borne system has been conducted and evaluated. A prototype sunseeker is described and evaluated. A theoretical and experimental investigation to determine the optimum tubing diameter and matching termination for good response of fluidic transmission lines as a function of line length is being carried out.

Defects are introduced into semiconductors by high-energy radiation. These defects influence the electrical, optical, and thermal properties of these materials. The luminescence that results from recombination of free holes with electrons trapped at these defects is a particularly sensitive means of determining the location of the energy levels arising from these defects and the nature of the interaction of the trapped charge with the lattice. The impurity band in highly-doped semiconductors has been investigated by studying the tunneling current between a superconductor, In, and the semiconductor, p-type Si. The results of these studies give information about the density of states of the impurity band and about the coupling of electrons to the K=0 optical phonon.

Computer statistics are reported. The properties of the CRT display are presented together with photographs of display output. Programming systems are described, and a new research program applying computer graphics to structural analysis is discussed.

Further observations of gas-composition effects are summarized; results of a study of the use of phosphors to provide displays with several colors are described; preliminary work on the use of plasma cells in logical structure is presented; and the problems of providing starting particles for the initial discharge in a sequence are discussed.

Work on the infrared-converter, thin-film display, has continued. The properties of light-emitting, tunnel-injection, CdS devices are given. Techniques for preparing films of semiconducting CdS, InSb, and insulating films are under development.

In the area of information retrieval, effort is continuing in establishing the data base, and theoretical investigations have been undertaken in clustering theory and file-organization techniques. The main effort, however, has concentrated on developing an interactive display system on the CDC 1604. New results have been obtained in coding theory, specifically as regards geometrical considerations on cyclic codes, decoding of BCH codes, and the general properties of linear residue codes. A study has been completed in row-column minimization of sequential machines and related problems, such as covering problems and identification of combinable classes. Several results have been obtained in the area of nonlinear filtering.

Pseudocuts of a graph are being studied in the belief that they will lead to necessary and sufficient conditions such that a linear graph can be mapped onto a doughnut. In addition, new topological formulas have been derived for the analysis of electrical networks containing ideal transformers. In the area of nonlinear circuits it has been found that a linear, time-invariant, passive RC network, in which is embedded a nonlinear time-varying capacitor with finite, positive, incremental capacitance, is always bounded-input, bounded-output, stable. Also, the behavior of a system of coupled oscillators is being studied. Some results have been obtained in the case of weakly-coupled oscillators, and the case where the coupling is very strong is under investigation. Some new frequency-domain criteria have been obtained for the stability of uniformly distributed networks.

Investigation of parameter-variation effects (sensitivity) on control-system performance is continuing. Emphasis has been placed on the design of minimum-sensitivity systems, using several techniques including comparison sensitivity, sensitivity functions, and the theroy of differential games. Several computer simulations have been made, and some numerical techniques for parameter optimization have been studied. An investigation of the connections between optimality and sensitivity is continuing.

Further progress is reported in methods for the selection and generation of diagnostic tests, and the modular decomposition of combinatorial logic. The relationship between flow graphs and the traveling salesman problem has been further investigated, and the results of the study of applicability of An+B codes to an error-checking arithmetic unit have been extended. Work on the Computer Compiler has been intensified.

Security Classification

DOCUMENT CONTROL DATA - R & D

Security classification of title, body of abstract and indexing annotation must be entered when the overall report is classified)

1. ORIGINATING ACTIVITY (Corporate author)

University of Illinois
Coordinated Science Laboratory
Urbana, Illinois 61801

2a. REPORT SECURITY CLASSIFICATION

Unclassified

2b. GROUP

3. REPORT TITLE

PROGRESS REPORT FOR MARCH 1967- AUGUST 1967

4. DESCRIPTIVE NOTES (Type of report and, inclusive dates)

5. AUTHOR(S) (First name, middle initial, last name)

6. REPORT DATE	7a. TOTAL NO. OF PAGES	7b. NO. OF REFS
October 2, 1967	292	

8a. CONTRACT OR GRANT NO.	9a. ORIGINATOR'S REPORT NUMBER(S)
DAAB-07-67-C-0199	
b. PROJECT NO	
c.	9b. OTHER REPORT NO(S) (Any other numbers that may be assigned this report)
d.	

10. DISTRIBUTION STATEMENT

Qualified requesters may obtain copies of this report from DDC.

11. SUPPLEMENTARY NOTES	12. SPONSORING MILITARY ACTIVITY
	Joint Services Electronics Program thru U.S. Army Electronics Command Ft. Monmouth, New Jersey 07703

13. ABSTRACT

Measurements of the adsorption and desorption of N_2, CO, and H_2 on polycrystalline, 110, and 111 tungsten have been made utilizing the Auger electron-emission technique. These measurements indicate various type of adsorption states having, in general, complex desorption characteristics. The electron spectrometry technique developed in this laboratory has been applied to the study of the adsorption of gasses on polycrystalline tungsten and platinum. The instrument is being modified to allow temperature control of the sample over a wide temperature range starting at about 100°K. The heating technique has also been modified. Work on the experiment for the study of the angular distribution of secondary electron has proceeded. Preliminary measurements with the analyzer system have been made showing some design changes to be necessary. Initial measurements with the improved system are being started. An experiment to study the emission of ions from solid surfaces due to electron impact has been started. Progress in the design and construcion of this instrument is discussed. Some measurements of the yield of photons emitted from surfaces by impinging ion have been made indicating values in reasonable agreement with theoretical predictions

Difficulties experienced in using an omegatron as a relative standard for comparing ionization-gauge sensitivities to ionization cross sections are reported. Size effects in thin, epitaxial gold films are discussed, as are the techniques used for the data analysis. The preparation of thin, unbacked, aluminum films for use as optical filters, and of replicas for electron microscopy of film surfaces

DD FORM 1 NOV 65 1473 (PAGE 1)

S/N 0101-807-6811

Security Classification

14 KEY WORDS	LINK A		LINK B		LINK C	
	ROLE	WT	ROLE	WT	ROLE	WT
Surface Physics						
Applied Physics						
Plasma Physics						
Rarefied Gas Dynamics						
High-Voltage Breakdown						
Space Sciences						
Semiconductor Physics						
Computer						
Plasma Display						
Infrared Converter						
Information Sciences						
Networks						
Controls Systems						
Switching Systems						